UC Riverside

UC Riverside Electronic Theses and Dissertations

Title

Genetically Encoded Approaches to Target Specific Neural Subtypes in Vivo

Permalink

https://escholarship.org/uc/item/67z5g3bq

Author

Ubina, Teresa Marie

Publication Date

2024

Copyright Information

This work is made available under the terms of a Creative Commons Attribution License, available at https://creativecommons.org/licenses/by/4.0/

Peer reviewed|Thesis/dissertation

eScholarship.org Powered by the California Digital Library
University of California

UNIVERSITY OF CALIFORNIA
RIVERSIDE

Genetically Encoded Approaches to Target Specific Neural Subtypes *In Vivo*

A Dissertation submitted in partial satisfaction
of the requirements for the degree of

Doctor of Philosophy

in

Neuroscience

by

Teresa Marie Ubina

September 2024

Dissertation Committee:
- Dr. Martin Riccomagno, Chairperson
- Dr. Sachiko Haga-Yamanaka
- Dr. Todd Fiacco
- Dr. Garret R. Anderson

Copyright by
Teresa Marie Ubina
2024

The Dissertation of Teresa Marie Ubina is approved:

_____

_____

_____

_____

Committee Chairperson

University of California, Riverside

ACKNOWLEDGEMENTS

I would like to thank the co-authors of the previously published work discussed here. I would like to thank my first PIs, Dr. Nicole Bournias-Vardiabasis and Dr. Paul Salvaterra for introducing me to research, training me, and allowing me to grow as a scientist. I would like to thank my committee members Dr. Sachiko Haga-Yamanaka, Dr. Todd Fiacco, and Dr. Garret Anderson for their guidance and mentorship during my PhD. To all of the mentors I have had over the years, whether it be in an official capacity or as my peers. Thank you to all of my lab mates, friends, and family who always supported me. Thank you to Marc Ubina for all of the love and for being my biggest supporter and cheerleader throughout my academic career and in life. Lastly, I would like to thank Dr. Martin Riccomagno for all his guidance and efforts into shaping me as a scientist. I would not be here without all your support, thank you.

In loving memory of my grandfather, Jose Luis Zaragoza.

ABSTRACT OF THE DISSERTATION

Genetically Encoded Approaches to Target Specific Neural Subtypes *in vivo*

by

Teresa Marie Ubina

Doctor of Philosophy, Graduate Program in Neuroscience
University of California, Riverside, September 2024
Dr. Martin Riccomagno, Chairperson

Neural cell-types are incredibly heterogenous. How the diversity of neural cell subtypes comes to be during development is a topic of intense study. New tools and techniques are essential for examining cell-type diversity and its implications for healthy brain functions. Differences in development likely contribute to the varied responses of cell subpopulations during neuroinflammation. This collection of works presents the design and generation of three tools to label and manipulate subtypes of cells. In Chapter 1, we introduce the Expression by Boolean Exclusion (ExBoX) AAV-based tool. ExBoX encodes expression of a gene of interest (GOI) that is turned on by one recombinase (Cre or Flp) and turned off by the other. Its simple design allows for insertion of larger cargo than similar tools. ExBoX can be used to express a GOI in a subset of neural cells, or to regulate GOI expression for a defined critical period. We show proof of concept utilization of ExBoX in the tight regulation of labeling both *in vitro* and *in*

vivo. In chapter 2 we describe the design, generation, and characterization of a knock-in mouse line (*Lcn2CreERT2*) to specifically target subsets of astrocytes that become reactive in disease. *Lcn2CreERT2* labels a subset of reactive astrocytes (RAs) across a wide range of neuroinflammatory insults. Using the *Lcn2CreERT2* line we show RAs labeled during systemic inflammation remain in the brain following the resolution of inflammation and largely revert to a pre-inflammatory state. Next, we provide an extended protocol for induction and labeling of RAs in the *Lcn2CreERT2* mouse. Finally, we designed and generated the *C3-FlpOER^{T2}* mouse line. The *C3-FlpOER^{T2}* line can label a subset of RAs under some neuroinflammatory conditions. We show this subset of RAs is labeled only in certain models of neuroinflammation caused by direct insult to the brain, and that *C3-FlpOER^{T2}* expressing RAs are not proliferative. Additionally, we show this tool can be used in combinatorial ways to drive robust and specific reporter expression in RAs. Overall, we show the design, generation, and utility of these newly generated mouse lines and viral tools for use in investigating cellular diversity during development and disease.

Table of Contents

Introduction 1

Neuronal heterogeneity 1

Astrocyte development and diversity 5

Astrocyte heterogeneity in disease 10

Targeting specific cell types and subpopulations to understand development and disease 13

Chapter 1: ExBoX – a simple Boolean exclusion strategy to drive expression in neurons 17

Abstract 18

Introduction 19

Materials and Methods 23

Results 31

Discussion 42

Chapter 2: A genetic tool for the longitudinal study of a subset of post-inflammatory reactive astrocytes 47

Abstract 48

Introduction 49

Materials and Methods 52

Results 60

Discussion 78

Chapter 3: Induction of neuroinflammation for the longitudinal study of reactive astrocytes in *Lcn2CreERT2* mice 86

Abstract 87

Before you begin 89
Low-dose LPS 96
High-dose LPS 99
Intrastriatal LPS 102
Cryopreservation and sectioning of tissue 106
Immunohistochemistry 107
Troubleshooting 110
Chapter 4: A novel FlpO recombinase mouse line to target a subset of reactive astrocytes 115
Abstract 116
Introduction 117
Materials and Methods 119
Results 127
Discussion 147
Conclusion 152
References 155

List of Figures

Chapter 1

Figure 1.1 Design for CreOnFlpOff and FlpOnCreOff constructs..... 23

Figure 1.2 Validation of ExBoX in Neuro2A cells. 32

Figure 1.3 Direct fluorescence for CreOn-FlpOff-EGFP in Neuro2A cells and Off recombinase detection. 34

Figure 1.4 Direct fluorescence for FlpOn-CreOff-tdTomato in Neuro2A cells and Off recombinase immunocytochemistry. 35

Figure 1.5 The ExBoX system can be used in multiple ways..... 37

Figure 1.6 Temporal control of FlpOn-CreOff-tdTomato expression in vivo. 39

Figure 1.7 Temporal control of CreOn-FlpOff during AAV delivery. 40

Figure 1.8 Temporal control of FlpOn-CreOff during AAV delivery. 41

Chapter 2

Figure 2.1 Design of the *Lcn2CreERT2* transgene. 51

Figure 2.2 Expression of *Lcn2CreERT2* following repeated low-dose LPS treatment..... 62

Figure 2.3 Cell type markers in *Lcn2CreERT2; Ai9* brains following repeated low-dose LPS treatment. 64

Figure 2.4 Expression of *Lcn2CreERT2* in a parasitic model of neuroinflammation 67

Figure 2.5 *Lcn2CreERT2; Ai9* tdTomato labeling after intrastriatal LPS injections 69
Figure 2.6 Astrocytes that were initially reactive remain in the brain after resolution of inflammation. 72
Figure 2.7 Morphological changes in astrocytes pre and post inflammation 75
Figure 2.8 Reactive markers return to baseline levels in astrocytes that were initially reactive 77

Chapter 3

Figure 3.1 Graphical abstract of low-dose, high-dose, and intrastriatal LPS protocols 88
Figure 3.2 Summary of the timing of treatments for low-dose protocol 96
Figure 3.3 Low-dose LPS expected outcome. 98
Figure 3.4 Summary of the timing of treatments for high-dose protocol 99
Figure 3.5 High-dose LPS expected outcome. 101
Figure 3.6 Summary of the timing of treatments for intrastriatal LPS protocol 102
Figure 3.7 Intrastriatal LPS expected outcome 105

Chapter 4

Figure 4.1 Complement 3 is upregulated during direct insults to the brain 129

Figure 4.2 Design of the *C3-FlpOERT2* mouse 130

Figure 4.3 Intrastriatal LPS labeling in *C3-FlpOERT2; RC::FLTG* mice 132

Figure 4.4 Cells labeled in the *C3-FlpOERT2* line are primarily astrocytes 134

Figure 4.5 Low- and high-dose LPS in *C3-FlpOERT2; RC::FLTG* animals 136

Figure 4.6 *C3-FlpOERT2; RC::FLTG* tdTomato expression 7, 30, and 60 days after FPI 138

Figure 4.7 Intrahippocampal kainic acid does not induce labeling of cells in *C3-FlpOERT2* mice..... 140

Figure 4.8 *C3-FlpOERT2* labeling of astrocytes during acute and chronic *T. gondii* infection..... 142

Figure 4.9 *C3-FlpOERT2* labeled astrocytes are not proliferative..... 143

Figure 4.10 *C3-FlpOERT2* can be used in combinatorial approaches. 146

List of Tables

Chapter 3

Table 3.1 List of required materials required for the low-dose, high-dose, and intrastriatal LPS protocols. 95

Chapter 4

Table 4.1 Antibodies, dilutions, suppliers, and catalog numbers used in this work 126

INTRODUCTION

The mammalian brain controls many aspects of an animal's daily life from relatively simple innate autonomic behaviors such as breathing, to more complex behaviors like learning, memory, and reasoning. The ability of the brain to control such a wide array of tasks and functions is, in part, related to its incredible cell diversity. How this diversity comes to be during development has been intensely studied. Here I discuss the development of subtypes of cells within populations and how these differences in development may contribute to their varied responses during injury and disease.

Neuronal heterogeneity

For decades, the study of neural cells and their functions often led to the assumption that these cell types were somewhat homogenous. This simplistic assumption contrasts with our current knowledge that suggest that most areas and circuits of the brain are incredibly diverse, and that this diversity is essential to their ability to process information (Sanes & Reh, 2019). Neurons exhibit remarkable diversity in their functions, morphology, electrophysiological properties, and genetic expression profiles (Sanes & Reh, 2019). Single-cell profiling has further uncovered cell heterogeneity in populations that were once thought to display less complexity (Darmanis et al., 2015). Generally, neurons can be classified into various subtypes based on their neurotransmitter profiles, connectivity patterns, marker expression and functional roles (Sanes & Reh,

2019). This heterogeneity is critical for the brain's ability to process information, form memories, and execute complex behaviors.

Neurogenesis and specification

To exemplify how this diversity arises during development, we will focus on one area of the brain, the neocortex. The neocortex is responsible for a wide range of functions that include behavior, motor control, memory, sensory processing, and spatial navigation (Sanes & Reh, 2019). The cortex is a laminated structure organized into 6 layers, comprising various cell types, each with its own subtypes, including glia, inhibitory and excitatory neurons (Sanes & Reh, 2019). Each of these layers has a specific cell makeup and connectivity (Adesnik & Naka, 2018; Sanes & Reh, 2019). The layered organization of the cortex is essential for the flow of information. For example, sensory information typically enters the cortex from the thalamus at layer IV, which is densely populated with stellate neurons. These stellate neurons then distribute the sensory input to other cortical layers for further processing.

The development of the mammalian cerebral cortex is a highly orchestrated process involving the generation, migration, and differentiation of neurons and macroglial cells (Sanes & Reh, 2019). Neurogenesis of glutamatergic pyramidal neurons in the developing mouse cortex begins with the proliferation of neural progenitor cells (NPCs) in the ventricular zone (VZ) and subventricular zone (SVZ) (Sanes & Reh, 2019). NPCs undergo asymmetric divisions to produce intermediate progenitor cells (IPCs) and post-mitotic

neurons (Sanes & Reh, 2019). A type of NPC, radial glial cells (RGCs), serve as both progenitors and scaffolding for newly born neurons (Sanes & Reh, 2019). Newborn glutamatergic neurons migrate radially from the ventricular zone along the radial glial scaffold to their destination within the cortical plate (Sanes & Reh, 2019). Specification of glutamatergic neurons in the cortex begins at cell division from NPCs in the VZ (Tropepe et al., 2001). Subpopulations are specified through asymmetric division, internal, and external cues (Tropepe et al., 2001).

As mentioned above, the cortex is organized into 6 layers. The layers form in an inside first, outside last manner. That is, the deepest layers from first and the more superficial layers are born last. Layer VI is the deepest and first formed layer and the other layers follow VI in development, apart from layer I. Layer formation and neuron identity within these layers is partially dependent on when neurons are born in development. Interestingly, layer identity seems to be a function of a progressive loss of multipotency that is the result of changing expression profiles for the progenitors (Desai & McConnell, 2000). For example, neurons born during layer III formation will go on to form layer III neurons and neurons born during layer IV will go on to form layer IV neurons (Desai & McConnell, 2000). Transplant studies have shown that as cortical development progresses the ability of progenitors to produce neurons of any layer decreases over time (Desai & McConnell, 2000). For example, when layer IV progenitors are transplanted to layer III they will produce layer III neurons, but when layer IV progenitors are transplanted to layer VI they will retain their layer IV identity

(Desai & McConnell, 2000). Single cell RNA sequencing (scRNA seq) is a recent advancement that has revolutionized our ability to detect neural cell subtypes (Tang et al., 2009). One study using scRNA seq has identified at least 56 pyramidal neuron subtypes within the cortex (Tasic et al., 2018). This same group connected specific subtypes in layer V of the motor cortex to specific roles in movement preparation using combinatorial methods (Economo et al., 2018). Here we see how timing of birth from progenitors can contribute to subpopulations (layers) of glutamateric neurons within the cortex.

Glutamateric neurons born from the SVZ are not the only subpopulations of neurons within the cortex. One subpopulation of neurons known as GABAeric neurons, or inhibitory interneurons, are born from progenitors in the Medial- and Caudal-Ganglionic Eminences (MGE and CGE, respectively) and travel tangentially in the intermediate zone (IZ) to the cortex where they then travel radially along RGCs to their final layer position (S. A. Anderson et al., 1997; Nakajima, 2007; Tamamaki et al., 1997). The MGE is the primary source for cortical parvalbumin- and somatostatin-containing GABAeric interneurons (S. J. B. Butt et al., 2005; Valcanis & Tan, 2003; Wichterle et al., 2001; Q. Xu et al., 2004). Other interneurons, known as vasoactive intestinal polypeptide- and calretinin-containing interneurons and originate from the caudal ganglionic eminence (CGE) (S. J. B. Butt et al., 2005; López-Bendito et al., 2004; Miyoshi et al., 2010; Q. Xu et al., 2004). Interneurons from the ganglionic eminences primarily migrate to the layer that was being formed at the time they were born

(Miyoshi et al., 2007, 2010). Heterochronic experiments show that these interneurons are specified before they migrate to their cortical layer (Valcanis & Tan, 2003). Here we see that the location of birth and origin progenitors contribute to subpopulations of interneurons within the cortex.

The subtypes of glutamateric and interneurons are not only specified by progenitor and temporal origins but also have regional identities specified by morphogen gradients across the cortex (Molyneaux et al., 2007; Sanes & Reh, 2019). For example, positional cell type markers were used to show regionalization of the cortex is affected in individual knockouts of *Emx1, Emx2,* and *Pax6* (Bishop et al., 2002). Other studies have shown that Shh, BMPs, Wnts, and FGFs are other morphogens that control regional cortex formation (Moore & Iulianella, 2021).

Astrocyte development and diversity

Astrocytes are a type of glial cell which have traditionally been viewed as only having support functions for neurons but are now recognized as having active roles in modulating neural circuits and maintaining brain homeostasis (Matyash & Kettenmann, 2010). These active roles are played by many astrocytic subtypes and this diversity in the astrocytes of healthy tissue is evident across different brain regions as they display distinct functional properties and molecular signatures (Laug et al., 2018). The diversity of their functional properties and molecular signatures begins at development.

Cortical astrocyte production begins following the production of cortical neurons. At this time a switch to gliogenesis begins in ventricular NSCs and they now begin to produce astrocyte and oligodendrocyte precursors (Gallo & Deneen, 2014). This switch is characterized by inhibition of neurogenesis and a shift towards gliogenic fates, also known as the gliogenic switch. During the gliogenic switch expression of neurogenic genes is suppressed and gliogenic genes are now permitted to express. Many pathways are involved in neurogenesis inhibition with Notch signaling being one of the best characterized (Gaiano et al., 2000). Neuronal fate is suppressed through expression of delta like 1 and jagged 1 that act as notch receptor activators for neighboring NSCs (Namihira et al., 2009). When the notch receptor is activated by jagged and delta, the notch intracellular domain (NICD) translocates to the nucleus and interacts with the recombining binding protein Suppressor Of Hairless (RPB-J) (Namihira et al., 2009). This then leads to the remodeling of chromatin structures, DNA methylation of neurogenic genes, and demethylation of astrocytic genes allowing for astrocytic transcription (Sanosaka et al., 2017). Notch signaling is considered to be permissive in this case because it does not induce expression of glial genes, but rather suppresses neuronal (Deneen et al., 2006).

One initial point of astrocytic diversity is there are multiple sources of astrocytes in the brain: neural progenitors (NP) in the SVZ, RGCs in the VZ, and self-replication (Ge & Jia, 2016; Hasel et al., 2021; Lee et al., 2022). In mice RGCs and NPs give rise to astrocytes beginning around E16 and continues

postnatally until about P3 (Su Akdemir et al., 2020). The proliferative phase generates most adult astrocytes and because these locally produced astrocytes are in different environments this makes it unlikely that their developmental progression is the same as their parent cells (Ge & Jia, 2016). During this proliferative stage lineage tracing studies also suggest that these locally proliferating astrocytes can also produce at least 3 subtypes (Clavreul et al., 2019). Astrocytes can broadly be classified by their morphology as protoplasmic or fibrous but there is a spectrum of these two morphologies (Matyash & Kettenmann, 2010; Retzius, 1894). Protoplasmic astrocytes are found in grey matter and have a large volume that is the result of their many fine and branching processes (Reichenbach & Wolburg, 2005). Fibrous astrocytes are found in white matter and have less volume and branching than their grey matter counterparts (Reichenbach & Wolburg, 2005). Interestingly, Olig2 seems to be important in the formation of fibrous astrocytes, but not protoplasmic (Cai et al., 2007). Other studies have further divided astrocytes into many more subtypes based on co-staining of GFAP and other markers, specific functional features and expression analyses (Ben Haim & Rowitch, 2016; Chai et al., 2017; Emsley & Macklis, 2006; Endo et al., 2022). Even within the cortex, astrocytes seem to display regional specialization based on expression profiles (Bayraktar et al., 2020). In fact, astrocytes are so diverse there does not exist any single marker that labels all astrocytes and not any other cell type, though some like Aldh1l1 and GLAST do come close (Beyer et al., 2021; Perego et al., 2000; Regan et al., 2007).

One of the prominent functional differences seen in subtypes of astrocytes is in gap junction numbers, coupling, and composition. For example, astrocytes in the cortex have many gap junction couplings while white matter astrocytes have very little (B. Haas et al., 2006). These couplings differ across cortical layers as the superficial layers have more elongated and transvers connections while deeper layers have more circular shaped couplings (B. Haas et al., 2006). Gap junction coupling groups also differ within the hippocampus. The center of the stratum radiatum has circular couplings while areas closer to the pyramidal cell layer have a more elongated pattern that are parallel to the pyramidal cell layer (Houades et al., 2006, 2008). Another difference found within astrocytic gap junctions is differences in the connexins used to form them. Proportions of connexin 43 and connexin 30 are higher in barrel fields and lower in between fields (Houades et al., 2006).

Given the diversity in gap junction coupling it is unsurprising that astrocytes also vary in their membrane currents. For example, astrocytes in the hippocampus and spinal cord have at least 4 subpopulations based on their membrane currents and the currents of Bergmann glia change as development progresses (Müller et al., 1994; Pastor et al., 1995; Steinhaüser et al., 1992). In comparison to neurons, astrocytes have a hyperpolarized resting membrane potential, though the typical resting membrane potential of any given astrocyte varies depending on its location in the brain (Du et al., 2016). For example, astrocytes in the deeper layers of the cortex typically rest at about -85mV, while

those seen at the optic nerve are around -62mV (A. M. Butt & Jennings, 1994; Mishima & Hirase, 2010). This heterogeneity in resting membrane potential is also seen within regions such as the hippocampus where some astrocytes have a resting membrane potential of around -80mV and others closer to -90mV (Deemyad et al., 2018; Mishima & Hirase, 2010; Zhong et al., 2016). A more negative resting membrane potential is linked to the ability to buffer K^+ and neurotransmitter reuptake and this may be reflective of the needs of the area where these astrocytes are located (Ryoo & Park, 2016; Zhong et al., 2016).

K^+ buffering is one of the key functions of astrocytes (Beckner, 2020). Astrocytes regulate extracellular concentrations of K^+ via different types of K^+ permeable channels and redistribute ion concentrations through gap junctions (Beckner, 2020). The most common and highly expressed of the inward rectifying K^+ channels in astrocytes is $K_{ir}4.1$ (Beckner, 2020). Unsurprisingly, expression of $K_{ir}4.1$ varies across the CNS in astrocytes (Beckner, 2020). Expression of Kir4.1 in astrocytes of the spinal cord is higher in the ventral horn than in the dorsal horn which implies differences in their ability for potassium clearance (Olsen et al., 2007). Kir4.1 levels seem to vary in the cortical layers as well (Higashi et al., 2001). K^+ buffering also changes throughout development and can be seen in BGCs over development. Early postnatal BGCs are characterized by delayed inward- and outward-rectifying K^+ currents while later BGCs are characterized as having large voltage and time-independent currents (Müller et al., 1994).

Ca^{2+} signaling is another feature of astrocytes that varies across the CNS. There are two distinct forms of calcium waves; spontaneous oscillations and coordinated waves (Scemes & Giaume, 2006). Astrocytes in the somatosensory cortex of rats have layer-specific oscillations of calcium waves (Takata & Hirase, 2008). Additionally, astrocytes in the hippocampus have been found to have Ca^{2+} channels while BGC are not known to have any (Duffy & MacVicar, 1994; Fraser et al., 1995). Interestingly, cortical Ca^{2+} waves primarily depend on gap junctions, however in the striatum there are few gap junctions so Ca^{2+} waves there are dependent on ATP release (J. S. Haas et al., 2006; Schipke et al., 2002).

Astrocytes are key regulators of extracellular glutamate in the CNS. They primarily do this with the reuptake glutamate transporters GLAST and GLT-1. Reuptake of glutamate by astrocytes allows them to recycle it into glutamine to be transported to the synaptic cleft where neurons can take it up and synthesize it into glutamate once again (Cuellar-Santoyo et al., 2023). Astrocytic GLT-1 is found to be present in about 10-fold lower amounts in the spinal cord than in the brain (Regan et al., 2007). Additionally, GLAST is found to be upregulated during development in RGCs, but downregulated in adult RGCs (Regan et al., 2007).

Astrocyte heterogeneity in disease

During inflammatory insults to the brain, healthy astrocytes can change their morphology, gene expression, and functions (M. A. Anderson et al., 2014; Li et al., 2019). Astrocytes that undergo these changes are known as reactive

astrocytes (RAs) (Escartin et al., 2021). RA responses can vary across disease state, location in the brain, and proximity to the insult (M. A. Anderson et al., 2014). The diversity of astrocytes during development likely contributes to their heterogeneity in disease. Factors such as disease type, proximity to the lesion, and disease stage can all influence astrocyte behavior and function (M. A. Anderson et al., 2014; Moulson et al., 2021; Okuda, 2018). Reactive astrocytes (RAs) play critical roles in the progression of various neurological disorders and our understanding of their heterogeneity and specific roles in disease progression remains limited and is still under investigation.

RAs undergo morphological, transcriptional, and functional changes in response to injury and disease (M. A. Anderson et al., 2014; Burda & Sofroniew, 2014; Sofroniew & Vinters, 2010). RAs are known to exhibit both protective and detrimental effects depending on inflammatory and disease context (M. A. Anderson et al., 2014). They may support neuronal survival and tissue repair by releasing neurotrophic factors and clearing debris, but they can also contribute to inflammation and neurodegeneration by releasing pro-inflammatory cytokines and/or reactive oxygen species (Cameron et al., 2024; Linnerbauer & Rothhammer, 2020; Reid & Kuipers, 2021; K. Yang et al., 2024). The balance between these opposing roles likely depends on the specific astrocyte subtypes involved and their interactions with other cell types in the injured or diseased brain.

The late Ban Barres' laboratory was one of the earliest research groups to use RNA sequencing to examine RAs under ischemic stroke or systemic LPS (Zamanian et al., 2012). They found similarities in gene expression of RAs between both, but several differences as well. These suggest heterogeneity in RA responses between neuroinflammatory models. Importantly, this study identified *Lipocalin 2* (*Lcn2*) as a potential marker for reactivity in both models (Zamanian et al., 2012). In chapter 2, we describe the in-depth characterization of a newly generated mouse line that uses the endogenous *Lcn2* promoter as a driver for Cre recombinase (Agnew-Svoboda et al., 2022). This *Lcn2CreERT2* line labels a subset of RAs across many neuroinflammatory models (Agnew-Svoboda et al., 2022).

Another notable example of heterogenous RA responses can be seen in RA volume regulation in response to ischemic stroke. One subpopulation was found to have large volume increases and membrane depolarization 20 minutes after ischemic stroke while another subpopulation was found to have a small volume increase and small membrane potential change (Benesova et al., 2009). These changes are likely the result of differences in GFAP and $K_{ir}4.1$ levels (Benesova et al., 2009).

Another varied response by astrocytes is proliferation. In spinal cord or optic nerve crush injuries only a subpopulation of astrocytes proliferates (Cameron et al., 2024; T. Yang et al., 2020). One group identified 2 subpopulations of complement 3^+ (C3) "neurotoxic" astrocytes and 6

subpopulations of “neuroprotective” astrocytes (Cameron et al., 2024). Of the subpopulations identified, a small number was $C3^+$ and another larger subpopulation was $C3^-$ (Cameron et al., 2024). Complement 3 is often used to define neurotoxic RAs, however the field is moving away from the simple categorization of harmful vs beneficial as this does not fully encompass the wide range of responses from RAs and often leads to the wrong assumption that astrocytic responses are binary. Regardless of this, it is clear that C3 expression defines a subset of RAs in models of neuroinflammation.

Spatial transcriptomics have revealed that astrocytes in different areas of the brain overall experience different upregulation of “modules” of genes previously defined as clusters in scRNA data (Hasel et al., 2021). This study also found 9 subpopulations during systemic LPS challenge and found expression of DEGs in these clusters changed over time (Hasel et al., 2021). Additionally, some clusters identified in healthy tissue were also identified as clusters in LPS treated astrocytes with upregulation of inflammatory genes, showing that RAs do not lose their “healthy” subpopulation identity (Hasel et al., 2021).

Targeting specific cell types and subpopulations to understand development and disease

Understanding the development and progression of injury and disease in the brain requires precise tools capable of targeting specific cell types within the brain. Recent advances in single-cell RNA sequencing and spatial

transcriptomics have revealed distinct transcriptional profiles, owing to the extensive diversity of neuronal subtypes (Adesnik & Naka, 2018; Darmanis et al., 2015; Molyneaux et al., 2007; Sanes & Reh, 2019; Tropepe et al., 2001). These methods have revealed the extent of neural heterogeneity and now we need ways to specifically target and manipulate these newfound subpopulations. Neural subpopulations are often defined by expression of more than one identifier, or these identifiers are expressed by more than one cell type making it difficult to isolate them with traditional genetic approaches. Combinatorial approaches are one way to overcome this limitation.

Early developmental lineage tracing strategies used vital dyes or direct observation (Keizer et al., 1983; Sulston et al., 1983). From there, fluorescent proteins were discovered and specific cell targeting became easier. (Luskin et al., 1988). After the discovery of Cre and recombinases and its first use in mammalian cell lines, the ability to lineage trace and target cell types became more accessible (Sauer, 1987, 2006; Sauer & Henderson, 1988). The further introduction of tamoxifen inducible recombinases allowed for even greater control of the timing at which Cre is active (Feil et al., 1997). However, this level of control, normally based on expression from a single promoter might be insufficient to target highly specialized subsets of cells. For example, a recent study found that a subset of dopaminergic neurons rich in *RIT2* are more vulnerable to Parkinson's disease pathogenesis (Wang et al., 2024). These subtypes could become targets for future gene therapies (Man et al., 2018).

Genetic combinatorial strategies are increasingly being utilized to specifically target subpopulations of neural cells and perform fate-mapping studies (Matho et al., 2021). Strategies using viral delivery can further enhance these types of approaches and are also currently being utilized to identify monosynaptic inputs from more than one area of the brain, label subtypes of neurons, and manipulate their activity (Kitanishi et al., 2022; Ubina et al., 2021; J. Xu et al., 2022). Viral tools using Boolean logic operations are increasingly being designed (Fenno et al., 2020; Hughes et al., 2024; Ubina et al., 2021). More recent tools have even combined the use of 5 different ribozymes in combination with recombinases that allow for even greater specificity (Hughes et al., 2024).

The brain's capacity to regulate a diverse range of behaviors and functions is intimately linked to its incredible cell diversity. This extensive heterogeneity of neural cell types arises from complex developmental processes and influences cell behavior in the healthy brain, but also during injury or disease. As we uncover this heterogeneity, design and generation of new types of tools and combinatorial strategies to target subpopulations of cells is becoming increasingly important. With this in mind, in chapter 1 we designed an adeno associated virus-based tool that uses Boolean exclusion to drive expression in neurons. In chapter 2, we describe the generation of the *Lcn2CreERT2* mouse line which labels a subset of RAs and show that these labeled RAs remain in the brain after the resolution of inflammation and largely return to their pre-inflammatory state after systemic LPS. In chapter 3, we provide detailed

protocols for the induction of neuroinflammation in the *Lcn2CreERT2* line. Finally, in chapter 4 we describe the generation and use of the *Complement 3-FlpOER^{T2}* (*C3-FlpOER^{T2}*) line for labeling a subset of RAs in various neuroinflammatory models. We also show that *C3-FlpOER^{T2}* labeled RAs are not proliferative and are labeled during direct insults to the brain.

CHAPTER ONE

ExBoX – a simple Boolean exclusion strategy to drive expression in neurons

Teresa Ubina[1,2], Tyler Vahedi-Hunter[1,2], William Agnew-Svoboda[1,2], Wenny Wong[1,2], Akshay Gupta[1,2], Vijayalakshmi Santhakumar[1,2], Martin M. Riccomagno[1,2]

[1] Neuroscience Graduate Program, University of California, Riverside, Riverside, CA 92521, USA
[2] Department of Molecular, Cell, and Systems Biology, University of California, Riverside, Riverside, CA 92521, USA

Published in final edited form as:

Teresa Ubina*, Tyler Vahedi-Hunter*, Will Agnew-Svoboda, Wenny Wong, Akshay Gupta, Vijayalakshmi Santhakumar, Martin M. Riccomagno; ExBoX – a simple Boolean exclusion strategy to drive expression in neurons. *J Cell Sci* 15 October 2021; 134 (20): jcs257212. doi: https://doi.org/10.1242/jcs.257212

*Authors contributed equally to this work.

Abstract

The heterogeneity and complexity of cell populations has been increasingly revealed by modern single-cell techniques. This increased complexity has made intersectional genetic approaches more vital to the investigation of cellular heterogeneity. In this work we establish a simple adeno-associated virus (AAV)-based approach to identify cell subpopulations by Boolean exclusion logic (AND NOT). The Expression by Boolean exclusion (ExBoX) system encodes a gene of interest (GOI) turned on by one recombinase (Cre or FlpO) and turned off by the other one. In use, ExBoX allows for transcription of a GOI in only the cells that contain the activating recombinase, but not in cells expressing both the activating and deactivating recombinases (AND NOT). The ExBoX system can tightly regulate expression of fluorescent reporters both *in vitro* and *in vivo*. The simple strategy and ease of use of ExBoX expands on the molecular tools available for not only cell-specific, but also temporal gene expression in various systems.

Introduction

The development of new genetic tools is critical to advancing our knowledge of biological processes. One critical genetic tool developed in mammals was the discovery and use of homologous recombination to generate loss-of-function alleles in mice (Capecchi, 1989). The discovery and utilization of recombinases as genetically encoded tools to conditionally target genetic alleles then made it possible to control genetic deletion in a tissue-specific way (Gu et al., 1994; Tsien et al., 1996). Recombinase-dependent systems, region-specific gene knockouts, and progenitor tracing are now all routine strategies used in mouse genetics (Branda and Dymecki, 2004).

Single-cell profiling has uncovered the complexity and heterogeneity of cell populations and reshaped how we view some organs (Darmanis et al., 2015). The ability to study cellular complexity is limited by the tools available to manipulate cells with increased specificity. Expansion of the existing tissue- and population-specific recombinase lines is one way to overcome this, however this would require the generation and characterization of each transgenic recombinase mouse line for each new cell population. Taking advantage of existing transgenic lines by incorporating genetically encoded intersectional approaches could be a complementary alternative to the generation of new transgenic lines (Awatramani et al., 2003). Intersectional approaches provide more specificity by selection of targets based on their overlapping or sequential

expression of different recombinases (Andersson-Rolf et al., 2017; Jensen and Dymecki, 2014; Robles-Oteiza et al., 2015). Intersectional strategies using the expression of two recombinase systems (Cre/lox and Flp/FRT) were first used in fate-mapping of neural progenitors which were previously difficult to track (Dymecki et al., 2010). These strategies are capable of targeting subpopulations and can do so with a variety of Boolean logic operations (AND, NOT, OR) (Daigle et al., 2019; Plummer et al., 2015). Using intersectional and subtractive strategies with multiple recombinase systems allows for specific targeting of subpopulations of cells (Farago et al., 2006).

The use of genetically encoded strategies has advantages over surgical delivery of viral expression systems in that it is non-invasive and has broad applicability for difficult to access tissues or during embryonic stages (Jensen and Dymecki, 2014). However, utilization of viral vectors is an alternative method to drive conditional and intersectional expression: Their power resides in the ease of generation and the regional control of expression by selecting the time and location of injection (Schnütgen et al., 2003; Atasoy et al., 2008; Gradinaru et al., 2010; Fenno et al., 2014; Zhang et al., 2007; Sternson et al., 2016). Many versions of recombinase-dependent AAVs now exist and more recently intersectional versions have been created (Atasoy et al., 2008; Saunders et al., 2012; Xue et al., 2014; Kakava-Georgiadou et al., 2019; Fenno et al., 2014; Fan et al., 2020). Understanding molecular diversity of cell populations and any

phenotypic differences they may be responsible for will undoubtedly benefit from combining viral and genetically encoded approaches.

The use of intersectional approaches is not only useful in parsing out functional diversity but can also be used in developmental biology to turn on and off expression of genes of interest during critical periods or developmental windows (Wiesel and Hubel, 1963; Kozorovitskiy et al., 2012). Using Boolean exclusion with intersectional approaches is one way to address this need. Expression of a GOI could be turned on by one recombinase at one time point and expression of this same GOI could be turned off at a later time (AND NOT) by a different recombinase. Some AAV-driven intersectional systems do exist, however they have some limitations in that they are long and intricate in design which somewhat restricts their use (Fenno et al., 2014). We set out to create a tool capable of controlling expression and labeling subsets of cells with more specificity using Cre and Flp recombinases that follow Boolean exclusion logic (called ‘expression by Boolean exclusion’ or ExBoX).

We first generated the CreOn-FlpOff version of this system (CreOn-FlpOff). CreOn-FlpOff contains a cassette with a coding sequence (CDS) of interest in-frame with a hemagglutinin tag (HA), P2A site, and an EGFP fluorescent reporter all inverted with respect to the promoter. In the CreOn-FlpOff vector, the expression of a coding sequence is turned on by Cre recombinase and expression is abolished by Flp recombinase. The human synapsin I promoter was chosen for these experiments because it is a well characterized

postmitotic neuronal promoter (Glover et al., 2002). Each side of the CreOn-FlpOff inverted cassette contains Frt sites and double-lox sites (lox2722 and loxP) in inverse orientation (DIO) (Schnütgen et al., 2003) (Fig. 1.1A). When Cre-mediated recombination occurs and HA-tagged CDS and EGFP are flipped into the forward orientation and robust Cre-dependent expression of the CDS and EGFP in neurons occurs. To turn off this expression, Flp-mediated recombination causes removal of the cassette and EGFP expression is abolished (Fig. 1.1A). The orientation of the recombination sites allows the CDS to be expressed in the presence of Cre AND NOT Flp.

We then designed a sister system called FlpOn-CreOff in which Flp is the activating recombinase and Cre is the deactivating recombinase. FlpOn-CreOff is designed similarly to CreOn-FlpOff except the expression cassette contains a tdTomato fluorescent reporter and is floxed by lox2722 sites and a Flp DIO switch (fDIO or fFLEX) with F14 and Frt sites (Xue et al., 2014) (Fig. 1.1B). In the FlpOn-CreOff system, Flp-mediated recombination results in expression of the CDS and tdTomato reporter, and Cre-mediated recombination excises the entire cassette resulting in abolished expression of the CDS and tdTomato (Fig. 1.1B). In FlpOn-CreOff, CDS expression would only occur when Flp is present AND NOT Cre.

This work describes the design and characterization of a system that uses Boolean exclusion logic driven by a single AAV. This system uses vectors that are simpler and shorter in length which allows for expression of longer GOIs. In

this work we validate the ExBoX system in neuronal populations and generate several ExBoX vectors for regulating neuronal activity *in vivo*.

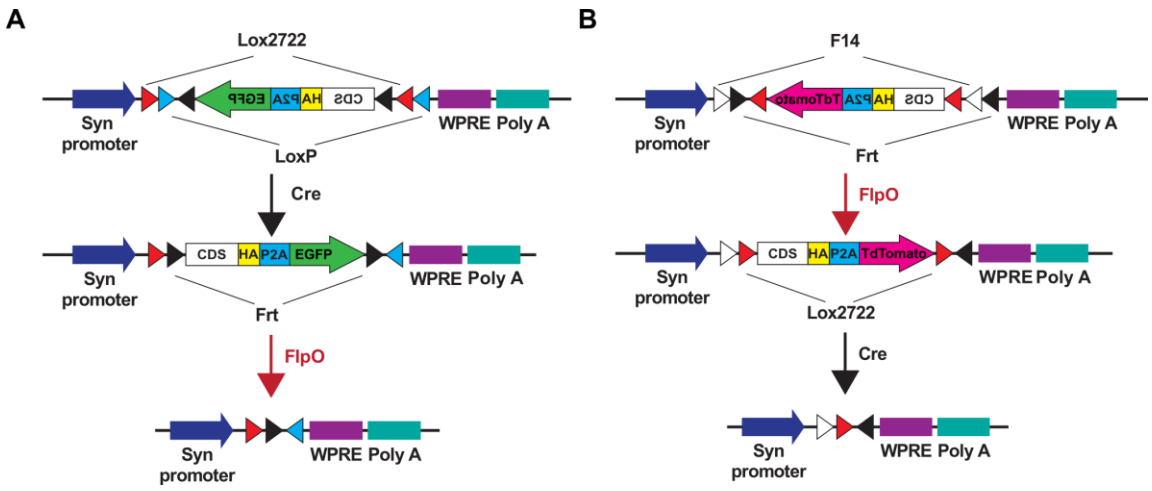


Figure 1.1: Design for CreOnFlpOff and FlpOnCreOff constructs. (A) Schematic representation of the CreOn-FlpOff construct. It is composed of an inverted expression cassette encoding for a coding sequence (CDS) fused to an HA tag, a P2A site and EGFP, which is flanked by Frt, lox2722 and loxP sites. Presence of Cre recombinase results in inversion of the cassette and expression. Presence of FlpO results in removal of the cassette. **(B)** Schematic representation of the FlpOn-CreOff construct. The inverted expression cassette is flanked by lox2722, F14 and Frt sites. Presence of Flp recombinase results in inversion of the cassette and expression. Presence of Cre results in removal of the cassette.

Materials and Methods

Animals

The ICR mouse strain was purchased from Taconic Biosciences. The *Grik4-Cre* transgenic mouse strain was purchased from The Jackson Laboratory. Generation of the *Grik4-cre* transgenic mouse line has been described previously (Nakazawa et al., 2002). Mice were housed in a controlled environment maintained at approximately 22°C on a 12hr light–12hr dark cycle. Mouse chow and water were provided ad libitum. The day of vaginal plug observation was designated as embryonic day 0.5 (E0.5), and the day of birth as postnatal day 0

(P0). For *in vivo* experiments where n=3 at least one female and one male were tested. For n=5, at least 2 males and 2 females were tested. No overt differences in expression of ExBoX constructs were observed between males and females. All animal procedures presented were performed according to the University of California Riverside's Institutional Animal Care and Use Committee (IACUC) guidelines and approved by UC Riverside IACUC.

Viral constructs

The CreOn-FlpOff and FlpOn-CreOff ExBoX viral constructs were designed using ApE (https://jorgensen.biology.utah.edu/wayned/ape/) and Vector Builder (https://en.vectorbuilder.com/) free software. The plasmids were synthesized and assembled by Vector Builder. Plasmid DNA was purified using the Qiagen Maxi Prep kit (Qiagen Cat#10023). AAVs were also packaged by Vector Builder into AAV2/9. pENN.AAV.CamKII 0.4. Cre. SV40 (AAV5) (deposited by James M. Wilson; Addgene #105558; RRID:Addgene_105558), pAAV-CAG-tdTomato (AAV5) (deposited by Edward Boyden; Addgene #59462; RRID:Addgene_59462) and pCAG-FLEX-EGFP-WPRE (AAV9) (deposited by Hongkui Zeng; Addgene #51502;; RRID:Addgene_51502) were obtained from Addgene (Oh et al., 2014). rAAV5/AAV-EF1α-FlpO-WPRE and rAAV9/CAG-GFP were obtained from the UNC GTC Vector Core. pENN.AAV.hSyn.Cre.hGH was Addgene #105555 (RRID:Addgene_105555) deposited by James M. Wilson. All the ExBoX constructs designed for this study, along with the maps and sequences, have been deposited in Addgene.

In utero electroporation

Pregnant ICR mice at E15.5 or E16.5 were anesthetized with isoflurane and an abdominal incision was made to expose the uterus. Pups were visualized through the uterine wall. Plasmids diluted in Fast Green dye and PBS (3µg/µl) were injected through sharpened glass capillary needles into the lateral ventricle; 5mm paddles were used to deliver five 40V (E15.5) or 37V (E16.5) pulses of 50ms each with 950ms intervals across the hemispheres. Uterine horns were repositioned inside the female and the abdominal cavity was filled with 5x penicillin/streptomycin (pen/strep; Gibco cat# 15140-122) in sterile PBS. Pups were collected at E17.5 or postnatally via transcardial perfusion with PBS and 4% paraformaldehyde (PFA) and fixed in 4% PFA for 4 h at 4°C, rinsed with PBS, and sectioned coronally at 150µm on a vibrating microtome (VT100S; Leica). Plasmids were diluted in a 4:1:1 ratio of CreOn-FlpOff-EGFP:pCAG-IRES-Cre:pCAG-IRES-DsRed/pCAG-mCherry-IRES-FlpO or FlpOn-CreOff-tdTomato:pCAG-FlpO:pCAG-EGFP/pCAG-Cre-IRES-GFP. For experiments involving temporal control using tamoxifen-dependent Cre recombinase, the plasmid ratios were 2:1:4:1 of FlpOn-CreOff-tdTomato:pCAG-FlpO:pCAG-ERT2-Cre-ERT2: pCAG-EGFP. For these experiments, pups were birthed and orally gavaged with tamoxifen (Sigma cat# T5648) in corn oil (150µg/g) or corn oil alone daily for 4 days starting at P10 until P13 and tissue collected at P23. Immunohistochemistry was performed as described previously (Polleux and Ghosh, 2002). Nuclei were visualized with DAPI (1µg/ml) and primary antibodies

used were chicken anti-GFP (1:500, Aves Labs Cat# GFP-1010) and rabbit anti-DsRed (1:500, Takara Bio Cat# 632475) with secondary antibodies goat anti-chicken-IgY conjugated to Alexa Fluor 488 (1:1000, Thermo Fisher Scientific Cat# A-11039) and goat anti-rabbit-IgG conjugated to Chromeo 546 (1:1000, Abcam Cat# ab60317). Sections were mounted on glass microscope slides with Fluoro-Gel (Electron Microscopy Sciences Cat# 1798502) and imaged with a laser-scanning confocal microscope (Leica SPEII). Fluorescence signals for both GFP and RFP in Fig. 1.6 have been amplified. The fluorescent signals for GFP and RFP in Fig. 1.5C, 1.6A are unamplified and only DAPI was added to visualize nuclei.

Neuro2A cell culture

Neuro2A cells from the ATCC were maintained in Dulbecco's modified Eagle's medium (DMEM) with pen/strep (Gibco Cat#15140-122) and 10% fetal bovine serum and incubated in 5% CO_2 at 37°C. Cells were visually inspected for contamination daily and routinely tested for Mycoplasma infection using the ATCC Universal Mycoplasma Detection Kit (Cat# 30-1012K). Cells were plated on laminin and poly-D-lysine (8.3 µg/ml) coated 12mm coverslips in a 24-well plate at 7.8×10^4 cells/cm^2. Cells were transfected 24hrs later with Metafectene PRO (Biontex Cat# T040-1.0) according to the manufacturer's suggested protocol with a 1:4 DNA to Metafectene ratio. Plasmid ratios were as follows 4:1:1 ratio of CreOn-FlpOff-EGFP:pCAG-IRES-Cre:pCAG-IRES-DsRed, CreOn-FlpOff-EGFP:pCAG-IRES-Cre:pCAG-mCherry-IRES-FlpO, FlpOn-CreOff-

tdTomato:pCAG-FlpO:pCAG-EGFP, or FlpOn-CreOff-tdTomato:pCAG-FlpO:pCAG-Cre-IRES-GFP. Cells were fixed 48hrs after transfection with 4% PFA for 5 min, rinsed with PBS, stained with DAPI (1µg/ml) for 1hr, then rinsed again three times with PBS for 5 min. Coverslips were mounted with Fluoro-Gel onto a glass slide and examined with confocal microscopy. In experiments where Neuro2A cells were stained for recombinases (Cre 1:500, EMD Millipore cat# MAB3120; Flp 1:500, Origene cat# TA160030; Figs. 1.2, 1.3, and 1.4) the protocol was as described above, except the Triton X-100 concentration was increased to 0.5% for antibody solutions. Secondary antibody used for Cre recombinase was goat anti-mouse-IgG conjugated to Alexa Fluor 647 (1:1000, Life Technologies Cat# A21236) and for Flp recombinase goat anti rabbit-IgG conjugated to Alexa Fluor 647 (1:1000, Invitrogen Cat# A21244). For experiments where tamoxifen was used, Neuro2A cells were plated at a density of 2.1×10^4 cells/cm^2 24hrs before transfection and the plasmid ratio was 4:1:1:1 FlpOn-CreOff-tdTomato:pEF1a-Flp:pCAG-ERT2-Cre-ERT2:pCAG-GFP. 4-hydroxytamoxifen (4OHT; Sigma cat# H7904) in 100% ethanol was added to culture medium to 10µM final concentration or equal volume 100% ethanol for vehicle control 48hrs after transfection and replaced daily for 3 days with fresh 4OHT or vehicle, then replaced with regular medium as needed until they were collected 4 days after the last day of tamoxifen.

Stereotactic and intracerebroventricular injections

Stereotactic injections were performed as described previously (Cetin et al., 2007). Mice were put under anesthesia for the duration of the procedure using isoflurane. P1 intracerebroventricular injections were performed as previously described with AAV-CreOn-FlpOff-EGFP or AAV-FlpOn-CreOff-tdTomato in a 1:1 ratio with their corresponding On recombinase AAV (AAV-hSyn-Cre 2.3×1013 GC/ml or rAAV5/EF1α-FlpO-WPRE 2.6×1012 GC/ml) (Mathiesen et al., 2020; Passini and Wolfe, 2001). In experiments where animals were initially injected at P1 and subsequently injected with Off recombinase into the cortex as adults, 150nl of viral cocktail was injected at the following coordinates: A/P −1.70 mm; M/L ±1.50 mm; D/V, −0.50 mm. Off recombinases (AAV-hSyn-Cre or rAAV5/EF1α-FlpO-WPRE) were injected 1:1 with pAAV-CAG-tdTomato or rAAV9-CAG-GFP. Controls were injected 1:1 with pAAV-CAG-tdTomato or rAAV9-CAG-GFP and sterile PBS to ensure concentration of viral particles was the same. Tissue was collected 3 weeks after the second injection. Mice were perfused and fixed with 4% paraformaldehyde overnight at 4°C, rinsed in 1× PBS, and sectioned coronally on a vibratome (150 μm). Sections were incubated in DAPI and mounted onto slides with Fluoro-Gel fluorescence mounting medium (Electron Microscopy Sciences Cat# 1798502). Expression was observed via confocal microscopy.

Image analysis

Neuro2A and primary cortical neuron image analysis was performed with FIJI (Schindelin et al., 2012). GFP+, RFP+, and Cre+ or Flp+ cells were all manually

counted. The percentage of transfected cells in which recombinase activity resulted in fluorescent reporter (RFP or GFP) expression were calculated as $\frac{\#GFP \text{ or } RFP}{\#positive\ for\ ON\ recombinase} x100$ (Fig. 1.2). The percentage of on cells for Neuro2A transfections for direct fluorescence were calculated as $\frac{\#GFP}{\#transfected} x\ 100$ for CreOn-FlpOff and $\frac{\#RFP}{\#transfected} x\ 100$ for FlpOn-CreOff (Figs. 1.3, 1.4, and 1.5). The datasets in figures 1.2-1.8 were tested for normality with the Shapiro–Wilk test and QQ plot. A one-way ANOVA with Tukey's multiple comparisons test was done for Neuro2A transfections (Fig 1.2).

Images from P1 animals intracerebroventricularly injected with AAV-CreOn-FlpOff plus AAV-hSYN-Cre that were later cortically injected with rAAV5/EF1a-FlpO-WPRE and pAAV-CAG-tdTomato or pAAV-CAG-tdTomato alone (Figs 1.7 and 1.8) were quantified by counting the number of On (tdTomato or GFP positive) cells that overlapped with the fluorescent reporter in the second injection of a 100 µm tall counting area (approximately layer V) that spanned the area of the second injection site and dividing by the number of fluorescent reporter positive cells in the same counting area. For example, CreOn-FlpOff was calculated as $\frac{\#GFP}{\#RFP} x\ 100$. AAV-FlpOn-CreOff images were quantified in the same way $\frac{\#RFP}{\#GFP} x\ 100$. All statistical analyses were performed using GraphPad Prism version 9.2.0 for Windows, GraphPad Software, San Diego, California USA (www.graphpad.com).

Acknowledgements

We would like to thank Drs Edward Zagha and Kevin Wright for critically reading the manuscript and providing helpful comments. We would like to thank the University of North Carolina Chapel Hill Gene Therapy Center Vector Core for packaging of viral constructs.

Author contributions

Conceptualization: M.M.R.; Methodology: T.U., T.V.-H., W.A.-S., A.G., V.S., M.M.R.; Validation: T.U., T.V.-H., A.G.; Formal analysis: T.U., T.V.-H., A.G., M.M.R.; Investigation: T.U., T.V.-H., W.A.-S., A.G., W.W.; Data curation: T.U., T.V.-H., M.M.R.; Writing - original draft: T.U., T.V.-H., M.M.R.; Writing - review & editing: W.A.-S., A.G., W.W., V.S., M.M.R.; Visualization: T.U., T.V.-H., W.A.-S., M.M.R.; Supervision: V.S., M.M.R.; Project administration: V.S., M.M.R.; Funding acquisition: V.S., M.M.R.

Funding

This work was supported by grants from the National Institutes of Health (R21MH118640 and R01NS104026 to M.M.R.; R01NS069861 and R01NS097750 to V.S.) and a Hellman Foundation Fellowship to M.M.R. Open access funding provided by University of California, Riverside. Deposited in PMC for immediate release.

Results

Validation of ExBoX functionality in Neuro2A cells

To test feasibility, we first generated a plasmid containing only EGFP in the cassette of the CreOn-FlpOff system. We transfected the CreOn-FlpOff-EGFP plasmid with pCAG-IRES-Cre, pCAG-mCherry-IRES-FlpO, or both pCAG-IRES-Cre and pCAG-mCherry-IRES-FlpO in Neuro2A cells (Fig. 1.2A). A pCAG-mCherry plasmid was used as a transfection control when pCAG-mCherry-IRES-FlpO was not transfected. When CreOn-FlpOff-EGPF was transfected with the pCAG-mCherry control plasmid alone there was no EGFP expression seen. When CreOn-FlpOff-EGFP was co-transfected with pCAG-IRES-Cre (the activating recombinase), the cassette was inverted and EGFP expression was observed in 95.5±4.2% (mean±SEM, n=3) of Cre positive cells are EGFP positive (Fig. 1.2B). Co-transfecting the CreOn-FlpOff-EGFP plasmid with pCAG-mCherry-IRES-FlpO, or with pCAG-IRES-Cre and pCAG-mCherry-IRES-FlpO, resulted in no EGFP+ cells, which suggests that the FlpO is efficiently turning off reporter expression (Fig. 1.2A,B). Similar results were observed by direct fluorescence when quantifying the EGFP+-to-mCherry+ cell ratio, or by staining for FlpO recombinase (Fig. 1.3). This data suggests that the ExBoX CreOn-FlpOff vector can be manipulated through Boolean exclusion in Neuro2A cells.

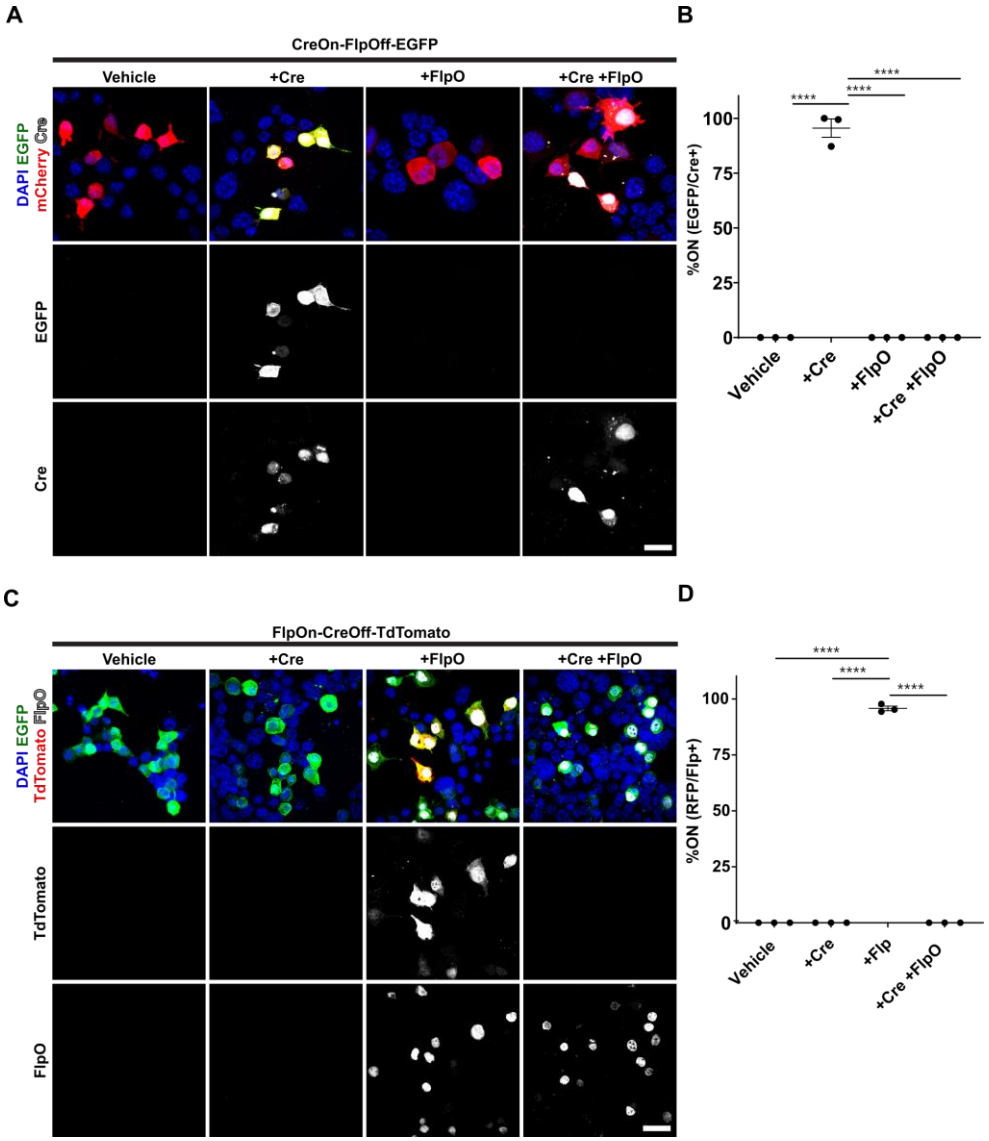


Figure 1.2: Validation of ExBoX in Neuro2A cells. (A) Expression of fluorescent reporter proteins in Neuro2A cells transfected with CreOn-FlpOff-EGFP construct (green) and pCAG-mCherry (red, loading control). Co-transfection with pCAG-Cre plasmid causes inversion of the cassette into the 'on' position and EGFP expression. Co-transfection of pCAG-FlpO deletes the cassette and abolishes EGFP expression. **(B)** Quantification of Neuro2A cell transfections with CreOn-FlpOff-EGFP. Upon transfection with Cre, the CreOn-FlpOff-EGFP construct results in 95.5±4.2% of Cre-positive cells expressing EGFP, while co-transfection with FlpO results in abolishment of EGFP expression. **(C)** Expression of fluorescent reporters in Neuro2A cells transfected with FlpOn-CreOff-tdTomato construct (red) and pCAG-EGFP (green, transfection control) in Neuro2A cells. Co-transfection with pCAG-FlpO causes inversion of the cassette into the 'on' position and tdTomato expression. Transfection with pCAG-Cre removes the cassette and abolishes tdTomato expression. **(D)** Upon transfection with FlpO, the FlpOn-CreOff-tdTomato construct results in detectable expression of reporter in 95.8±1.0% of Flp positive cells, while co-transfection with Cre results in abolishment of tdTomato expression. Values given are mean±SEM. n=3 independent experiments (30–40 cells in each experiment). ****P<0.0001 (one-way ANOVA; Tukey post-hoc test). Scale bar: 30 µm.

Similarly, we generated the FlpOn-CreOff vector that contains only a tdTomato fluorescent reporter. FlpOn-CreOff-tdTomato plasmid was co-transfected with pCAG-Cre-IRES-EGFP, pCAG-FlpO, or both pCAG-Cre-IRES-EGFP and pCAG-FlpO. In the absence of pCAG-Cre-IRES-EGFP, a pCAG-IRES-EGFP plasmid was used as transfection control. When FlpOn-CreOff-tdTomato was co-transfected with pCAG-FlpO, 95.8±1.0% (mean±SEM) of Flp+ cells were positive for tdTomato (Fig. 1.2C,D). No tdTomato-expressing cells were seen when FlpOn-CreOff-tdTomato plasmid was co-transfected with pCAG-Cre-IRES-EGFP alone. Lastly, co-transfecting FlpOn-CreOff-tdTomato with pCAG-Cre-IRES-EGFP and pCAG-FlpO results in no expression of the tdTomato reporter (Fig. 1.2C,D). Similar results were seen with direct fluorescence, and by Cre recombinase immunocytochemistry (Fig. 1.4). These results confirm that Cre can successfully excise the cassette and stop expression even when Flp is present (Fig. 1.2C,D, 1.3). Expression of the FlpO-CreOff construct was only present in the presence of Flp AND NOT Cre.

Complementary published work by us confirmed that expression of both CreOn-FlpOff and FlpOn-CreOff ExBoX are tightly controlled by recombinase co-expression in primary cortical neuron culture, as well as *in vivo* through *in utero* electroporation (IUE) and AAV injection (Ubina et al., 2021).

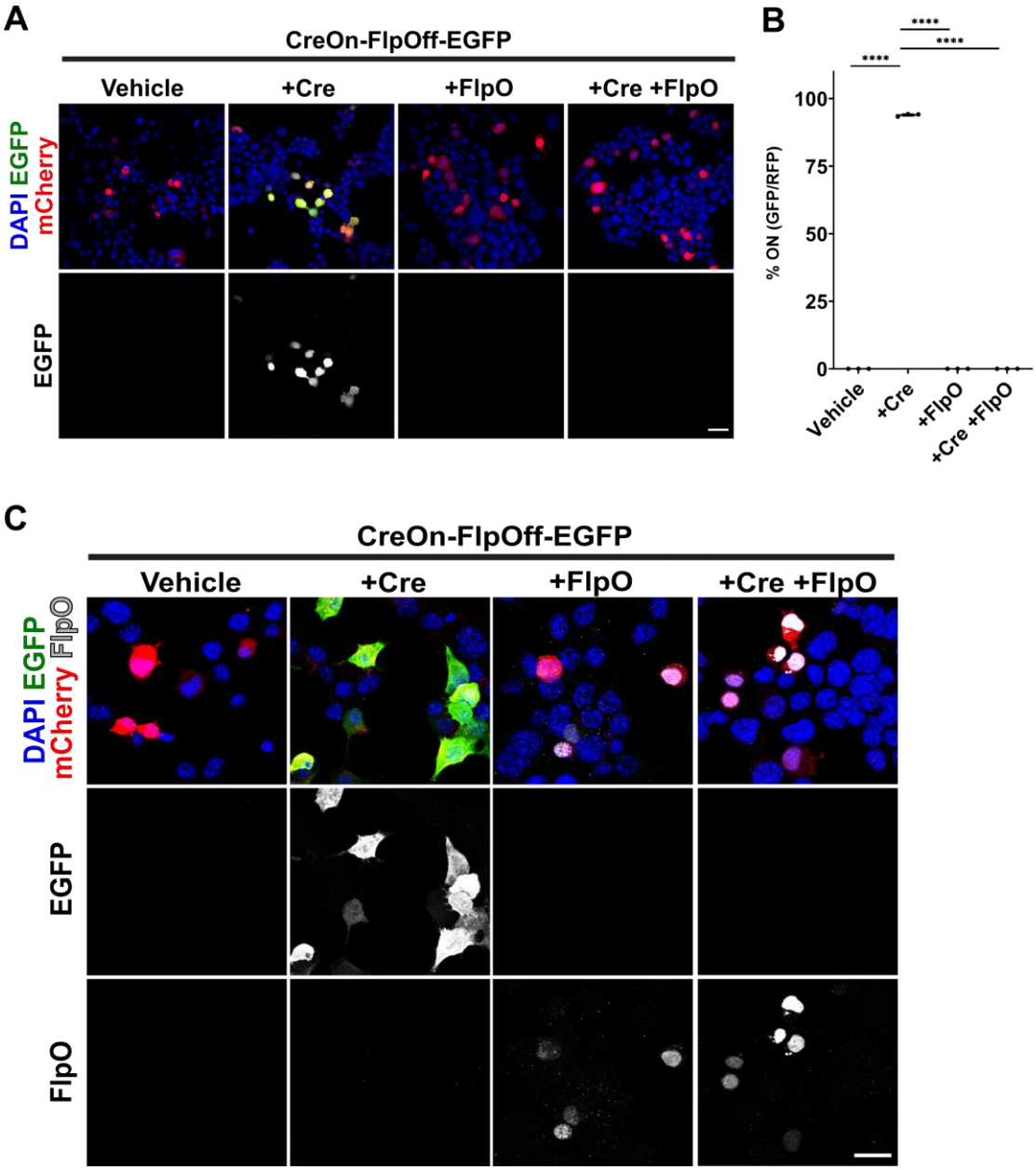


Figure 1.3: Direct fluorescence for CreOn-FlpOff-EGFP in Neuro2A cells and Off recombinase detection. (A) Unamplified images of Neuro2A cell transfection. **(B)** Quantification of unamplified images shows 93.9%±0.3 of cells transfected with Cre expressing EGFP, while co-transfection with FlpO results in abolishment of EGFP expression. N=3 independent experiments, error bars ±SEM. ANOVA $p<0.001$; Tukey post-hoc test ****$p<0.0001$ vs. all other transfections. **(C)** Immunocytochemical staining for the Off recombinase, Flp, reveals no Flp positive cells remaining in the On condition (EGFP expression). Values given are mean±SEM. Scale bars 30 µm.

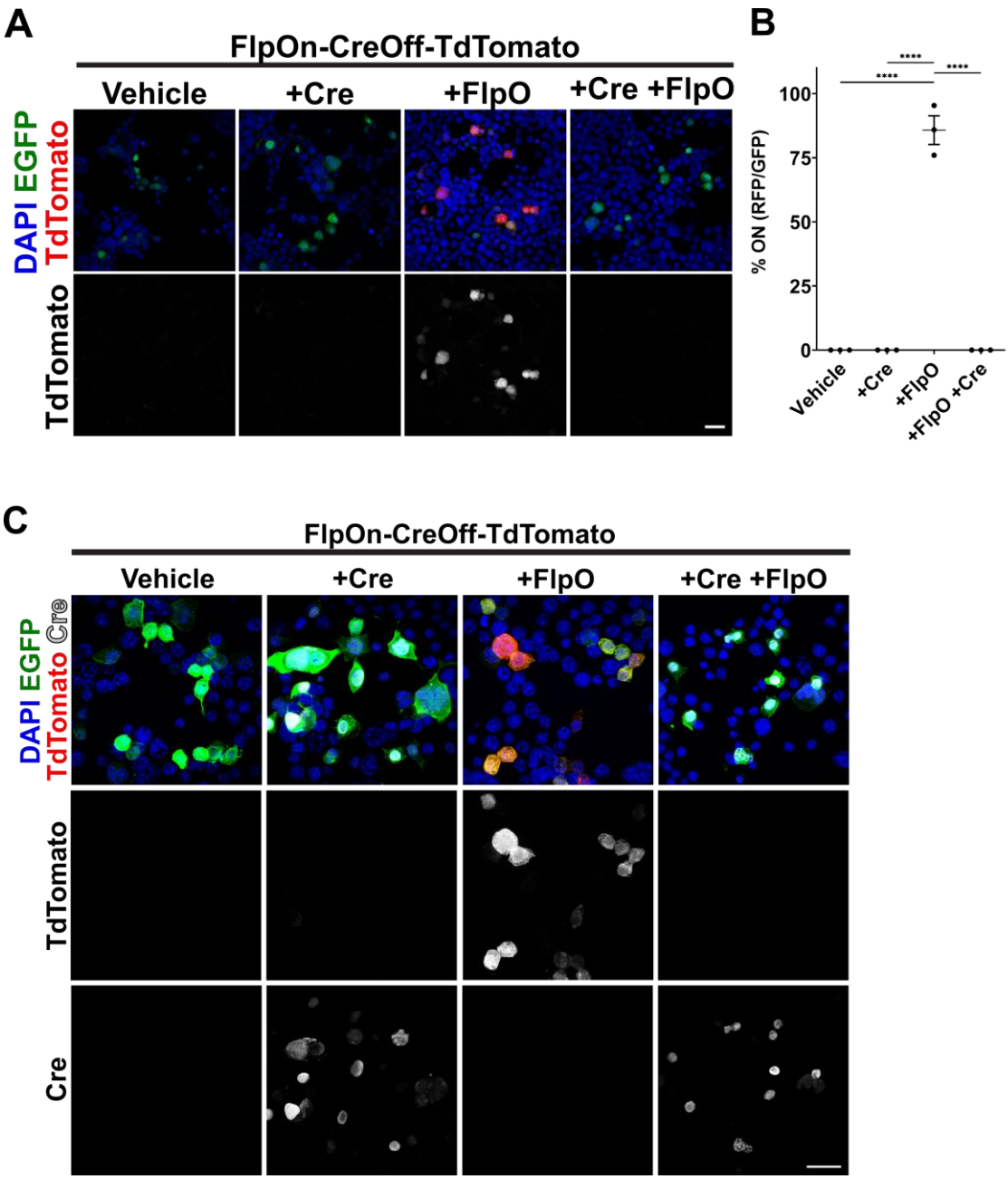


Figure 1.4: Direct fluorescence for FlpOn-CreOff-TdTomato in Neuro2A cells and Off recombinase immunocytochemistry. (A) Unamplified images of Neuro2A cell transfection. (B) Quantification of unamplified images show expression of reporter in 85.8%±5.6 of transfected cells, while co-transfection with Cre-IRES-EGFP results in abolishment of TdTomato expression. N=3 independent experiments, error bars ±SEM. ANOVA $p<0.01$; Tukey post-hoc test ****$p<0.0001$. Scale bar 30μm. **(C)** Immunocytochemical staining for Cre recombinase reveals no Cre positive cells expressing TdTomato (On condition). Values given are mean±SEM. Scale bar 30 μm.

Temporal and spatial control of expression using ExBoX

So far our data suggest that the ExBoX system can be used to efficiently control expression of multiple genes of interest in a Cre- and Flp-dependent manner through AND NOT Boolean operations. Thus, this system has the potential to be a powerful tool to control expression temporally and spatially (Fig. 1.5A,B). To test the usefulness of the ExBoX vectors for temporal control of expression, we established a simple *in vitro* paradigm. Neuro2A cells were transfected with FlpOn-CreOff-tdTomato, pCAG-FlpO, pCAG-ERT2-Cre-ERT2, and pCAG-EGFP (Matsuda and Cepko, 2007). 48hrs after transfection cells were treated with 4-hydroxytamoxifen (4OHT) or vehicle for 3 days in culture and collected for analysis four days later. Before treatment 87.7±1.7% (mean±SEM) of transfected cells were tdTomato positive (On condition) (Fig. 1.5C,D). In vehicle-treated cultures 96.1±1.8% of transfected cells were positive for tdTomato, while only 3.2±1.0% of 4OHT-treated EGFP+ cells remained tdTomato positive, a highly significant decrease (Fig. 1.5C,D). These results show robust temporal control of ExBoX-driven expression in Neuro2A cells.

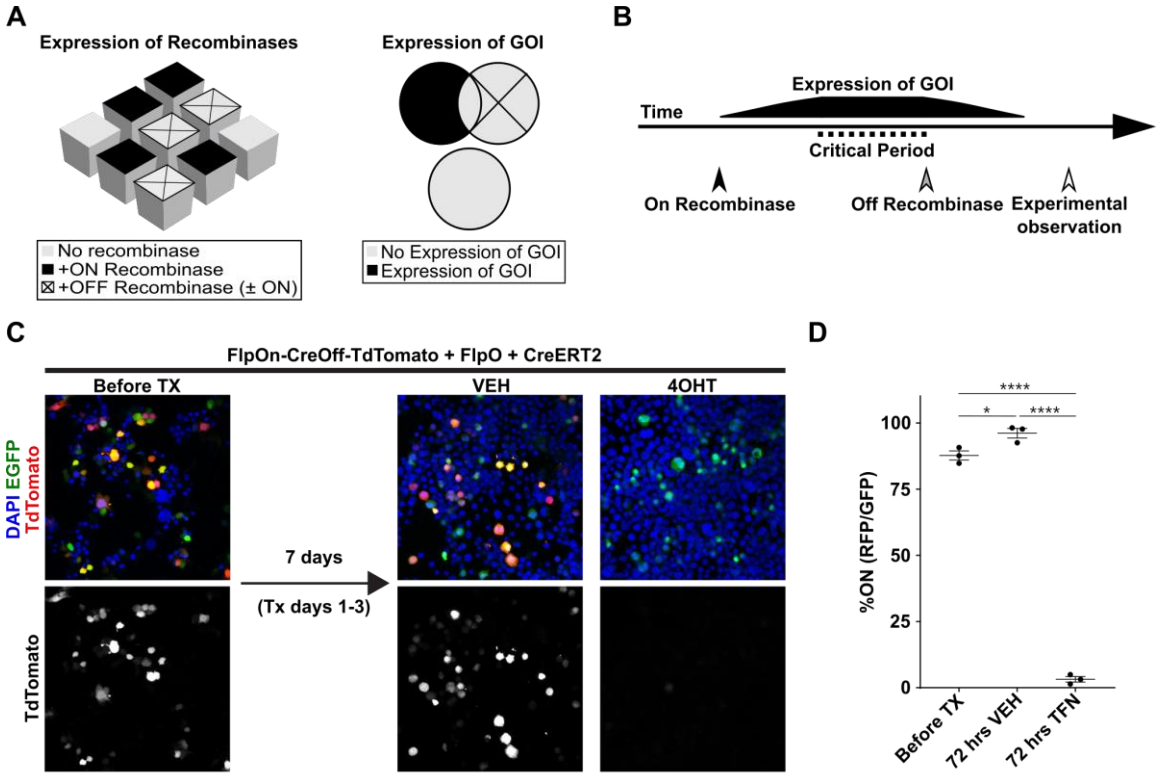


Figure 1.5: The ExBoX system can be used in multiple ways. (A) Expression of a gene of interest (GOI) can be restricted to a specific subpopulation of cells. Only the subpopulation of cells expressing the on recombinase, but not the Off recombinase, will express the GOI. **(B)** ExBoX can also be used for temporal control of expression. In this scheme, activation of the on recombinase is used just prior to a critical period of interest. Introduction or activation of the Off recombinase at the end of this critical period will turn off expression of the GOI. This serves to reduce confounding factors during later experimental observation, as GOI expression is no longer present. **(C)** Neuro2A cells were transfected with FlpOn-CreOff-TdTomato, FlpO, ERT2-Cre-ERT2, and EGFP. Beginning 48hrs after transfection, cultures were treated with 4-hydroxytamoxifen (4OHT) or vehicle (VEH) for 3 days and collected for imaging and quantification 4 days after that. **(D)** Before treatment 87.7±1.7% of cells were on. After treatment with the vehicle 96.1±1.8% of cells were on, while only 3.2±1.0% of cells treated with 4OHT remained on. Values given are mean±SEM. n=3 independent experiments (183–712 cells in each experiment). *P=0.0205, ****P<0.0001 (one-way ANOVA; Tukey post-hoc test). Scale bar 50 μm.

To further demonstrate the ability of ExBoX to provide temporal control of expression *in vivo*, we performed IUEs at E16.5 with FlpOn-CreOff-tdTomato in combination with pCAG-FlpO, pCAG-ERT2-Cre-ERT2, and pCAG-EGFP. After birth, pups were orally gavaged with tamoxifen or vehicle oil from P10 to P13 (4 days) and collected for visualization 10 days later (P23). Pups orally gavaged with vehicle showed 80.9±1.4% of EGFP+ cells also expressing tdTomato (Fig. 1.6A,B). Tamoxifen-treated pups displayed a significant decrease in EGFP+ cells expressing tdTomato, with only 2.1±0.6% remaining in the On condition after treatment (Fig. 1.6A,B). Taken together, these experiments corroborate that FlpOn-CreOff ExBoX constructs can be used in combination with tamoxifen-inducible Cre recombinase to control temporal expression of GOIs *in vitro* and *in vivo*.

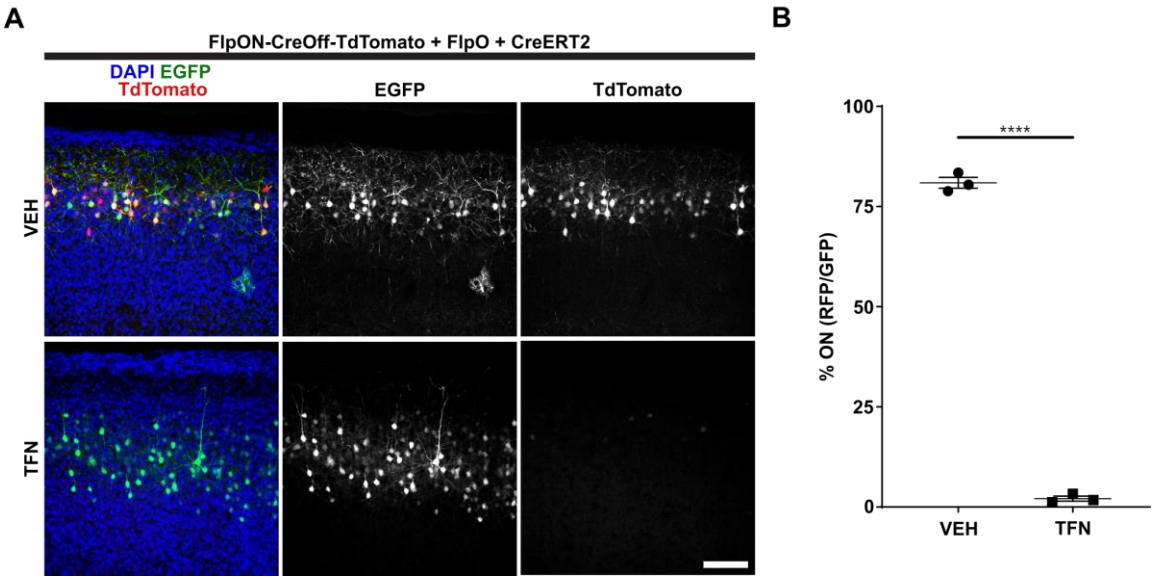


Figure 1.6: Temporal control of FlpOn-CreOff-TdTomato expression *in vivo*. (A) IUE was performed with the same combination of plasmids as in figure 1.5. Pups were gavaged with oil or tamoxifen from P10-P13 and collected for visualization 10 days later. **(B)** In vehicle treated pups, 80.9±1.4% of transfected cells co-expressed EGFP and TdTomato. Tamoxifen treatment resulted in a significant decrease of TdTomato expression in EGFP positive cells (2.1±0.6%). Values given are mean±SEM n=3 independent injections (62–330 cells in each experiment). ****P<0.0001 (two-tailed unpaired t-test). Image fluorescence is unamplified. Scale bar: 100 μm.

Finally, we sought to demonstrate that ExBoX-driven expression can be temporally and spatially controlled by performing successive viral injections. ICR pups were initially injected into the lateral ventricles with AAV-CreOn-FlpOff-EGFP and AAV9-hSyn-Cre at postnatal day 1 (P1) to obtain robust expression in layer V of the cortex (Mathiesen et al., 2020). These animals were injected 3 weeks later (P22) with pAAV-CAG-tdTomato alone or in combination with AAV-EF1a-FlpO into the primary somatosensory cortex (S1). Tissue was collected for analysis 3 weeks after the P22 injection. Because the initial P1 injection robustly labels layer V, quantification was limited to this layer at the site of the second injection. Only injections that were surrounded by expression of the CreOn-FlpOff-EGFP construct on both sides were scored. We found that 46.8±7.1% of

labeled cells co-expressed EGFP and tdTomato when the control pAAV-CAG-tdTomato vector was injected (Fig. 1.7A,B). Notably, co-injection of pAAV-CAG-tdTomato and pAAV-EF1α-FlpO resulted in a strong and significant decrease in expression, with only 7.6%±2.1 of the cells co-expressing EGFP and tdTomato (Fig. 1.7A,B).

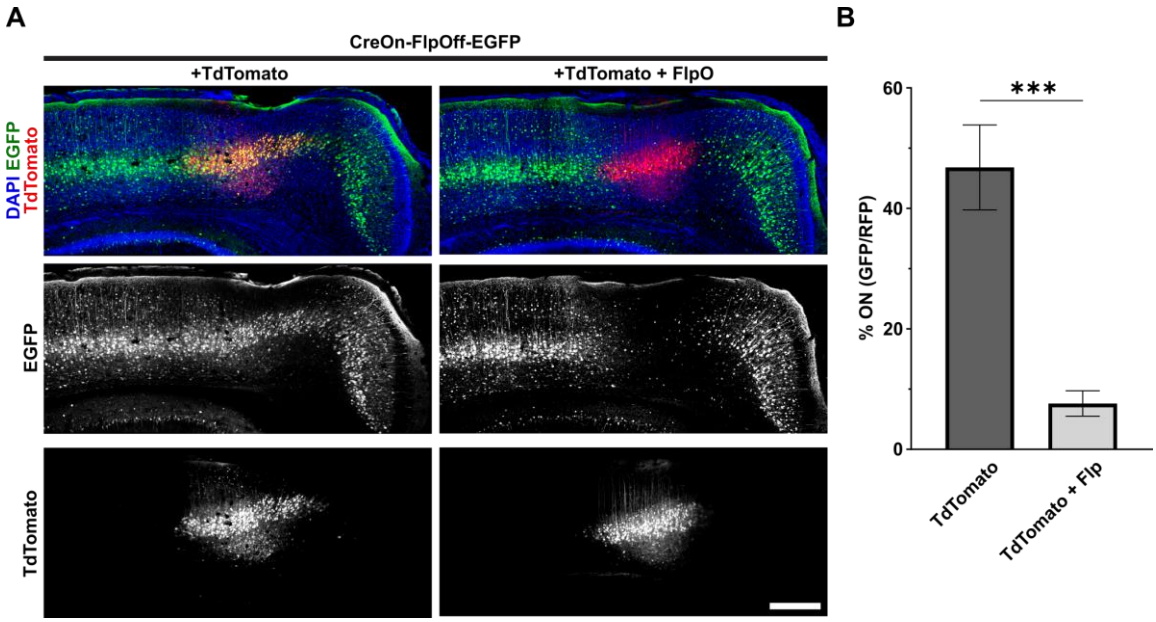


Figure 1.7: Temporal control of CreOn-FlpOff during AAV delivery. (A) Detection of AAV-CreOn-FlpOff-EGFP co-injected intracerebroventricularly with AAV-hSyn-Cre at P1. pAAV-CAG-TdTomato alone or in combination with AAV-EF1α-FlpO into layer V of S1 at P22. **(B)** Quantification of A. 46.8±7.1% of LV cells injected with pAAV-CAG-TdTomato alone express EGFP. A significant decrease in the number of EGFP-expressing cells is observed in animals co-injected with pAAV-CAG-TdTomato and AAV-EF1α-FlpO (7.6±2.1%). Values given are mean±SEM. n=5 independent injections (183–572 cells in each experiment). ***P=0.0007 (two-tailed unpaired t-test). Scale bars: 300 μm.

A similar proof-of-principle experiment was performed to validate the temporal and regional control of expression of the FlpOn-CreOff AAV constructs. AAV-FlpOn-CreOff-tdTomato and AAV-EF1a-FlpO were co-injected into the lateral ventricles of P1 pups. Three weeks later, AAV-CAG-EGFP alone or in combination with AAV9-hSyn-Cre were injected stereotactically into S1. In

animals injected with AAV-CAG-GFP alone, 40.0±3.8% of layer V cells co-expressed EGFP and tdTomato (Fig. 1.8A,B). Animals injected with AAV-CAG-GFP and AAV9-hSyn-Cre showed a significant 9-fold decrease in the number of cells co-expressing EGFP and tdTomato (4.31±0.5%; Fig. 1.8A,B). Though not shown here, the initial assessment of AAVs carrying neuromodulatory cargo show very few escaper cells when injected into the DG (Ubina et al., 2021). Overall, our data suggest that the ExBoX system can be used to provide temporal and spatial control of expression of genes of interest in a Cre- and Flp-dependent manner.

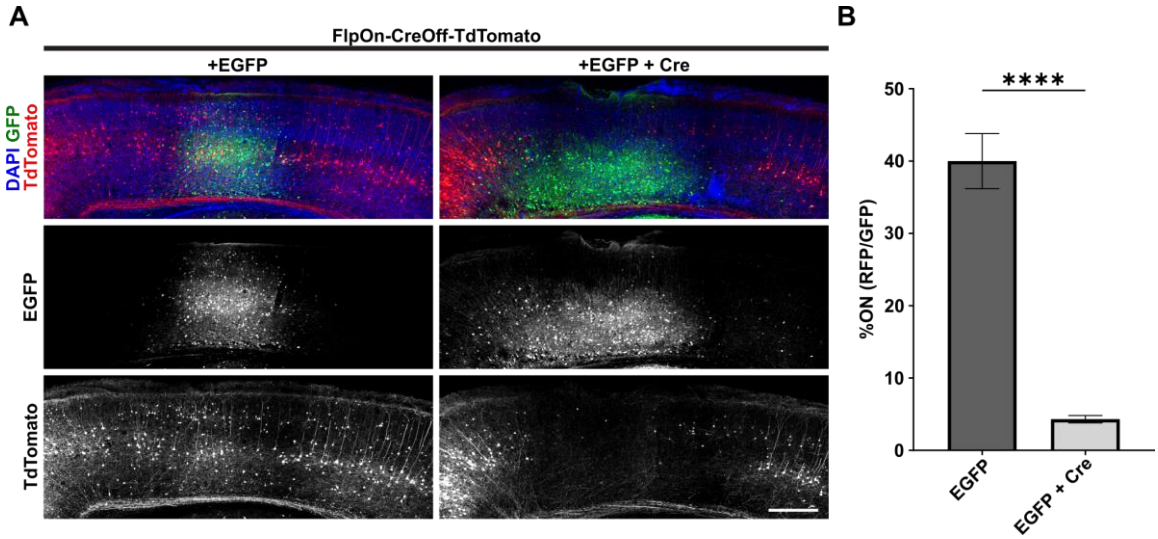


Figure 1.8: Temporal control of FlpOn-CreOff during AAV delivery. (A) AAV-FlpOn-CreOff-TdTomato expression when co-injected with AAV-EF1α-FlpO intracerebroventricularly at P1. pAAV-CAG-GFP alone or with AAV-hSyn-Cre into layer V of S1 at P22. **(B)** Injection of pAAV-CAG-GFP alone results in 40.0±3.8% of cells at the injection site in the on condition (expressing TdTomato). A significant decrease of TdTomato-expressing cells (4.3±0.5%) at the injection site was observed when pAAV-CAG-GFP and AAV-hSYN-Cre were co-injected. Values given are mean±SEM. n=3 independent injections for EGFP control, n=5 independent injections for EGFP+Cre (56–442 cells in each experiment). ****P<0.0001 (two-tailed unpaired t-test). Scale bar: 300 µm.

Discussion

Design of a simpler, more space-efficient Boolean exclusion expression system

Until recently, methods for cell targeting were limited to populations expressing a single marker and/or reporter. This made the study and targeting of specific subpopulations of cell types difficult. Many intersectional strategies have been recently developed to address these difficulties (Andersson-Rolf et al., 2017; Atasoy et al., 2008; Fenno et al., 2014; Gradinaru et al., 2010; Jensen and Dymecki, 2014; Plummer et al., 2015; Robles-Oteiza et al., 2015; Schnütgen et al., 2003). A previous study generated a system called INTRSECT that uses Boolean logic and is packaged in a single AAV (Fenno et al., 2014). INTRSECT uses a modular system with introns and can drive expression using many Boolean logical operations (AND, NOT, AND NOT, XOR, and NAND) (Fenno et al., 2014). Additionally, a new system following a similar design but using three recombinases (Triplesect), was published while this article was in preparation (Fenno et al., 2020). The design of these systems is elegant but are somewhat constrained in that the AND NOT construct design contains the same internal logic as the AND INTRSECT and Triplesect constructs. This constraint causes a few shortcomings in the existing AND NOT system. There are two introns that increase the length of the construct by 194 base pairs. This does not significantly impede their use in plasmid form, but may cause difficulty when using them with viruses such as AAV that have a limited packaging capacity (Dong et al., 1996). The introns also increase the difficulty of designing and cloning other sequences

into them. The ExBoX system was created in part to solve some of these constraints in that there is more cargo space, and it has a simpler design which allows for replacement of the CDS in the cassette with a simple cloning step.

The ExBoX system has strong expression in the presence of only the On recombinase and this expression can be easily inactivated in the presence of the Off recombinase (Figs. 1.2-1.8). We have validated the use of viral or plasmid ExBoX in embryonic and postnatal tissue both *in vitro* and *in vivo* (Figs. 1.2-1.8). Very few or no escaper cells still expressed the ExBoX constructs in the presence of the Off recombinase when the On and Off recombinases were active simultaneously (Figs. 1.2–1.8) or when the Off recombinase was activated by tamoxifen treatment over several days (Figs. 1.5 and 1.6). Considering how efficient the off switch appeared to be *in vitro* and *in vivo* when using the plasmid vectors (Figs. 1.2-1.6), the very few escapers observed in the AAV injections (Figs. 1.7 and 1.8) could be explained in part by incomplete or uneven co-infection – the recombinases and the fluorescent markers were driven by independent viral vectors (Maturana et al., 2023). However, a small but more noticeable number of escapers was observed when FlpO and Cre recombinases were expressed sequentially *in vivo* (Figs. 1.7 and 1.8). It is important to note that in addition to the sequential injection and the aforementioned use of independent viral vectors to drive the recombinases and the fluorescent markers, the titers and ratios for the ExBoX and recombinase vectors were not optimized for these AAV experiments. It will be necessary to carefully calibrate these parameters on

a case-by-case basis, based on the promoters used to drive expression of the recombinases and the ExBoX constructs, and the stability of the protein of interest in the cells to be studied.

A Boolean system to control expression with temporal and cell-type specificity

The ExBoX system can also be used to study cell populations that were previously inaccessible. ExBoX can be used to drive expression of a GOI or reporter in a subpopulation in cases where there is a recombinase driver for the broader population (Figs. 1.5A, 1.7, and 1.8). For example, it can be used to label or manipulate *5HTR3*$^{+}$*; VIP*$^{-}$ interneurons in the cortex by turning on expression of CreOn-FlpOff with *5HTR3a-Cre* and excluding inhibitory neurons that have *VIP-FlpO* (Fig. 1.3A) (Tremblay et al., 2016; Che et al., 2018; He et al., 2016; Gerfen et al., 2013).

Temporal control can also be achieved with ExBoX (Figs. 1.5B-D, 1.7, and 1.8). This becomes especially useful when studying topics with defined critical periods such as development or degenerative diseases. Expression of the On recombinase would specify cell type while the Off recombinase could be used to turn off expression at a desired time point (Figs. 1.5B, 1.7, and 1.8). For example, ExBoX AAVs containing a GOI can be injected at a desired time point into *Grik4-Cre* mice and a window of expression can be created by turning off expression with Flp. Our proof-of-principle experiments demonstrated that ExBoX expression can be shut off in the order of a few days (Figs. 1.7 and 1.8). Even with a highly efficient system, it is unlikely that protein expression will be turned

off within a few hours, but this will be ultimately dependent on the mRNA and protein stability for each gene of interest. Thus, we think the ExBoX system will be most powerful when studying developmental events that take place over days, but the inclusion of an in-frame PEST sequence might allow for the study of processes with shorter time windows (Rogers et al., 1986). The timing of expression can also more easily be controlled by delivering a tamoxifen-dependent Off recombinase at the same time as ExBoX delivery and easily turn off expression later by dosing with tamoxifen.

Expanding the toolkit to study gene function

Owing to the simple design of ExBoX, it can be easily modified to work with additional or alternative recombinase systems. For example, one could achieve even greater specificity by including the Dre-Rox system in addition to Cre-lox and Flp-frt (Plummer et al., 2015). Using the Dre-Rox system one could even utilize AND-NOT-NOT Boolean operations, opening up more possibilities. Changing the promoter of this system will allow ExBoX to drive expression in any cell type or tissue of interest. The wide array of possibilities and simplicity of this system makes the use of ExBoX particularly useful for gene therapy applications.

Here we created a new viral tool that drives expression using Boolean exclusion logic. The design of ExBoX allows for strict spatial and temporal control of gene expression, and its simplicity allows for easy modification to drive any GOI. Additionally, ExBoX improves on the CDS cargo capacity over previous designs (by 194bps) (Fenno et al., 2014, 2020). We believe that the simplistic

design of ExBoX will help to make the use of combinatorial approaches more widespread, cementing it as a valuable new addition to a series of recently developed intersectional viral systems (Fenno et al., 2014, 2020; Fan et al., 2020; Sabatini et al., 2021).

CHAPTER TWO

A genetic tool for the longitudinal study of a subset of post-inflammatory reactive astrocytes

Teresa Ubina[1,2], William Agnew-Svoboda[1,2], Zoe Figueroa[1,3], You-Cheung Wong[2,5], Edward A. Vizcarra[3,4], Bryan Roebini[2], Emma H. Wilson[1,3,4], Todd A. Fiacco[1,2,4], Martin M. Riccomagno[1,2,4,6]

[1] Neuroscience Graduate Program, University of California, Riverside, Riverside, CA 92521, USA
[2] Department of Molecular, Cell, and Systems Biology, University of California, Riverside, Riverside, CA 92521, USA
[3] Division of Biomedical Sciences, University of California, Riverside, Riverside, CA 92521, USA
[4] Biomedical Sciences Graduate Program, University of California, Riverside, Riverside, CA 92521, USA

Published in final edited form as:

Willaim Agnew-Svoboda, Teresa Ubina, Zoe Figueroa, You-Cheung Wong, Edward A. Vizcarra, Bryan Roebini, Emma H. Wilson, Todd A. Fiacco, Martin M. Riccomagno. A genetic tool for the longitudinal study of a subset of post-inflammatory reactive astrocytes (2022). *Cell Reports Methods*, 2(8), 100276. https://doi.org/10.1016/j.crmeth.2022.100276

Abstract

Astrocytes are vital support cells that ensure proper brain function. In brain disease, astrocytes reprogram into a reactive state that alters many of their cellular roles. A long-standing question in the field is whether downregulation of reactive astrocyte (RA) markers during resolution of inflammation is because these astrocytes revert back to a non-reactive state or die and are replaced. This has proven difficult to answer mainly because existing genetic tools cannot distinguish between healthy versus RAs. Here we describe the generation of an inducible genetic tool that can be used to specifically target and label a subset of RAs. Longitudinal analysis of an acute inflammation model using this tool revealed that the previously observed downregulation of RA markers after inflammation is likely due to changes in gene expression and not because of cell death. Our findings suggest that cellular changes associated with astrogliosis after acute inflammation are largely reversible.

Introduction

Astrocytes are critical regulators of homeostasis within the CNS and have many functions that include facilitating transport of nutrients and waste, maintaining the blood-brain barrier, and providing synaptic support (Engelhardt & Sorokin, 2009; Jessen et al., 2015; Panatier & Robitaille, 2016; Sofroniew & Vinters, 2010). When immune insults or inflammation occur in the CNS reactive gliosis occurs as a response (Escartin et al., 2021). During reactive gliosis, astrocytes and microglia undergo multiple transcriptional, functional, and structural changes. While initially increased expression of GFAP and cellular hypertrophy were recognized and used as the sole markers of astrocyte reactivity, other changes in protein expression and functionality are now recognized (Burda et al., 2022; Cahoy et al., 2008; Dai et al., 2023; Jurga et al., 2021b; Lee et al., 2009; Sung et al., 2003; Eng et al., 1971; Jurga et al., 2021a). Reactive astrocytes (RAs) are a feature of many CNS inflammatory responses and have been observed after a variety of insults such as penetrating brain injuries, epilepsy, and Alzheimer disease (Binder & Steinhäuser, 2009; Burda & Sofroniew, 2014; Katsouri et al., 2020; Laird et al., 2008). RAs can also proliferate, migrate, and polarize to become part of the glial scar as a response to nervous tissue damage (Ferrer-Acosta et al., 2017; Wanner et al., 2013).

Based on a growing body of research, RAs can be beneficial or harmful to CNS repair and recovery after injury. Recent work suggested that RAs can be

neurotoxic under certain conditions or disease states, while in other contexts they are neuroprotective: i.e preventing or reverting reactivity led to worse outcomes and delayed healing (Katsouri et al., 2020; Liddelow et al., 2017; Okada et al., 2006; Shinozaki et al., 2017; Yun et al., 2018). Recent research has shown there are different subtypes of RAs and their responses, whether beneficial or harmful, can differ across disease models and even regionally within the brain (Anderson et al., 2014; Burda et al., 2022; Park et al., 2021; Smith et al., 2022; Yun et al., 2018; Zamanian et al., 2012). Existing tools have provided many insights into RA morphology, physiology, and transcriptomic changes. However, many of these tools have the limitation of also being expressed in healthy astrocytes, making it difficult to target only RAs during the progression of inflammation or disease (Cahoy et al., 2008; Robel et al., 2009; Sofroniew, 2009). The recent identification of genes that are upregulated only in RAs has provided a means to begin to address these limitations. Lcn2 is an ion chelator that is expressed at negligible levels in the healthy brain but is highly upregulated in RAs of murine models of neuroinflammation (Zamanian et al., 2012). Initially deemed a pan-RA marker, Lcn2 has more recently been shown to be upregulated to varying degrees in a large pool of astrocytes in several disease models, with some exceptions (Diaz-Castro et al., 2019, 2021; Habib et al., 2020; Hasel et al., 2021; Liddelow et al., 2017; Zamanian et al., 2012). Based on this knowledge, we developed a *Lcn2CreERT2* mouse that expresses a tamoxifen-dependent Cre

recombinase (Cre-ERT2) under the *Lcn2* promoter (Fig. 2.1). Pilot validation of *Lcn2* as an RA marker has previously been performed (Agnew-Svoboda, 2021).

In this study we examine RAs in a variety of neuroinflammatory models and identify RAs for single cell studies using the *Lcn2CreERT2* mouse. The *Lcn2CreERT2* mouse can be used to permanently label RAs during neuroinflammation and follow them post inflammation. Permanent labeling of RAs allows for longitudinal studies of their morphology, physiology, and transcriptomic changes during and after onset of reactivity. Here we demonstrate that RAs labeled during inflammation remain in the CNS after the resolution of inflammation and expression of reactive markers returns to pre-inflammatory levels. This work suggests that most RAs remain in the brain after the resolution of inflammation and gene expression seems to return to pre-inflammatory levels. Interestingly, some morphological changes may remain at least one month after the inflammatory insult. Our experiments underscore the potential of the *Lcn2CreERT2* mouse to contribute to the body of literature pertaining to RAs and elucidate new disease mechanisms.

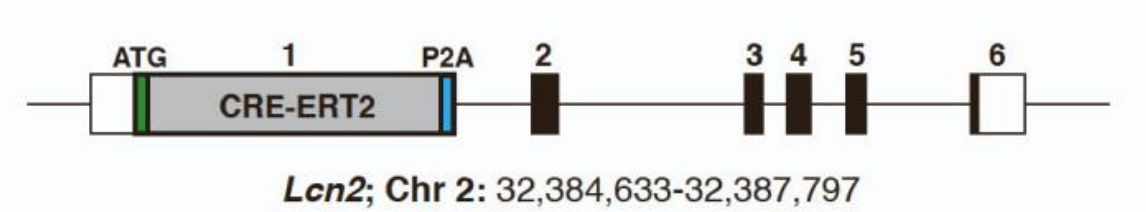


Figure 2.1: Design of the Lcn2CreERT2 transgene. CreErt2 followed by a P2A signal was targeted downstream of the Lcn2 promoter and start codon, but upstream of the remainder of the first coding exon.

Materials and Methods

Animals

Wild-type Swiss Webster mice were used for histology to examine Lcn-2 expression in the naive and inflamed brain. *Lcn2CreERT2* animals were maintained in the Swiss Webster background and crossed into the *Ai9* tdTomato reporter line (strain #007909) available from JAX for experiments. Cre-negative controls were *Lcn2CreERT2* negative littermates, while saline controls were performed on Cre positive littermates. All procedures were done on animals 4-6 months of age. For each experiment at least one male and 1 female were included. Mice were maintained in a 12-hour light/dark cycle with ad libitum food and water at room temperature. All animal procedures detailed in the following sections were performed according to the University of California, Riverside's Institutional Animal Care and Use Committee (IACUC) guidelines.

T. gondii

The Me49 Toxoplasma strain was maintained *in vivo* by passaging consecutively in Swiss Webster (SW) and CBA mice (JAX).

Generation of Lcn2CreERT2 mice

The mouse line carrying a CreERT2 between the Lcn2 promoter and the 5′ untranslated region (UTR) of the Lcn2 gene was generated using the vector pBS-PGK-DTA-pa, modified by Bac recombineering (Liu et al., 2003). The *Lcn2CreERT2neo* allele was engineered to encode for an ERT2 tagged Cre recombinase upstream of the 5′ UTR and an FTR-flanked neomycin cassette.

Targeting and selection of Embryonic Stem (ES) cells, and production of chimeric mice by injection of targeted ES cells into blastocysts was performed by the Transgenic Mouse Facility (TMF) at the University of California, Irvine. Germline transmission of the *Lcn2CreERT2*neo allele was verified by southern blot and a PCR genotyping strategy. In order to eliminate the neomycin cassette, *Lcn2CreERT2neo/+* animals were crossed to the deleter mice carrying ACT-FlpE, which expresses FlpE recombinase under the ACTB promoter. Expression of FlpE generates the *Lcn2CreERT2* allele by removal of the neomycin gene while leaving a single FRT site in the genomic DNA. All breeding at the chimera stage was conducted in C57/B16J mice and subsequently outbred to the Swiss Webster background for at least 3 generations. PCR genotyping of the *Lcn2CreERT2* mouse was conducted using the following primers: *Lcn2CreERT2* Forward: 5′-GGCAGTCCAGATCTGAGCTGC-3′ and *Lcn2CreERT2* Reverse: 5′-TGCATCGACCGGTAATGCAGG-3′.

Low-dose and high-dose LPS treatments

Lcn2CreERT2 animals crossed into the *Ai9* tdTomato reporter line were separated into 4 treatment groups; Oil and Saline, Oil and LPS, tamoxifen and saline, and tamoxifen and LPS. Animals in the two tamoxifen treated groups were given an oral gavage of 150 µg/g of tamoxifen (Sigma Aldrich, T5648) dissolved in corn oil (Sigma Aldrich, C8267), while animals in the two oil groups received an equivalent dose of corn oil. Tamoxifen/oil treatments were given every 24 hours for 6 consecutive days. Twenty-four hours after the first tamoxifen

or oil treatment, animals in the two LPS treatment groups received intraperitoneal (IP) injections of 1.5 mg/kg lipopolysaccharide (Sigma Aldrich; L2880, Lots 68M4053v and 39M4004v) dissolved in sterile 1x phosphate buffered saline (PBS), while animals in the two saline treated groups received an equivalent dose of sterile 1x PBS. LPS/saline treatments occurred every 24 hours for 5 consecutive days. Animals were collected for tissue processing 24 hours to 1 month following the final treatment.

For experiments utilizing 5-ethynyl-2′-deoxyuridine (EdU), *Lcn2CreERT2;Ai9* mice were treated with the low-dose LPS protocol described above and given 150 mg/kg of EdU (Molecular Probes, cat#E10187) IP on days 4 and 5 of LPS treatment and the following day (3 total doses). Animals collected at the 24-hour post LPS timepoint were given EdU 2 hours prior to collection. Animals were also collected 7 days or 1 month following LPS treatment.

The same treatment groups as described for the low-dose experiment were used for the high-dose LPS treatments. However, for these experiments tamoxifen/oil treatments were given every 24 hours for only 3 consecutive days. Twenty-four hours after the first tamoxifen or oil treatment, animals in the LPS treatment groups received a single IP injection of 10 mg/kg lipopolysaccharide dissolved in sterile 1x PBS, while animals in the saline treated groups received an equivalent dose of sterile 1x PBS. Animals were collected for tissue processing 24 hours to 1 month following the final treatment.

Toxoplasma gondii injections

To induce chronic Toxoplasma infection, mice were infected via IP with the cyst forming Me49 Toxoplasma strain maintained *in vivo* by passaging consecutively in Swiss Webster (SW) and CBA mice (JAX). Brains from CBA mice were harvested, homogenized in 3ml sterile 1X Phosphate Buffer Saline (PBS) through needle passing, and cysts counted using a 30ul aliquot and a light microscope (average cyst burden/brain ~3000). Cyst homogenate was then diluted in sterile 1X PBS and 10 Me49 cysts injected via 200ul IP injections. This amount mimics a physiological Toxoplasma infection that initiates in the gut of the host and travels through the blood stream to eventually enter the brain to form cysts in neurons. Mice were monitored closely immediately after infection to watch for any adverse effects. Three weeks following the initial infection date, when acute systemic inflammation has subsided and infection is localized to the brain, *Lcn2CreERT2; Ai9* tdTomato mice were given 150 ug/g tamoxifen dissolved in corn oil. Tamoxifen treatments continued 3 times per week for 4 weeks. Twenty-four hours after the final tamoxifen treatment, animals were collected for tissue processing.

Intrastriatal LPS

Lcn2CreERT2 animals crossed into the *Ai9* tdTomato reporter line were given 150 ug/g tamoxifen dissolved in corn oil every 24 hours for 3 consecutive days. Striatal LPS was injected as described in Hunter et al. (2009). Briefly, on the day of the second tamoxifen treatment animals were stereotactically injected with 1 µl

of sterile saline or 1 µl of 7.5 mg/ml LPS in four locations in the striatum using the following coordinates from Bregma: a/p +1.18 mm, m/l ± 1.5 mm, and d/v −3.5 mm as well as a/p −0.34 mm, m/l ± 2.5 mm, and d/v −3.2 mm. Injections were performed at 0.5 µl/minute and the needle was kept in place for 5 minutes prior to withdrawing. Animals were kept on a heating pad and received sterile saline subcutaneously until they became hydrated and free moving. Seven days after the injections, animals were collected for tissue processing.

Fluorescent in situ hybridization: RNAscope

Fluorescent in situ hybridization was performed on mouse tissue using the RNAscope Multiplex Fluorescent Detection kit v2 (Advanced Cell Diagnostics, ACD, 323110). In this assay, the target RNAs are hybridized to single stranded DNA “z-probes” composed of a complementary ∼20 nucleotide sequence to the RNA of interest, a spacer sequence, and a 14 nucleotide tail region. Twenty-eight nucleotide -reamplifier oligos bind to the tail region of z-probe pairs bound to adjacent sequences in the RNA, which are then bound to amplifiers that are labeled with horseradish peroxidase (HRP) enzyme molecules. Tyramide-conjugated fluorophores are added, leading to HRP enzymatic conversion of tyramide into a highly oxidized intermediate which covalently binds to proteins near the HRP label, thus depositing a large number of detectable fluorophores. Multiple RNA targets can be labeled with the use of detection probes in different channels with distinct tail sequences which allow for the generation of unique amplification trees for each target. Each target/probe is then sequentially

developed using tyramide signal amplification by using channel specific HRP labels and tyramide conjugated dyes Opal 520 and Opal 690 (Akoya Biosciences, FP1487001KT and FP1497001KT). Probes used were: *Slc1a3* (ACD, 430781), *Lcn2* (ACD, 313971), *Pecam1* (ACD, 316721), *Lrrc8a* (ACD, 458371), *Slc1a2* (ACD, 441341), *Aldh1l1* (ACD, 405891) and *Gfap* (ACD, 313211). At the end of signal development, sections were counterstained with DAPI (Thermo Scientific, 62248) or selected for immunohistochemistry as described below.

Immunofluorescence

Mice were perfused and extracted brains were fixed with 4% paraformaldehyde for 2 hours to overnight at 4°C, rinsed, and sunk in 30% sucrose overnight prior to being frozen in Optimum Cutting Temperature media (OCT, Tissue-Tek, 4583) for cryopreservation. Coronal sections (20 μm) were obtained on a Leica CM3050 cryostat. Sections that were immediately used for immunohistochemistry were next blocked in 10% goat serum and 0.1% Triton-X100 (Thermo Fisher, A16046.AP) for 1 hour at room temperature. This step was skipped for sections that had been previously used for RNAscope, but all steps following were the same. Sections were then incubated overnight at 4°C with primary antibodies. Following incubation, sections were washed with PBS and incubated with secondary antibodies and DAPI. Sections were washed in PBS and mounted using Vectorshield hard-set fluorescence mounting medium (Vector Laboratories, H-1400-10). Confocal fluorescence images were taken using a

Leica SPE II microscope. Primary antibodies used in this study include rabbit anti-DsRed (Takara Bio, 632496, 1:500), rat anti-GFAP (Invitrogen, 13-0300, 1:1000), chicken anti-Foxo3 (EnCor CPCA-FOX3, 1:1000), rabbit anti-Iba1 (Fuijifilm, 019-19741), and chicken anti-GFP (AVES, GFP-1020, 1:1000). Tomato-lectin (Vector Laboratories, B-1175-1, 1:75) was combined with primary antibodies. Secondary antibodies used in this study include goat anti-rabbit 488 (Invitrogen, A-11034), goat anti-rat 488 (Invitrogen, A-11006), goat anti-rat 647 (Invitrogen, A-21247), goat anti-chicken 488 (Invitrogen, A11039), streptavidin 488 (Invitrogen, S32354). For EdU experiments, the Click-iT EdU Cell Proliferation Kit from Invitrogen was used according to manufacturer instructions (cat# C10337).

Quantification and statistical analysis

All images were analyzed using FIJI (Schindelin et al., 2012). Cells expressing tdTomato were counted by thresholding to create a binary image, the "watershed" function was used and followed by the "analyze particles function" to count cells with a size between 20-2000 pixels^2. Colocalization of IHC markers was performed by manual counting. Cells expressing tdTomato were identified and their area was turned into outlines. For EdU experiments the number of EdU and tdTomato copositive cells was taken as a percentage of total tdTomato labeled cells. Cells showing expression of markers labeled in the green or far-red channel within the outlined areas were then manually counted.

Astrocytes were traced using Neurolucida 360 version 2021.1.3 (MBF Bioscience, Williston, VT USA) and analyzed as previously described (Wilhelmsson et al., 2006). Briefly, the number of cellular processes leaving the soma were counted as well as the number of processes at 15 μm away from the soma. Volume was measured by taking 0.2 μm optical sections and calculating volume from the tdTomato labeling of astrocytes.

Total expression of RNAs identified through FISH was performed by analyzing total fluorescent area in selected ROIs. ROIs were drawn around the thalamus. Background fluorescence was subtracted with the “subtract background” function. The “measure” function was then used to look at total fluorescent area in the drawn ROI. For measuring expression of reactive markers within tdTomato positive astrocytes, the tdTomato positive cells were outlined and the outline was turned into an ROI. The fluorescent channel corresponding to the RNA was then made binary, the watershed function applied, and particles were analyzed within the ROI using the “analyze particles” function. All counts are reported with ± standard error of the mean.

Statistical analyses were performed using GraphPad Prism version 9.3.1 for Windows, GraphPad Software, San Diego, California USA, www.graphpad.com. Each figure panel and legend contains information on statistical tests performed along with sample sizes and p values. $*p < 0.05$; $**p < 0.01$; $***p < 0.001$; $****p < 0.0001$ for all statistical analyses presented in figures. Sample sizes are mentioned in figure legends.

Acknowledgments

The authors thank the Transgenic Mouse Facility (TMF) at the University of California, Irvine, for the generation of the *Lcn2CreERT2* mice. This work was supported by grants from the National Institutes of Health R03AG063264 and R21NS109918 to T.A.F. and M.M.R.; R01DA048815 to E.H.W., T.A.F., and M.M.R.; and R01DA048815-03S1 to E.H.W. The funders had no role in study design, data collection and analysis, decision to publish, or preparation of the manuscript.

Results

Validation of the Lcn2CreERT2 mouse during systemic inflammation

Validation of the *Lcn2CreERT2* mouse was carried out by crossing into the Cre-reporter mouse line *Ai9* (Madisen et al., 2010). The mice resulting from this cross express the fluorescent reporter tdTomato in a Cre- and tamoxifen-dependent manner. We utilize a 5-day low-dose LPS protocol with tamoxifen to induce systemic inflammation (Catorce & Gevorkian, 2016). Control animals were given saline and tamoxifen, saline and oil, or LPS and oil. One day after the last treatment brains were collected and immunohistochemistry (IHC) was done. This type of analysis revealed that tdTomato was highly expressed in animals treated with LPS and tamoxifen, but negligible in other treatment groups suggesting that *Lcn2CreERT2*-dependent recombination is inflammation- and

tamoxifen-dependent (Fig. 2.2). Since the most robust expression was in the thalamus, later experiments focused on this region.

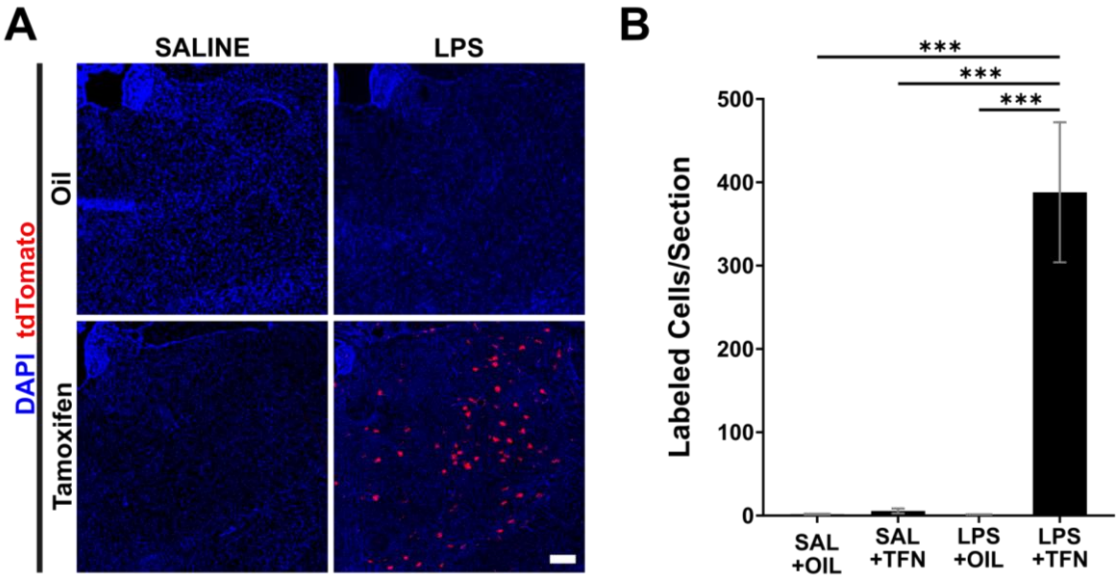


Figure 2.2. Expression of Lcn2CreERT2 following repeated low-dose LPS treatment. (A) Immunostaining for tdTomato in *Lcn2CreERT2;Ai9* brains. Animals were given one of the following four treatments for 5 consecutive days: Saline and corn oil, saline and tamoxifen, LPS and corn oil, LPS and tamoxifen. Sections were counterstained with DAPI. **(B)** Quantification of total number of red cells/section from animals in (A). ***p < 0.001 ANOVA and Tukey's post hoc test, n = 5 animals per treatment. Scale bars 250μm. Error bars ± SEM. Panel A courtesy of William Agnew-Svoboda.

We next explored the cell types expressing the Cre-dependent reporter in *Lcn2CreERT2; Ai9* brains using IHC for cell-type markers (Figures 2.3A and 2.3B). No tdTomato+ cells were positive for the neuronal marker NeuN. Approximately 51±2.2% of tdTomato+ cells are co-positive for lectin (a marker for monocytes and endothelial cells) and 45±1.8% are co-positive for the astrocytic marker GFAP. GFAP co-positive cells were unequivocally identified as astrocytes, while lectin-positive cells appeared to be endothelial cells based on their morphology. Only a small subset of tdTomato+ cells was co-positive for Iba1 (1.1% ± 0.4%), a marker of microglia, suggesting that the majority of Lectin+ tdTomato cells are indeed endothelial cells. Together, these results suggest that *Lcn2CreERT2* is expressed only after an inflammatory insult and this expression is primarily located in RAs and endothelial cells.

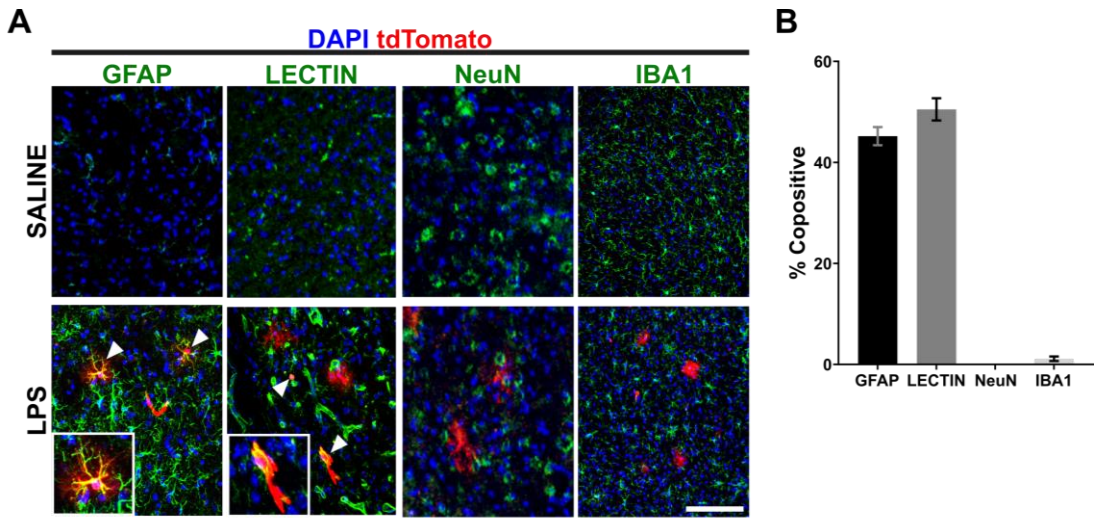


Figure 2.3: Cell type markers in Lcn2CreERT2;Ai9 brains following repeated low-dose LPS treatment. (A) Immunostaining of brains from saline- (top row) or LPS-treated (bottom row) *Lcn2CreERT2;Ai9* animals for tdTomato and the astrocytic marker GFAP (left), the endothelial and microglial marker lectin (middle left), the neuronal marker NeuN (middle right), and the microglial marker Iba1 (right). Sections were counterstained with DAPI. White arrowheads indicate co-positive cells for tdTomato and the panel maker. **(B)** Quantification of co-positive cells from (A). Scale bar 50μm. Error bars ± SEM.

Expression of Lcn2CreERT2 in other brain injury models

We next examined whether the *Lcn2CreERT2* mouse could serve as a tool for the study of RAs across a range of disease and brain injury models. Many neuroinflammatory models were tested; however, here we highlight parasitic infection by *Toxoplasma gondii* and intrastriatal injection of LPS (Figs. 2.4 and 2.5). *T. gondii* infection is a common human pathogen that exists in approximately one-third of the world's population and can cause serious life-threatening disease in the immune-compromised (Dubey et al., 2021). The parasite resides as cysts within neurons, requiring a continuous immune response in the brain to prevent reactivation and disease (Wohlfert et al., 2017). It therefore provides a model of chronic inflammation that is human disease-relevant. *Lcn2CreERT2; Ai9* mice were injected with *T. gondii* cysts via IP injection or given a saline sham injection (Noor et al., 2010). Three weeks after *T. gondii* infection, tamoxifen was given 3 times/week for 4 weeks and collected. Initial analysis of these mice demonstrated that tdTomato expression was only found in infected animals (Fig. 2.4A). The identity of the cells that turned on the reporter was investigated by co-labeling with neuronal, astrocytic, microglial, and endothelial markers. No tdTomato+ cells were co-positive with the neuronal marker NeuN. Cells co-positive for GFAP accounted for 64±3.4%, 37±1% were co-positive for tdTomato and lectin, and 2.3% ± 0.4% were positive for Iba1 (Fig. 2.4B,C). The robust upregulation of *Lcn2CreERT2* following chronic *T. gondii* infection primarily in astrocytes and endothelial cells was somewhat expected

based on the LPS experiments. Similarly, the percentages for each cell type are consistent with repeated low-dose LPS treatment. Additionally, these data showed long term tamoxifen treatment alone does not induce *Lcn2CreERT2*.

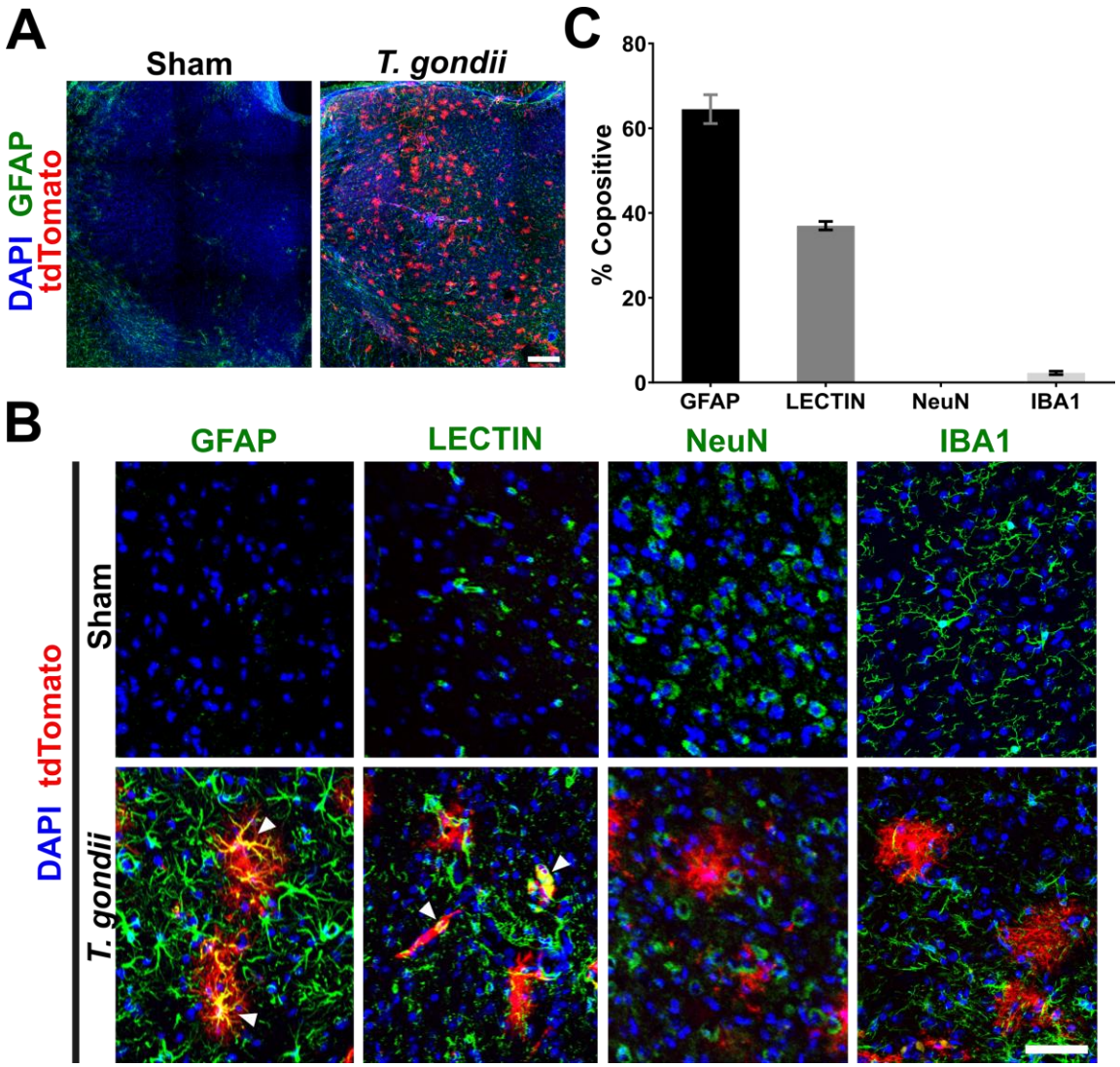


Figure 2.4: Expression of Lcn2CreERT2 in a parasitic model of neuroinflammation. (A) Immunostaining for tdTomato on *Lcn2CreERT2; Ai9* thalami 7 weeks after infection with *T. gondii*. (B and C) Tissue from animals described in (A) was immunostained for tdTomato and the astrocytic marker GFAP (left), the endothelial and microglial marker lectin (second column), the neuronal marker NeuN, and the microglial marker Iba1 (right). Co-positive cells indicated by white arrowheads, quantified in (C). n = 3 animals. Scale bars, (A) 250 μm, (B) 50 μm. Error bars ± SEM.

In addition to toxoplasma infection, we also determined the levels of *Lcn2CreERT2* activation after intrastriatal injection of LPS (IS LPS). This could serve as a relevant model of encephalitis since injection of LPS directly into the striatum induces inflammation within the brain and loss of dopaminergic neurons in the substantia nigra (Hunter et al., 2009). tdTomato expression in IS LPS injected brains was found throughout the brain and restricted to the injection site for IS saline (Fig. 2.5A,B). As observed in the other inflammation models, tdTomato was almost exclusively expressed by astrocytes and endothelial cells (Fig. 2.5C,D). Taken together, our results suggest that many conditions that induce an inflammatory immune response in the brain will result in *Lcn2* expression, highlighting the utility of the *Lcn2CreERT2* mouse for the study of reactivity across multiple disease and brain injury models.

Lcn2CreERT2-expressing astrocytes remain in the CNS following resolution of inflammation

One longstanding question in the field is whether RAs remain or die off after the resolution of inflammation (Escartin et al., 2021; Zamanian et al., 2012). Markers of RAs are rapidly induced after LPS treatment but return to basal levels within 1 month (Escartin et al., 2021; Zamanian et al., 2012). Whether this overall decrease in expression of RA markers is a result of programmed cell death and generation of new cells, or downregulation of expression of these genes within RAs cannot be determined without an approach that permanently labels astrocytes at the onset of gliosis.

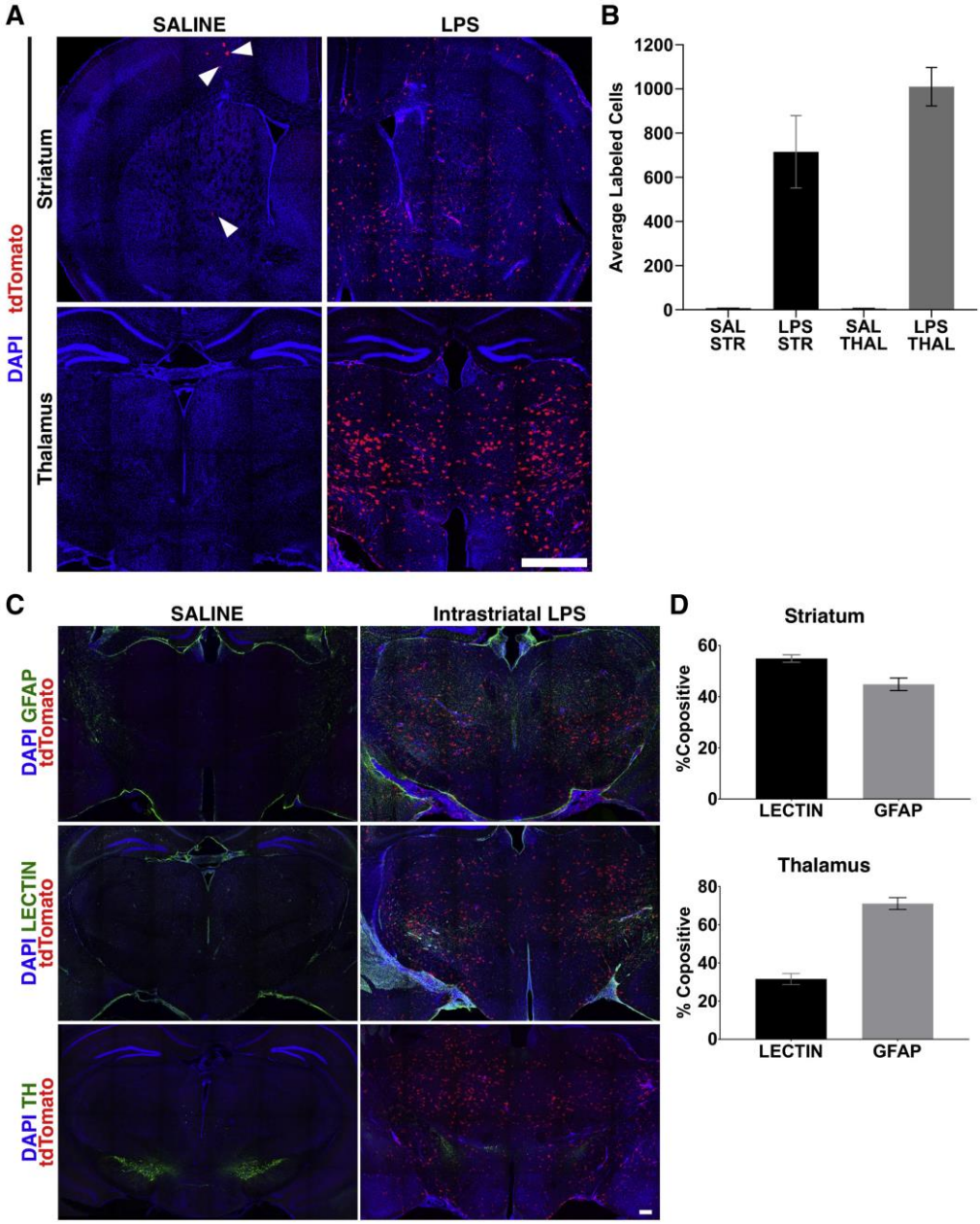


Figure 2.5: Lcn2CreERT2; Ai9 tdTomato labeling after intrastriatal LPS injections. (A) tdTomato immunostaining of *Lcn2CreERT2; Ai9* animals injected intrastriatally with LPS or sterile saline and gavaged with tamoxifen for 3 days. Sections were counterstained with DAPI. tdTomato+ cells lining the saline injection site are marked by white arrowheads. **(B)** Quantification of total number of labeled cells in the striatum and thalamic regions. **(C)** Representative images of brains collected after saline or LPS injections into the striatum (n = 4 animals). Coronal sections through the thalamus and ventral tegmental area were immunolabeled with anti-tdTomato antibody (red) and co-stained with DAPI (blue) and anti-GFAP (top, green), Lectin (middle, green) or tyrosine hydroxylase (bottom, TH, green). tdTomato signal partially co-localized with GFAP and lectin, but not with TH-positive catecholaminergic neurons. **(D)** Quantification of cells co-positive for tdTomato and GFAP or lectin. Scale bars, (A) 250 µm, (C) 500 µm. Error bars ± SEM. Data courtesy of William Agnew-Svoboda.

To address this question the low-dose LPS protocol was done on *Lcn2CreERT2; Ai9* mice. Tamoxifen was given only during the LPS treatment so only the cells activated by the initial LPS treatment were labeled. Brains were collected at 24 hours and 1 month post treatment when reactive markers are reported to return to baseline levels (Zamanian et al., 2012). tdTomato labeling again remained negligible in saline-treated animals and was highly expressed in animals at the 24 hour and 1 month time points (Fig. 2.6A,B). The number of tdTomato+ cells was not significantly different between the 24 hour and 1 month time points (Fig. 2.6B, $t(4)=0.32$, $p=0.38$). Moreover, analysis of RNAscope data revealed no significant difference in the number of tdTomato+ cells that expressed the astrocytic marker *ALDH1L1* at the two time points (Fig. 2.6C and 2.6D; $t = -1.000726$, $p = 0.160803$). These results suggest that astrocytes that had become reactive and expressed *Lcn2CreERT2* at the onset of inflammation remain in the CNS long after inflammation has resolved.

To confirm that the numbers of tdTomato+ astrocytes were not maintained via clonal expansion of just a few Lcn2+ RAs that remained alive soon after the inflammatory insult subsided, we labeled proliferating cells at the peak of inflammation with Ethynyl deoxyUridine (EdU; Fig. 2.6E–2.6G). EdU is a thymidine analog that is incorporated in cells undergoing the S-phase of the cell cycle and can be used to observe the fate of cells born at a specific timepoint (Salic & Mitchison, 2008). EdU was injected on the last 2 days of the low-dose LPS treatment and also 22 hours after. Brains were collected 24 hours, 7 days,

and 1 month after the low-dose treatment. Only a small percentage of tdTomato astrocytes appeared to be proliferative when collected at 24hrs post LPS. This tdTomato+/EdU+ population did not expand significantly, as the percentage remained almost constant at 7 days and 1 month after LPS (Fig. 2.6E–2.6G; NS; one-way ANOVA). These data suggest that acute inflammatory insult does not result in noteworthy proliferation of RAs and provides further support to the idea that the large majority of Lcn2+ RAs remain alive 1 month after inflammation.

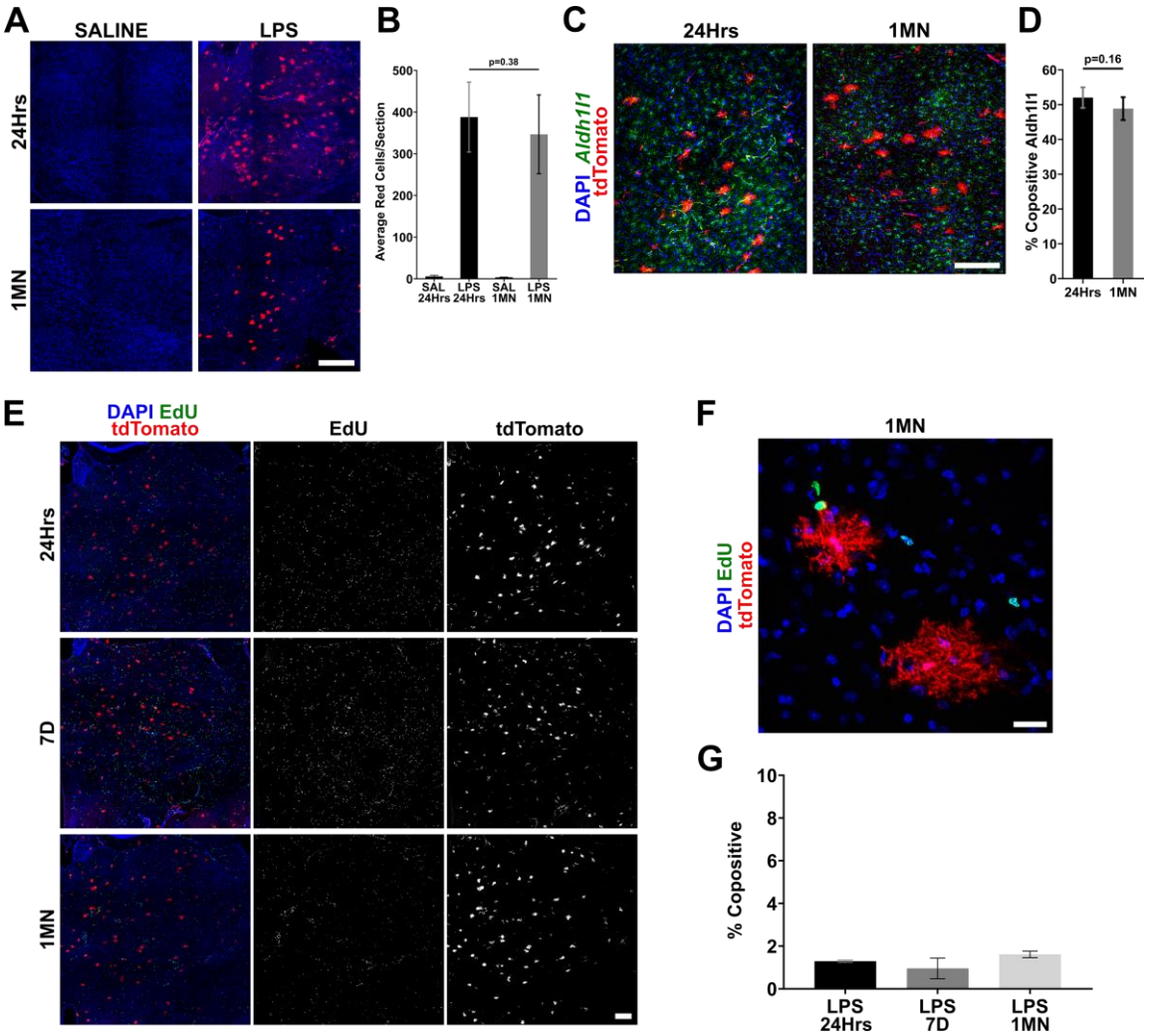


Figure 2.6: Astrocytes that were initially reactive remain in the brain after resolution of inflammation. (A) *Lcn2CreERT2; Ai9* brain sections immunostained for tdTomato and counterstained with DAPI. Animals were given tamoxifen and saline or LPS and collected at either 24hrs or 1 month after the last treatment. **(B)** Quantification of tdTomato-positive cells in the thalamic region. p = 0.38, ANOVA followed by Tukey's HSD post hoc, n = 5 animals. **(C)** RNAscope on *Lcn2CreERT2; Ai9* brain sections for the astrocyte marker *Aldh1l1* 24 h and 1 month after low-dose LPS treatment, followed by immunostaining for tdTomato and counterstaining with DAPI. **(D)** Quantification of *Aldh1l1* and tdTomato co-positive cells in (C). p = 0.16, paired t test. n = 18 pooled sections across three animals. **(E)** Co-labeling of tdTomato and EdU-positive astrocytes in *Lcn2CreERT2; Ai9* animals after LPS treatment. **(F)** High magnification image of labeled astrocytes and EdU-positive cells at 1 month. **(G)** Quantification of tdTomato and EdU co-positive astrocytes at 24 h, 7 days, and 1 month following LPS treatment. Error bars ± SEM. Scale bars, (A) 400 µm, (C, E) 200 µm, (F) 20 µm. Panels C and D courtesy of William Agnew-Svoboda.

Morphological and molecular changes in RAs following inflammation

Next, we investigated whether the tdTomato-expressing cells maintained their reactive markers, or if these returned to basal levels. tdTomato+ astrocytes from 24 hours and 1 month time points were examined by assessing independent measures of reactivity, i.e., alterations in volume and branching pattern (Escartin et al., 2021; Wilhelmsson et al., 2006). The use of a cytoplasmic tdTomato reporter has the advantage of allowing the visualization of the whole astrocyte and not just GFAP or other cytoskeletal features, thus providing a strong readout for morphological changes in thin astrocytic processes (Escartin et al., 2021). We compared the volume and branching pattern of tdTomato+ astrocytes in *Aldh1l1CreERT2; Ai9* animals treated with saline and tamoxifen, versus astrocytes in *Lcn2CreERT2; Ai9* mice 24 h and 1 month after low-dose LPS treatment (Fig 2.7A,B). Consistent with previous studies (Wilhelmsson et al., 2006), cell volume did not significantly change after insult (Fig. 2.7A,B; NS, one-way ANOVA). The number of total branches and the number of distal processes were significantly higher 24 h after LPS treatment versus saline treatment (Fig. 2.7B; $p = 0.0002$ and $p = 0.0068$, respectively, one-way ANOVA followed by Tukey post hoc test). Interestingly, while the overall number of branches returned to baseline 1 month after LPS treatment, the number of distal processes did not (Fig. 2.7A,B; saline versus 1 month, NS and $p < 0.0001$, respectively). This demonstrated that while some traditional markers of reactivity revert back to the

non-reactive baseline, there are some longer-lasting effects of acute inflammation on astrocyte morphology.

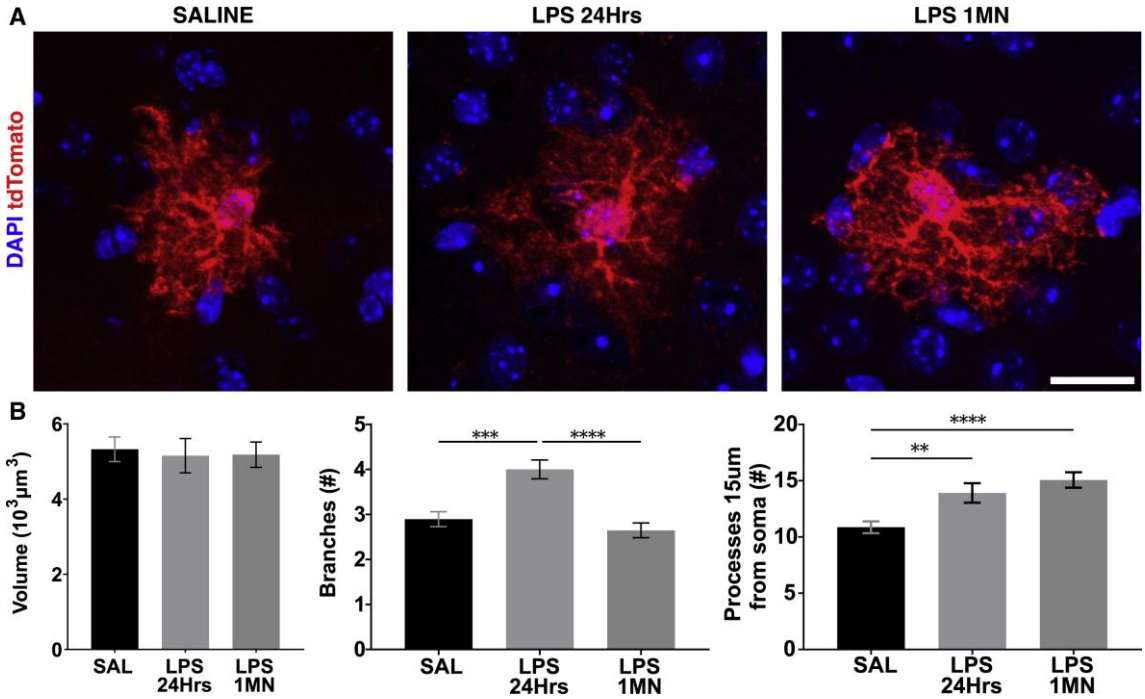


Figure 2.7: Morphological changes in astrocytes pre and post inflammation. (A) Representative morphology of tdTomato-positive astrocytes in *Lcn2CreERT2; Ai9* animals treated with saline or LPS, collected at 24 h and 1 month after treatment (top). **(B)** Quantification of volume (bottom left), number of primary branches (bottom, middle), and number of processes 15 µm from the soma (bottom, right). $^{**}p < 0.01$, $^{***}p < 0.001$, $^{****}p < 0.0001$, ANOVA followed by Tukey's honest significant difference post hoc test. n = 30 pooled astrocytes across three animals. Error bars ± SEM. Scale bar, 20 µm.

To gain a better understanding of the resolution process in astrocytes, we visualized the expression of three physiologically relevant astrocyte-expressed genes at different timepoints after inflammation using RNAscope (Fig. 2.8). Two glutamate transporters (Slc1a3 and Slc1a2) and the pore-forming subunit of the Volume-Regulated Anion Channel (VRAC, Lrrc8a) that are known to be mis-regulated in a variety of brain disease models were chosen for this assessment (Diaz-Castro et al., 2019; Hasel et al., 2021; Peterson and Binder, 2019; Yang et al., 2019). Saline-injected, tamoxifen-induced *Aldh1l1CreERT2; Ai9* animals were used to measure baseline expression. *Slc1a2* (*GLT-1/EAAT2*) expression in tdTomato+ astrocytes did not significantly change after LPS treatment compared with saline-injected mice (Fig. 2.8A; NS, one-way ANOVA). On the other hand, *Slc1a3* expression increased significantly 24 h after LPS treatment, but reverted back to baseline within 7 days (Fig. 2.8B; $p = 0.022$ saline versus 24hrs, $p = 0.99$ saline versus 7D, $p = 0.61$ saline versus 1 month). *Lrrc8a* showed a similar temporal pattern of expression as *Slc1a3*, increasing significantly in tdTomato+ astrocytes 24hrs after LPS treatment, but decreasing to the same level as saline-injected animals 7 days after LPS (Fig. 2.8C; $p = 0.0004$ saline versus 24hrs, $p = 0.3$ saline versus 7D, $p = 0.75$ saline versus 1 month). Taken together, our findings suggest that astrocytes that upregulate reactive markers following inflammation survive in the brain while no longer strongly expressing some of these markers after inflammation has resolved.

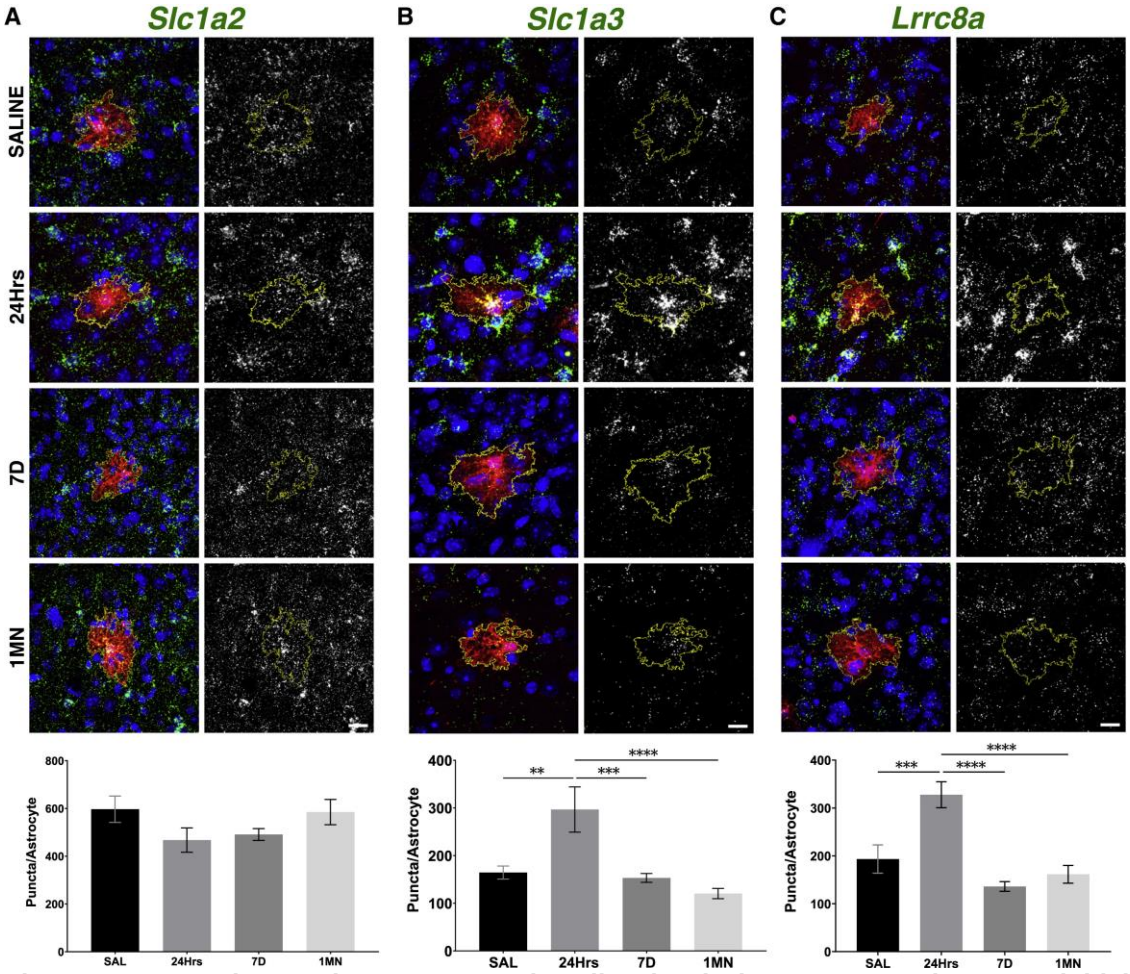


Figure 2.8: Reactive markers return to baseline levels in astrocytes that were initially reactive. (A–C) RNAscope staining (green) for *Slc1a2* (A), *Slc1a3* (B), and *Lrrc8a* (C) in *Lcn2CreERT2; Ai9* animals treated with saline or LPS. Sections were immunostained for tdTomato and counterstained with DAPI. Bottom: quantification of RNAscope puncta per tdTomato+ astrocyte. ∗∗p < 0.01, ∗∗∗p < 0.001, ∗∗∗∗p < 0.0001, ANOVA followed by Tukey's HSD post hoc test. n = 30 pooled astrocytes across three animals. Error bars ± SEM. Scale bars, 20 μm.

Discussion

Reactive gliosis is an early response to brain inflammation, which occurs universally in brain pathologies including infection, trauma, and neurodegenerative disease (Sofroniew, 2020). Despite RA observation in several pathologies and during injury, questions remain about the roles they play in outcomes (Escartin et al., 2021). These questions can begin to be answered by using tools such as the *Lcn2CreERT2* mouse that specifically targets RAs to further study the differences between responses or to target RAs. Here we introduce the *Lcn2CreERT2* mouse as a first step to selectively target and manipulate RAs in the diseased or injured brain when used in combination with traditional astrocytic tools.

Advantages and utility of the Lcn2CreERT2 mouse

There is strong upregulation of *Lcn2CreERT2* in many neuroinflammatory models and negligible expression in the healthy brain. Current tools target markers that are already abundantly expressed in the healthy CNS such as Aldh1l1 or GFAP (Brambilla et al., 2005; Cahoy et al., 2008; Robel et al., 2009; Sofroniew, 2009; Srinivasan et al., 2016). Thus, using tools in which expression can be controlled using Aldh1l1 or GFAP as the drivers can pose difficulties since not all astrocytes become reactive after insult; in these cases both reactive and non-reactive astrocytes would be targeted (Escartin et al., 2021). Thus, any tool that targets astrocytes before they become reactive has the potential downside of

impacting healthy brain function or diluting effects that specifically occur only in RAs. An advantage of the *Lcn2CreERT2* line is that *Lcn2* is minimally expressed in the healthy CNS and so CreERT2 is expressed highly only after injury in reactive cells. This ensures that Cre expression in astrocytes will only be turned on in a reactive setting.

During the development of the *Lcn2CreERT2* mouse it was decided to use the tamoxifen-dependent recombinase *CreERT2* since a there is currently already a large arsenal of floxed transgenic mouse lines and constructs available for use in the study of neuroinflammation (Birling et al., 2012; Daigle et al., 2019; Van Duyne, 2015). Having the *Lcn2CreERT2* mouse express a CreERT2 allows for temporal control of Cre activation. This approach opens up a number of experimental possibilities. Cre activity can be temporally controlled to only be active during experimental windows to prevent off-target recombinase activity. In addition, this allows for the study of reactivity during the course of the neuroinflammatory process. For example, tamoxifen can be given early or late in disease processes such as in the kainic acid model of epilepsy. In the kainic acid model there is a one-week latent period before the development of progressive seizures (Coulter & Steinhäuser, 2015). Giving tamoxifen early or late would allow for the study of RAs that are induced immediately or the RAs that are induced later in the chronic stage. It is very likely that the properties and functions of RAs are very different across time points in disease progression or recovery from injury. By FACS sorting and sequencing RAs at different time

points, heterogeneity of RAs within a disease process can begin to be appreciated.

One point to consider when designing a tool is its utility across many CNS injuries and diseases as RAs are observed in almost all cases. In the work that initially identified *Lcn2* as a gene highly upregulated in RAs, it was suggested to be a pan-RA marker, as its expression was observed in two very different injury models (Zamanian et al., 2012). These models, systemic inflammation by LPS injection and stroke, have since been reported to induce at least two broad categories of RAs that likely represent only two ends of a spectrum, with many subtypes in-between and even within a particular injury or disease process (Anderson et al., 2014; Liddelow et al., 2017). In addition to not being expressed prior to the onset of inflammation, we have thus far found *Lcn2CreERT2* expression in several of the disease models we have explored. *Lcn2CreERT2* upregulation is found in IP LPS, *T. gondii* infection, IS LPS, and other models briefly explored in this work (Figs. 2.2-2.5). Unsurprisingly, expression of tdTomato in the 5XFAD mouse was extremely sparse and restricted to thalamus, consistent with a previous mRNA sequencing study that showed that Lcn2 is not broadly or strongly upregulated in this AD mouse model (data not shown) (Habib et al., 2020). Future studies could continue to expand the number of diseases investigated with the *Lcn2CreERT2* mouse, which would shed light on heterogeneity of RAs.

Permanent fluorescent labeling of RAs using the *Lcn2CreERT2* mouse also opens other research avenues. In our study, we provided proof-of-concept for different directions one could take. FACS was used to isolate Lcn2CreERT2+ cells which will enable sequencing for the study of gene expression changes across a wide variety of not only inflammatory insults, but also examination of the transcriptomic changes that occur throughout the disease course (data not shown). In addition, we explored the fate of astrocytes after acute inflammation, a question that has remained unanswered despite recent advances in astrocyte molecular phenotyping (Diaz-Castro et al., 2021; Escartin et al., 2021; Hasel et al., 2021). By performing longitudinal studies, we observed that the astrocytes that were Lcn2+ 1 day after induction of inflammation remained in the CNS long after the inflammatory response subsided. Further, the expression of markers of astrocyte reactivity analyzed in our study returned to basal levels. These findings suggest that astrocytes that become reactive after an acute injury or insult have the capacity to largely revert their expression profiles to the non-reactive state after the immune and healing response is complete, rather than being tagged for programmed cell death and replaced. What this might mean for the development and progression of brain disease remains to be determined. Future studies could use the *Lcn2CreERT2* mouse to perform longitudinal analysis of the same astrocytes over time using 2-photon microscopy in living mice to address this question further.

Regarding the genes differentially regulated in the tdTomato+ cells of *Lcn2CreERT2; Ai9* mice after low-dose LPS treatment compared with saline controls, mining of previous datasets suggest that *Slc1a3/Glast* also trends toward being upregulated in multiple astrocytic populations 24 hours after high-dose LPS treatment (Hasel et al., 2021; https://www.liddelowlab.com/gliaseq; https://gliaseqrev.ue.r.appspot.com). A similar but more striking upregulation was also observed for *Lrrc8a* 24 hours after high-dose LPS (Hasel et al., 2021). Consistent with our findings, by 72 hours post-LPS treatment the expression of both of these genes appears to revert back to baseline, or at least become noticeably downregulated compared with 24 hours. Interestingly, *Lrrc8a* and other Lrrc8s are differentially regulated also in the R6/2 model of Huntington disease, but in that case, they are downregulated compared with non-carriers (Diaz-Castro et al., 2019). The exploration of the role of VRAC/Lrrc8 in the etiology and progression of a variety of brain disorders is an area of active interest (Mongin, 2016; Yang et al., 2019).

The observation that activated cells are likely to remain in the CNS raises a number of interesting questions for further study. RAs undergo many changes that may impact their normal homeostatic functions (Sofroniew, 2015). It is currently unknown if an RA that can revert to a non-reactive state is able to perform its key homeostatic functions as efficiently as before the injury. Our data showed that one morphological feature of reactivity, increased complexity of distal processes, fails to revert back to baseline levels even 30 days after

inflammation, suggesting that some effects of the inflammatory process might be long lasting. Given the emerging relationship between astrocyte morphology and function, in the future it will be interesting to investigate how this long-lasting effect on number of distal branches affects astrocyte physiology (Lawal et al., 2022). In this regard, the *Lcn2CreERT2* mouse will be useful to analyze many key functions of astrocytes before, during, and after injury (or in disease progression), such as glutamate uptake and potassium buffering, synaptogenesis and synaptic maintenance, regulation of the brain extracellular space, and cerebrovascular coupling, to name a few. Fluorescent labeling also opens the possibility to examine RAs in real time in living mice across disease and injury progression, allowing a live look-in at some of the more controversial aspects of reactivity, such as migration, proliferation, and changes in astrocyte connectivity (Escartin et al., 2021).

Limitations of the study

There are 3 main limitations in the study of RAs when using the *Lcn2CreERT2* mouse. The percentage of *Lcn2CreERT2* expressing astrocytes was lower than the percentage of cells which stained for GFAP or endogenous Lcn2. This limitation is compounded by the fact that *Lcn2*, which was initially thought to be upregulated in most mouse brain disease models, does not appear to be strongly upregulated in models of Alzheimer's or Huntington disease (Diaz-Castro et al., 2019; Habib et al., 2020; Zamanian et al., 2012). In addition, there seems to be some regional specificity to the expression of *Lcn2CreERT2* in

astrocytes. While most areas of the forebrain expressed tdTomato in *Lcn2CreERT2; Ai9* animals after induction of inflammation, labeling of astrocytes was widespread in thalamus and hypothalamus, somewhat limited in the dorsal cortex, and very low in the dorsal hippocampus. While there might be many reasons behind the specificity in *Lcn2CreERT2* expression, from alternative splicing of the targeted exon to existence of alternative *Lcn2* promoters, the expression pattern could be revealing underlying regional biological differences in RAs. Molecular, functional, and morphological differences have been noted for several other regions in the healthy and diseased brain, and this might just be one more example of astrocyte heterogeneity (Adams & Gallo, 2018; Anderson et al., 2014; Sofroniew, 2015).

The third potential limitation is expression of *Lcn2CreERT2* in non-astrocytic cells. *Lcn2CreERT2* is also expressed in endothelial cells following LPS, which was expected from our initial observations of endogenous Lcn2 expression. Therefore, *Lcn2CreERT2* could also be a useful tool for the study of reactive endothelial cells and the BBB in brain injury and disease. In order to focus our study on RAs specifically, we used a combinatorial approach in which an AAV viral construct AAV-GFAP(long)-FLEX-gCaMP7f was used to drive expression of Cre-dependent gCaMP7 under the GFAP promoter (data not shown) (Agnew-Svoboda et al., 2022). The use of this approach allowed us to intersect targeting of reactive cells (*Lcn2CreERT2*) with astrocytes (GFAP), thereby preventing LPS-induced endothelial expression of Cre. As we were able

to observe robust expression of GCaMP7 in astrocytes using this approach, it could be used in future studies to examine changes in RA calcium signaling. Similarly, the use of the *Lcn2CreERT2* line with intersectional transgenic drivers or viral vectors that selectively express GOIs based on the overlapping or sequential expression of multiple recombinases (e.g., Cre and Flp, Cre and Dre) will allow for labeling of subpopulations of reactive cells with greater specificity and also make a variety of Boolean logic operations (AND, NOT, OR) available (Awatramanil et al., 2003; Fan et al., 2020; Fenno et al., 2014, 2020; Ubina et al., 2021). For flow cytometry and FACS, combining tdTomato detection with an antibody for a surface marker of astrocytes like ACSA2 could be a suitable solution (G. Kantzer et al., 2017; Lattke et al., 2021). Overall, we view the *Lcn2CreERT2* mouse as a first-generation tool for the study of RAs. As heterogeneity of RAs is explored further, next generation tools could be designed to target other specific subsets of RAs that are predominantly expressed in a particular brain injury or disease process.

CHAPTER THREE

Induction of neuroinflammation for the longitudinal study of reactive astrocytes in *Lcn2CreERT2* mice

Teresa Ubina [1,3], William Agnew-Svoboda [1,3], Zoe A. Figueroa [1,4], Emma H. Wilson [1,2,4], Todd A. Fiacco [1,2,3,5,†], and Martin M. Riccomagno [1,2,3,5,6,*]

1. Neuroscience Graduate Program,
2. Biomedical Sciences Graduate Program,
3. Department of Molecular, Cell, and Systems Biology, University of California, Riverside, CA, 92521
4. Division of Biomedical Sciences, University of California, Riverside, CA, 92521
5. Technical contacts
6. Lead contact

*martinmr@ucr.edu
†toddf@ucr.edu

Abstract

During brain disease, astrocytes can reprogram into a reactive state that alters many of their functions. This protocol describes several methods utilizing lipopolysaccharide (LPS) from *E. coli* for the study of neuroinflammation and reactive astrogliosis. We employ the *Lcn2CreERT2* mouse crossed into a fluorescent Cre reporter line to label a subset of reactive astrocytes during and after inflammation. Using this strategy astrocytes remain labeled for at least 1-month post-inflammation, allowing for the longitudinal study of astrogliosis induction, progression and/or resolution.

For complete details on the use and execution of this protocol, please refer to Agnew-Svoboda et al., 2022.

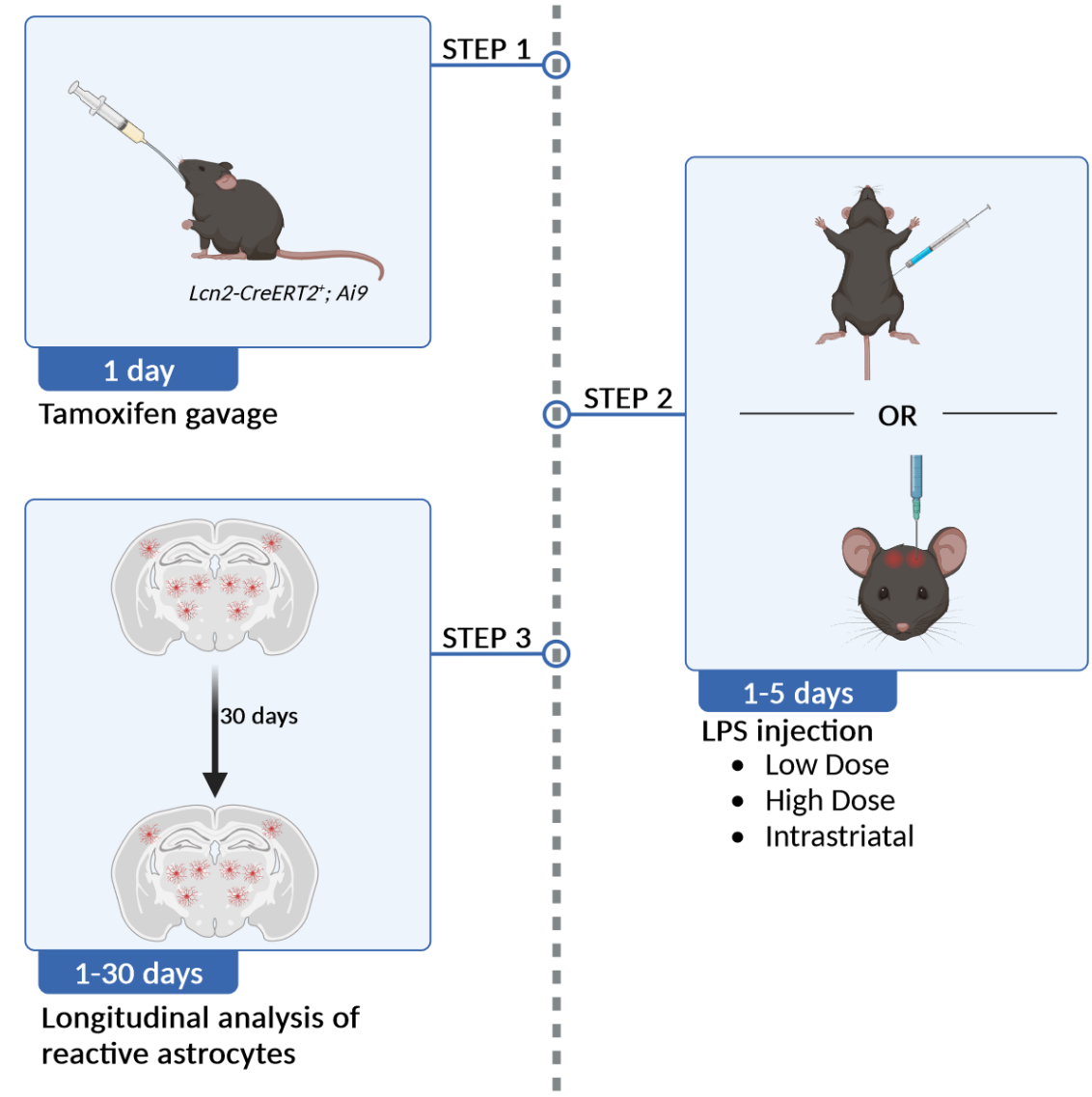


Figure 3.1: Graphical abstract of low dose, high dose, and intrastriatal LPS protocols

Before you begin

1. *Identify your institution's animal use regulatory committee and confirm that all experiments conform to their regulatory guidelines and standards.*
2. *The use of anti-inflammatories as analgesics is not recommended for these procedures since this will attenuate the inflammatory response. The authors suggest working with your institution's regulatory committee and a veterinarian to determine an alternative.*

This protocol describes three methods for the induction and labeling of reactive cells in models of neuroinflammation in the *Lcn2CreERT2* mouse. *Lcn2CreERT2* mice are first crossed into the *Ai9* Cre reporter line and the *Lcn2CreERT2*$^{+}$*; Ai9* offspring are aged to a minimum of 6 weeks prior to beginning one of the three neuroinflammatory induction methods. The low- and high-dose LPS protocols are designed to induce systemic inflammation and can be used to broadly study neuroinflammatory-related processes (Zhao et al., 2019). The injection of LPS into the striatum causes neuroinflammation that leads to a progressive loss of dopaminergic neurons in the substantia nigra (Hunter et.al., 2009). This progressive loss of dopaminergic neurons mirrors the progressive loss seen in Parkinsonian disorders (PD) and can be used to study the role of neuroinflammation in the progression of PD. The role of reactive astrocytes (RAs) in disease onset and progression has been difficult to study. The introduction of new tools to specifically label and target reactive astrocytes like

the *Lcn2CreERT2* mouse will aid in understanding astrocyte reactivity and the roles of RAs in disease processes.

Institutional permissions

All animal procedures detailed in the following sections were performed according to the University of California Riverside's Institutional Animal Care and Use Committee (IACUC) guidelines.

Generate *Lcn2CreERT2; Ai9* mice

Timing: 19 weeks

Before experiments can begin *Lcn2CreERT2*$^{+}$*; Ai9* animals must be generated. The lines used in this protocol are *Lcn2CreERT2* and the Cre-dependent reporter line *Ai9*. Both lines are on the C57BL/6N background. There are reports that certain strains may be resistant to LPS challenge (Catorce and Gevorkian, 2016). Results may vary if a different strain background is used. The *Ai9* line contains a CAG promoter and a floxed stop sequence followed by a tdTomato sequence inserted at the Rosa locus. Other Cre-dependent reporter lines may be used instead. For example, several Cre-dependent lines driving a variety of genetic tools have been generated by the Allen Institute for Brain Science (Madisen et al., 2015; Daigle et al., 2018; Madisen et al., 2010; Madisen et al., 2012). Of note, we find that the *Ai9* reporter provides robust labeling in astrocytes and intensity of the fluorescent labeling may vary if another reporter is used.

1. Cross *Lcn2CreERT2*$^{+}$ mice with homozygous *Ai9* mice (Jax strain 007909) to obtain *Lcn2CreERT2*$^{+}$*; Ai9* mice.

2. Extract genomic DNA from tissue samples and genotype the offspring via PCR for *Lcn2CreERT2* using the following primers: Forward 5'-GGCAGTCCAGATCTGAGCTGC-3' and Reverse 5'-TGCATCGACCGGTAATGCAGG-3'. The expected product size is 408bp.

    a. Use only animals positive for the *Lcn2CreERT2* transgene.

    b. The provided cycling conditions have been optimized with Promega GoTaq green master mix (cat# M7123). If a different master mix is used the optimal conditions may vary.

PCR reaction master mix

Reagent	Amount
DNA template	1ml
GoTaq (2x)	5 ml
Forward primer (10mM)	0.2 ml
Reverse primer (10mM)	0.2 ml
ddH_20	3.6 ml

PCR cycling conditions

Steps	Temperature	Time	Cycles
Initial Denaturation	95 °C	3 min	1
Denaturation	95 °C	30 sec	39 cycles
Annealing	59 °C	30 sec	
Extension	72 °C	45 min	
Final extension	72 °C	5 min	1
Hold	4 °C	forever	

3. Age animals to 6 weeks.

CRITICAL: The authors have not observed reporter induction in the absence of tamoxifen; however, we still suggest the following controls be used: tamoxifen +

saline; oil + LPS; and oil + saline. Be sure to generate enough animals for controls.

Tamoxifen

Timing: 1 hour to overnight

The *Lcn2CreERT2* line uses a tamoxifen dependent Cre. Thus, the *Lcn2CreERT2*$^{+}$*; Ai9* mice require tamoxifen for recombination and deletion of the stop cassette to allow expression of the red fluorescent protein tdTomato.

4. Weigh appropriate amount of tamoxifen and add to corn oil to create a stock of 20mg/ml tamoxifen in corn oil.
5. Protect container from light and place on a shaker for 1 hour to overnight at 37°C until fully dissolved.
    a. Occasionally tamoxifen may not enter solution. Vigorously vortexing or sonication may help to dissolve any difficult crystals.
6. Once tamoxifen has fully dissolved, store at 4°C and protect from light.
    a. Do not use prepared tamoxifen after 1 month from preparation date. It is recommended to make fresh tamoxifen aliquots weekly.
    b. Inspect mixture before each use. It should be clear and free of contaminants.

CRITICAL: Tamoxifen is toxic, be sure to use all proper precautions and dispose of contaminated waste appropriately.

CRITICAL: Be sure the corn oil being used is not rancid. Rancid corn oil can affect the survival of animals. Corn oil should be kept at room temperature.

CRITICAL: While gavage is a simple technique, care must be taken to avoid esophageal damage.

LPS

Timing: 15 min

Lipopolysaccharides (LPS) from *E. coli* are known to induce an inflammatory response when given intraperitoneally and when injected directly into the brain[1,3,4].

7. Reconstitute LPS from *E. coli* in sterile saline. The solution will be hazy and may have a yellow tint.
    a. 3.5mg/ml for low-dose intraperitoneal (IP) injection
    b. 7.5mg/ml for high-dose IP injection or intrastriatal injection
8. Aliquot and store at -20°C.
    a. Avoid freeze-thaw cycles and do not reuse thawed aliquots.
    b. Aliquot size will depend on the number of animals you plan to inject at once. Just prior to low-dose or high-dose injection, LPS will be diluted in sterile saline. Plan your aliquots accordingly as thawed aliquots cannot be refrozen and used later.

c. For low-dose LPS 25ml aliquots are typically enough for two doses for a 25g animal. For high-dose LPS 80ml aliquots are typically enough to dose one 25g animal twice. The aliquot sizes given are based on usage with low dead space syringes and needles. Do not forget to account for reagent loss in the dead space of syringes and needles when determining aliquot size.

Optional: Use of syringes and needles with low dead space such as insulin syringes are preferred to avoid loss of LPS but are not required.

d. The stability of LPS is affected by each freeze-thaw cycle and can be stored at -20°C for up to two years.

CRITICAL: LPS is extremely toxic to humans. Be sure to use all proper precautions and dispose of contaminated waste properly

Key resources table

REAGENT or RESOURCE	SOURCE	IDENTIFIER
Antibodies		
Rat anti-GFAP (1:500)	Invitrogen	13-0300
Tomato lectin (1:75)	Vector labs	B-1175-1
Rabbit anti-DsRed (1:500)	Takara	632496
Rabbit anti-Iba1 (1:500)	Fujifilm	019-19741
Chicken anti-Fox3 (NeuN) (1:500)	Aves labs	NUN-0020
Mouse anti-Tyrosine Hydroxylase (1:500)	R&D systems	MAB7566
Chicken anti-mCherry (1:500)	Aves labs	MCHERRY-0100
Chemicals, peptides, and recombinant proteins		
Lipopolysaccharides from *Escherichia coli*	Sigma-Aldrich	L2880
Sterile saline solution	Covetrus	069169
Tamoxifen	Sigma-Aldrich	T5648
Corn Oil	Sigma-Aldrich	C8267
GoTaq Green Master Mix	Promega	M7123
Fluoro-Gel	Electron Microscopy Sciences	17983
Critical commercial assays		
RNAscope Multiplex Fluorescent Detection kit v2	Advanced Cell Diagnostics	323110
Experimental models: Organisms/strains		
Lcn2CreERT2 mice	Riccomagno lab	
Ai9 mice	The Jackson Laboratory	Strain #007909
Oligonucleotides		
Lcn2CreERT2 forward primer	IDT	GGCAGTCCAGATCT GAGCTGC
Lcn2CreERT2 reverse primer	IDT	TGCATCGACCGGTAA TGCAGG
Other		
Animal feeding needle (gavage needle), 20g, 1.5”	Fisher	01-208-87
Leica DMi8 A Confocal microscope	Leica	DMi8 A
Leica CM1950 cryostat	Leica	CM1950
Fisherbrand Superfrost Plus Microscope Slides	Fisher	12-550-15

Table 3.1: List of required materials required for the low-dose, high-dose, and intrastriatal LPS protocols.

Step-by-step method details

Low-dose LPS

Timing: 8-30 days

In *Lcn2CreERT2; Ai9* mice low-dose IP LPS treatment will induce systemic inflammation, including reactive astrogliosis. When given tamoxifen during this inflammation the result will be fluorescent labeling of a subset of reactive cells[1]. Tissue may be harvested on day 8 or 30 for longitudinal studies of labeled astrocytes. A summary of the timing for low-dose treatments can be found in figure 3.2. Expected outcomes can be found in figure 3.3.

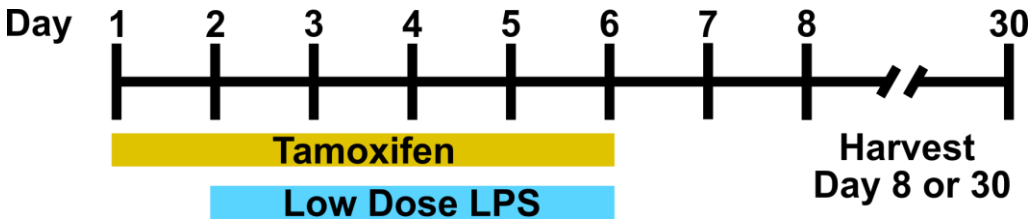


Figure 3.2: Summary of the timing of treatments for low dose protocol.

1. On day 1, weigh each animal and calculate the amount of tamoxifen in corn oil (20mg/ml) to orally gavage at 150mg/kg.
    a. Warm tamoxifen in corn oil to room temperature for at least 15 minutes prior to oral gavage.
2. Using an animal feeding needle (Fisher), orally gavage the appropriate amount of tamoxifen in corn oil for each animal.

Note: See troubleshooting 1

3. On day 2, weigh each animal and orally gavage tamoxifen as done on day 1.

4. Just prior to LPS injection, add sterile saline to a fresh LPS aliquot thawed on ice to a final concentration of 0.35mg/ml.

    a. Mix well and briefly vortex if needed. Store on ice until injection.

5. Calculate amount of LPS to be injected so that each animal receives 1.5mg/kg.

    a. It is not recommended to inject a volume greater than 10ml per kg of body weight.

6. Hand-restrain the animal and inject appropriate amount of LPS intraperitoneally.

Note: See troubleshooting 2

7. Repeat steps 3-6 for days 3-6.

8. Harvest tissue on day 8 or any desired time after gavage if performing longitudinal studies. We have harvested brains up to 30 days after gavage.

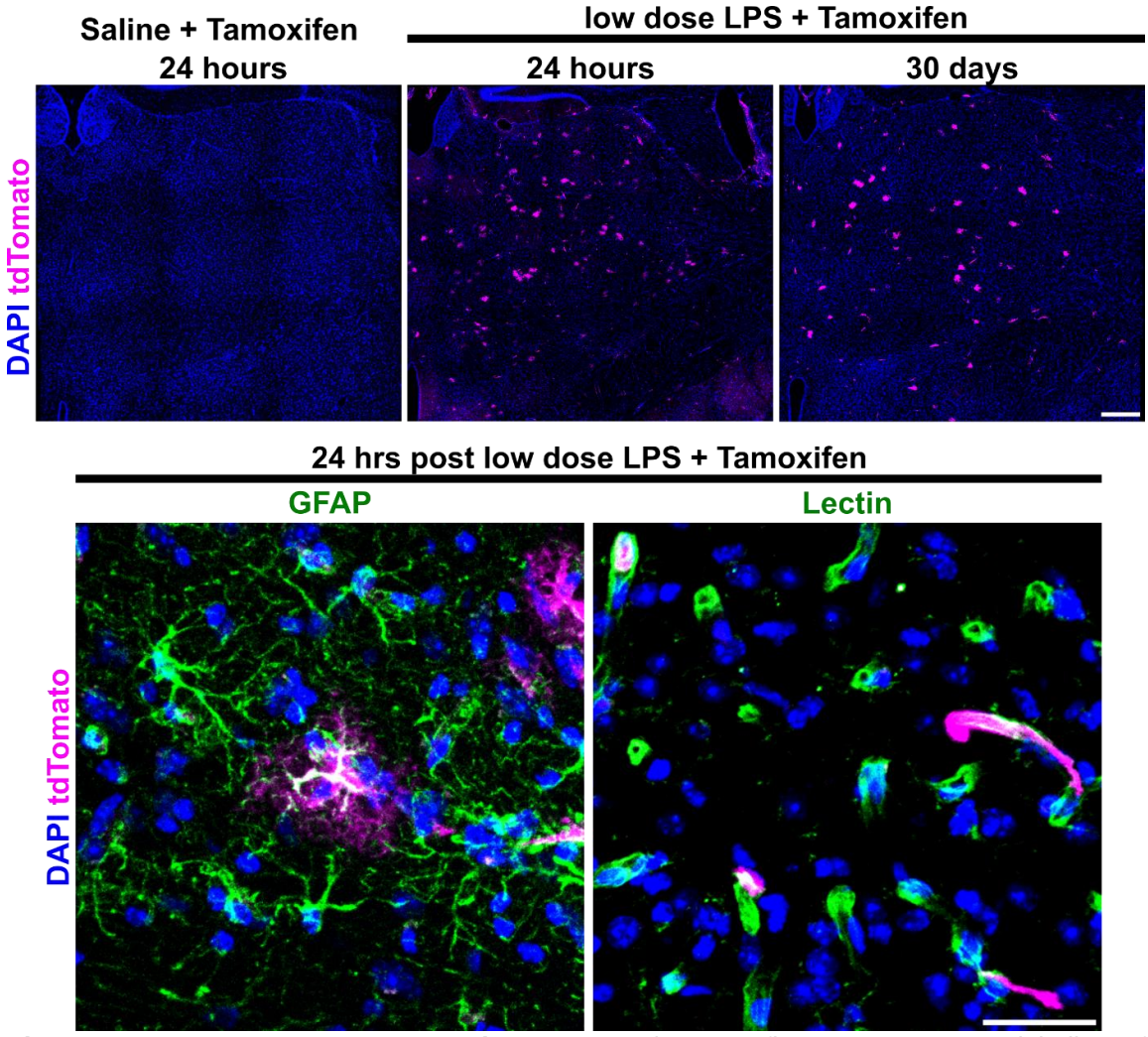


Figure 3.3: Low-Dose LPS expected outcome. tdTomato fluorescent reporter labeling of primarily reactive astrocytes and endothelial cells within the thalamus. No tdTomato labeling is observed in the saline control. Scale 300mm top, 30mm bottom. Sections are 20mm in thickness. Images were taken on a Leica DMi8 M confocal microscope.

High-dose LPS

Timing: 4-30 days

High-dose LPS treatment will induce systemic inflammation, including reactive astrogliosis[10]. Treating *Lcn2CreERT2; Ai9* mice with a single high-dose of LPS will result in the fluorescent labeling of reactive cells, including astrocytes. Tissue may be harvested as soon as day 4 or may be harvested at day 30 for longitudinal studies of labeled astrocytes. A summary of the timing for high-dose treatments can be found in figure 3.4. Expected outcomes can be found in figure 3.5.

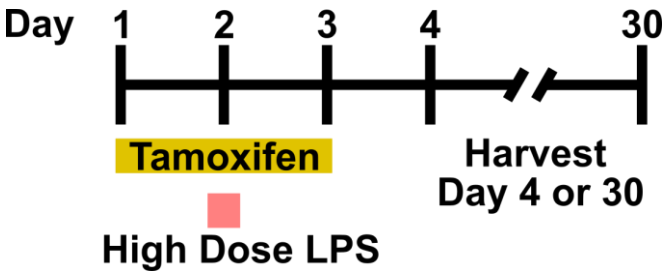


Figure 3.4: Summary of the timing of treatments for high-dose protocol.

9. On day 1, weigh each animal and calculate amount of tamoxifen in corn oil (20mg/ml) to orally gavage at 150mg/kg.
    a. Warm tamoxifen in corn oil to room temperature for at least 15 minutes prior to oral gavage.
10. Orally gavage the appropriate amount of tamoxifen in corn oil for each animal.

Note: See troubleshooting 1

11. On day 2, weigh each animal and orally gavage tamoxifen as done on day 1.

12. Just prior to LPS injection, add sterile saline to a freshly thawed LPS aliquot to a final concentration of 3mg/ml.

    a. Mix well and briefly vortex if needed. Store on ice until injection.

13. Calculate the amount of LPS to be injected so that each animal receives 10mg/kg.

14. Appropriately restrain the animal and inject LPS intraperitoneally.

Note: See troubleshooting 2

15. Orally gavage appropriate amount of tamoxifen in corn oil for each animal.

Note: See troubleshooting 1

16. On day 3, orally gavage with tamoxifen in corn oil.

Note: See troubleshooting 1

17. Harvest tissue on day 4 or any desired time after gavage if performing longitudinal studies. We have harvested brains up to a month after gavage.

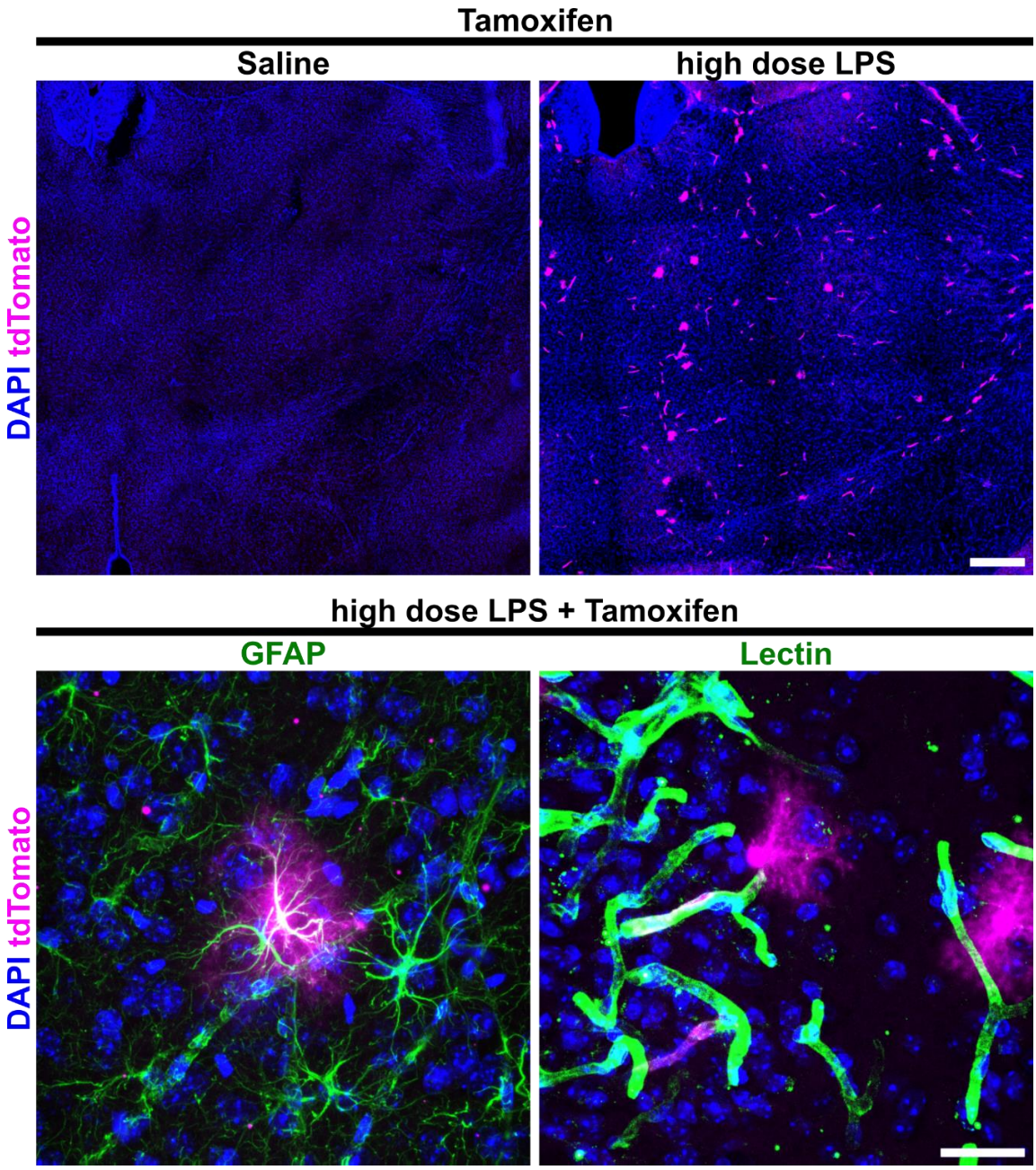


Figure 3.5: High-Dose LPS expected outcome. tdTomato fluorescent reporter labeling of primarily reactive astrocytes and endothelial cells. No tdTomato labeling is observed in the saline control. Scale 300mm top, 30mm bottom. Sections are 20mm in thickness. Images were taken on a Leica DMi8 M confocal microscope.

Intrastriatal LPS

Timing: 9 days

In *Lcn2CreERT2*$^{+}$*; Ai9* mice intrastriatally injected LPS will induce Parkinson-like symptoms and will result in fluorescent labeling of reactive cells, including reactive astrocytes (Agnew-Svoboda et al., 2022; Hunter et al., 2009). Tissue may be collected as soon as day 9 or later for longitudinal studies of labeled astrocytes. A summary of the timing of intrastriatal treatments can be found in figure 3.6. Expected outcomes can be found in figure 3.7.

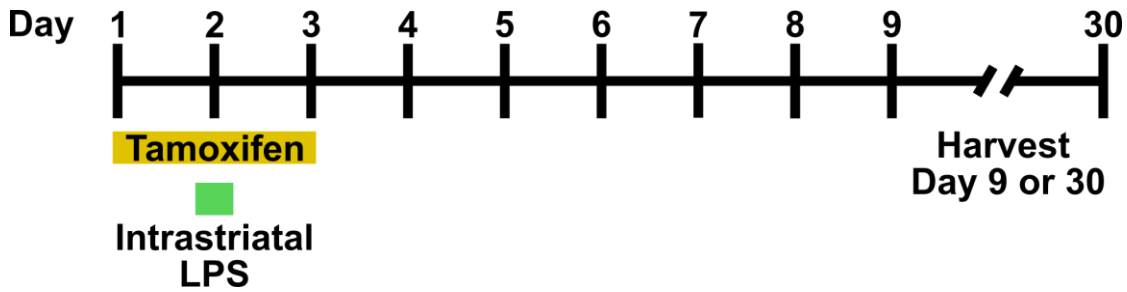


Figure 3.6: Summary of the timing of treatments for intrastriatal LPS protocol.

18. On day 1, administer tamoxifen in corn oil via oral gavage at a dose of 150mg/kg.

Note: See troubleshooting 1

19. On day 2, administer tamoxifen as done on day 1.

Note: See troubleshooting 1

20. Just prior to LPS injection thaw one 7.5mg/ml aliquot of LPS.

    a. Mix well and vortex briefly if needed. Store on ice until injection.

21. Anesthetize animal with Isoflurane in an induction chamber before mounting on a stereotaxic rig.
22. Once the animal is fully anesthetized, shave and aseptically prepare the incision site.
    a. Sufficient anesthesia is determined by the relaxed posture of the animal and insensitivity to toe and tail pinches.
    b. The authors find that maintaining Isoflurane at 1.5-2% is sufficient to keep the animal anesthetized at the appropriate level throughout the procedure.
23. Make an incision along the midline on the top of the head to expose the skull.
24. Level bregma and lambda landmarks on the skull.
25. Drill holes in the skull using a 0.7mm burr at the four following coordinates from Bregma: A/P +1.18mm, M/L ±1.5mm and A/P -0.34, M/L ±2.5mm
26. Load 1.5ml of 7.5mg/ml LPS into a Hamilton Neuros syringe with a 32G needle.
27. Inject 250nl of 7.5mg/ml LPS into each of four locations at a rate of 0.5ml/min, for a total of 1ul LPS injected. After each injection leave needle in place for 5 minutes prior to withdrawing.

a. Coordinates for injection from bregma: A/P +1.18mm, M/L ±1.5mm, D/V -3.5mm and A/P -0.34, M/L ±2.5mm, D/V -3.2mm.

Note: See troubleshooting 2

28. After the last injection close skin with Michel Suture Clips. Give 200ul of sterile saline subcutaneously. Monitor the animal after surgery on a heating pad until awake and freely moving.

CRITICAL: Heating pad must not be warmer than 37°C. Warmer temperatures may burn and injure the animal.

29. On day 3, administer tamoxifen as on day 1.

Note: See troubleshooting 1

30. Harvest tissue on day 9 (7 days after LPS injection) or later for longitudinal studies.

    a. If doing longitudinal studies suture clips must be removed 10-14 days after surgery.

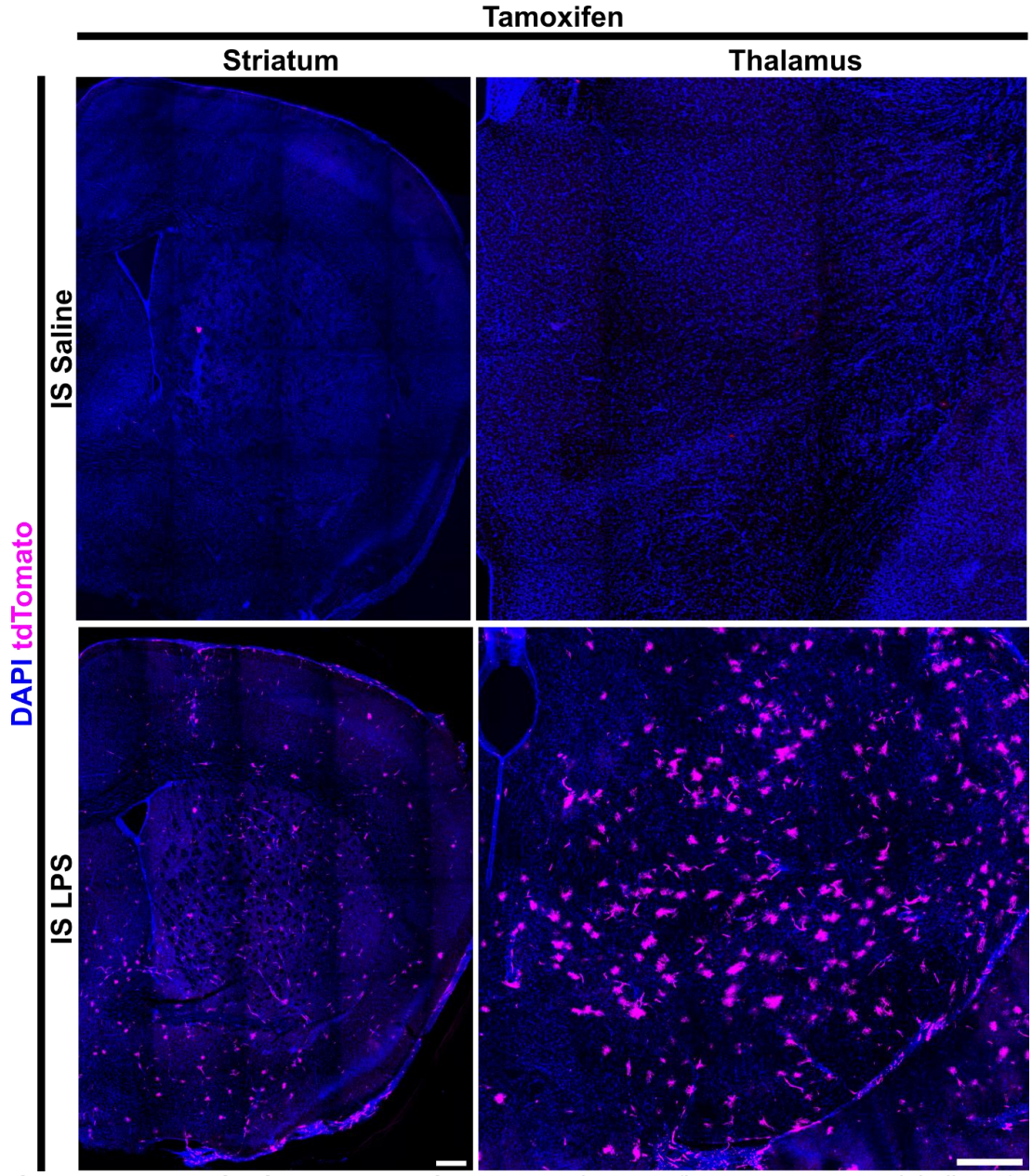


Figure 3.7: Intrastriatal LPS expected outcome. tdTomato fluorescent reporter labeling of primarily reactive astrocytes and endothelial cells in the striatum and thalamus. Scale 300mm. Sections are 20mm in thickness. Images were taken on a Leica DMi8M confocal microscope.

Cryopreservation and sectioning of tissue

Timing: 2-3 days

Cryopreservation of tissue is performed prior to sectioning on a cryostat.

Preparation and sectioning of cryopreserved tissue is performed as follows.

31. After perfusion and tissue collection, brains are fixed in 4% PFA overnight at 4°C in a 6-well plate filled with approximately 8ml.
32. Rinse tissue 3x in PBS, filling the well each time (~8ml).
33. Move brains to 30% sucrose and store at 4°C overnight.
34. The next day replace 30% sucrose. If the brain floats incubate overnight again at 4°C. Repeat sucrose replacement as necessary until brain sinks. Once the brains have sunk, dry on a paper towel for 5-10 minutes.
35. Rinse brains in OCT to coat and remove any surrounding bubbles, then put into an embedding mold filled with OCT.
36. Place mold on dry ice until fully frozen. Store at -80°C until ready to cut on a cryostat.
37. Cut 15-20mm sections on a cryostat and mount onto charged slides.
    a. Cut 15mm sections if preparing for RNAscope.

Note: See troubleshooting 3

38. After cutting, let the tissue dry on the slide for 2 hours. Cryosections can be used for RNAscope and/or immunohistochemistry (IHC). If doing RNAscope follow the manufacturer's suggested instructions. If doing IHC, proceed to the immunohistochemistry section of this protocol. Alternatively, slides can be stored at -80°C for future use but the drying step must be performed prior to storage.

    a. If you plan on performing a combination of RNAscope and IHC, complete the RNAscope procedures first and begin the immunohistochemistry procedures beginning at step 41.

Immunohistochemistry

Timing: 2 days

Immunohistochemistry is performed as follows:

39. Place slides into a slide mailer filled with PBS and incubate at RT for 15 minutes. If OCT is not removed after 15 minutes, repeat PBS wash.

CRITICAL: Treat slides gently. Vigorously pouring PBS or other liquids onto slides may result in the tissue dislodging.

CRITICAL: Tissue should not be allowed to dry at any time beyond this point. Drying out will drastically reduce the quality of your tissue and IHC.

40. Dry the slide around the tissue gently while taking care to keep the tissue moist. Draw around the tissue with a hydrophobic pen and let dry while keeping the tissue moist.

a. This may require gently pipetting PBS directly on top of your tissue occasionally while the hydrophobic barrier dries.

41. Block sections with 10% serum and 0.1-0.3% Triton-X100 in PBS for 1 hour at RT in a humidifying chamber with enough volume to cover tissue.

    a. A simple humidifying chamber can be made from a plastic slide box holder with damp paper towels at the bottom.

    b. Serum type will depend on your antibodies. Be sure to match the serum type to the secondary antibody host. If using goat secondary antibodies, goat serum is preferred.

    c. If performing IHC after RNAscope, block with 3% bovine serum albumin (BSA) in PBS.

42. Sections are then incubated overnight at 4°C in a humidifying chamber with primary antibodies in 1% serum and 0.1% Triton-X100 in PBS. Use enough volume to sufficiently cover the tissue.

    a. If using tomato lectin, add in with primary antibodies.

    b. If performing IHC after RNAscope, mix antibodies and/or lectin in 3% BSA in PBS.

43. Wash slides in a slide mailer filled with PBS for 10 minutes 3x at RT.

44. Incubate slides at RT in a humidifying chamber for 1-2 hours with secondary antibodies, 1% serum, and 0.1% Triton-X100 in PBS. DAPI at

1:1000 dilution may also be added at this step if desired to label cell nuclei. Use enough volume to sufficiently cover the tissue.

a. If using tomato lectin, a fluorescently-conjugated streptavidin is added at this step.

b. If performing IHC after RNAscope, mix antibodies and/or lectin in 3% BSA in PBS.

45. Wash slides in a slide mailer filled with PBS for 10 minutes 3x at RT.

46. Mount with Fluoro-Gel (or other desired mounting medium) and coverslip, then let the Fluoro-Gel dry before using nail polish to seal the coverslip.

Note: See troubleshooting 4

47. Store at 4°C until ready to image.

Limitations

These protocols were performed with animals on the C57BL/6N background. There are reports that LPS injection in certain strains may be resistant to LPS challenge. Keep this in mind when crossing *Lcn2CreERT2* animals onto different strain backgrounds[4].

The second potential limitation of using these approaches is that *Lcn2CreERT2* is also expressed in some non-astrocytic cells (mainly endothelial cells) following LPS injection (Zamanian et. al., 2012). While this makes the *Lcn2CreERT2* line a potentially useful tool for the study of reactive endothelial cells in brain injury and

disease, to selectively label reactive astrocytes we recommend using a combinatorial approach or co-labeling with an astrocyte-specific marker. Finally, Lcn2^{+} astrocytes represent only a subset of reactive astrocytes and there seems to be regional specificity to the expression of *Lcn2CreERT2* in these cells (Agnew-Svoboda et al., 2022; Wheeler et al., 2020; Zamanian et al., 2012; Liddelow et al., 2017). This should be carefully considered when interpreting observations stemming from the use of this system.

Troubleshooting

Problem 1: Oral gavage difficulty (related to step 2, 10, 15, 16, 18, or 19). Animals are difficult to gavage, are injured during gavage, or perish shortly after oral gavage.

Potential solutions:

- Inspect the gavage needle before each use and discard if there are any rough or sharp areas. Esophageal tissue is delicate and can be easily damaged by rough edges on the gavage needle.
- It is not recommended to orally gavage more than 10ml per kg body weight.
- Measure the end needle to the caudal portion of the sternum and visually note or mark where the mouth of the animal meets the needle. Do not advance the needle further than this point as internal injury to the animal is likely.

- Ensure the scruff of an animal is secure. A mobile head is dangerous for the animal and the person performing the gavage. A proper scruff ensures that the animal's head is not mobile. Starting the scruff closer to the head and tucking the tail in between the third and little fingers often helps to secure the animal. The authors find that an improper scruff is often the case with new users and is what causes the most difficulty.

- Begin gavage needle insertion on the animal's left (your right) side and gently guide it to the back of the throat, then gently guide the needle down. Gavage needle should easily slide down the esophagus, no force should be required to advance the needle. This should be done in one smooth movement. If any force is required to advance the needle, remove it and try again.

- The gavage needles provided in this protocol are straight, have a metal shaft, and a plastic bulb at the tip. This is based on user preference. There are many variations of feeding needles available and users may find they are more comfortable using a different type. It is not recommended that users new to oral gavage use a gavage needle with a plastic shaft as the animal may bite through this.

Problem 2: labeling of reactive astrocytes after LPS injection (related to step 6, 14, or 27).

No or low numbers of reactive astrocytes are labeled after injection.

Potential solutions:

- Mix LPS thoroughly.
- Check that LPS has not expired or experienced multiple freeze-thaw cycles.

Problem 3: Tissue integrity (related to step 37).

Tissue is cracked, difficult to cut, or otherwise looks poor.

Potential solutions:

- Freeze tissue shortly after collection. Longer times between collection and freezing will result in more degradation of tissue.
- Thaw tissue to -20°C for one hour prior to sectioning on cryostat.
- Change to a fresh blade.
- Cut tissue within one year of freezing.
- Ensure tissue does not dry at any point beyond step 39.
- Try a gentler treatment of tissue on slides.

Problem 4: Low or poor signal intensity (related to step 47).

IHC signal intensity is low or poor.

Potential solutions:

- It is best to image slides within one month of completion of IHC.

- Change post-fix timing. Longer fixation times may mask epitopes. A 2 hour or a 4 hour fixation time may yield better results.
- Increase Triton-X100 concentration. Nuclear epitopes tend to require more permeabilization.
- Change antibody concentrations.
- Check that antibodies are not old, expired, or have been mishandled.
- All antibodies used in the original paper[1] are known to work well with overnight fixation at a 1:500 dilution or 1:75 dilution for tomato lectin. Some antibodies may work best on vibratome floating sections (not frozen).
- RNAscope is harsh on tissue and not all epitopes will survive this process. Using the weakest protease possible during the RNAscope protocol will increase the chances of an antibody working. Fox3 (Encor, CPCA-FOX3) is one of the antibodies known to our lab to stain poorly after RNAscope. GFAP (Invitrogen, 13-0300) and ALDH1L1 (Cell Signaling, 85828S) work well after the RNAscope process.

Resource availability

Lead contact

Further information and requests for resources and reagents should be directed to and will be fulfilled by the lead contact, Martin Riccomagno martinriccomagno@ucr.edu.

Materials availability

The *Lcn2CreERT2* mouse line is available from the Riccomagno, Fiacco and Wilson labs upon request.

Data and code availability

This study did not generate and analyze datasets or code.

Acknowledgments

This work was supported by grants from the National Institutes of Health R03AG063264, R21NS109918, R01DA048815, and R01DA048815-03S1.

Author contributions

Teresa Ubina: Data collection and analysis, writing and editing manuscript.

William Agnew-Svoboda: Data collection and analysis

Zoe A. Figueroa: Data collection and analysis

Emma Wilson: Idea conception, editing manuscript, obtained funding for project.

Todd Fiacco: Idea conception, writing and editing manuscript, obtained funding for project.

Martin Riccomagno: Idea conception, writing and editing manuscript, obtained funding for project.

Declaration of interests

The authors declare no competing interests.

CHAPTER FOUR

A novel FlpO recombinase mouse line to target a subset of reactive astrocytes

Teresa Ubina[1,2], William Agnew-Svoboda[1,2], Zoe Figueroa[1,3], Jose L. Martin[3,4], Emma H. Wilson[1,3,4], Todd Fiacco[1,2], Martin M. Riccomagno[1,2]

[1] Neuroscience Graduate Program, University of California, Riverside, Riverside, CA 92521, USA

[2] Department of Molecular, Cell, and Systems Biology, University of California, Riverside, Riverside, CA 92521, USA

[3] Division of Biomedical Sciences, University of California, Riverside, Riverside, CA 92521, USA

[4] Biomedical Sciences Graduate Program, University of California, Riverside, Riverside, CA 92521, USA

Abstract

Astrocytes ordinarily execute vital processes for proper brain function but reprogram into “reactive” astrocytes (RAs) following injury. Astrocytes become reactive to varying degrees in virtually all neurodegenerative diseases and brain disorders. When astrocytes become reactive, they undergo changes in gene expression, morphology and function. This response varies based on the type of insult and brain region that is affected. With the aim of targeting, labeling and manipulating RAs, we have designed RA-specific recombinase lines. Our lab has previously generated an *Lcn2CreERT2* line that is capable of permanently labeling a subset of RAs and other reactive cells. Here, we describe the generation of a different recombinase line driven by the endogenous *Complement 3* (*C3*) promoter. C3 is involved in the complement cascade and has been shown to be significantly upregulated in a subset of RAs. We used this knowledge to develop an inducible FlpO knock-in mouse line (*C3-FlpOER^{T2}*) that targets a subset of RAs. We then characterized the *C3-FlpOER^{T2}* line in several models of neuroinflammation. The generation of a FlpO line opens the possibility of combinatorial approaches using well validated astrocytic Cre lines to study RA function and heterogeneity.

Introduction

Once viewed as purely supportive cells, astrocytes are now known to be active players in central nervous system (CNS) homeostasis and disease. In the healthy brain astrocyte functions include facilitating transport of nutrients and waste, maintenance of the blood brain barrier, synaptic support, and immune responses (Haydon & Carmignoto, 2006; Lovick et al., 2005; Sofroniew & Vinters, 2010; Volterra & Meldolesi, 2005). When responding to immune insults astrocytes can experience changes in morphology, gene expression, and function (Burda & Sofroniew, 2014; Sofroniew, 2015). These astrocytes are known as reactive astrocytes (RAs). Once astrocytes become reactive, they lose some of their homeostatic functions and gain other functions that may be harmful or beneficial in the progression of the insult (Matusova et al., 2023). For example, there are several studies that suggest that astrocytes contribute to the progression of Alzheimer's disease by overexpressing amyloid beta-producing enzymes, while other studies suggest they promote amyloid beta degradation (Jin et al., 2012; Jiwaji et al., 2022; Liddelow et al., 2017; Roßner et al., 2005). In other instances, such as in spinal cord injury, the glial scar was traditionally thought to be inhibitory to recovery, while more recent studies in which they are ablated or prevented from becoming reactive lead to worse outcomes (Anderson et al., 2016; Bush et al., 1999; Gu et al., 2019; Hara et al., 2017; Jones et al., 2003; McKeon et al., 1991, 1995). In models of Parkinson's disease RAs have been shown to be a source of accumulating a-synuclein while also having

increased secretion of neuroprotective molecules (Sonninen et al., 2020). This mix of conclusions and more recent sequencing data attest to the incredible diversity of RAs (Cameron et al., 2024; Escartin et al., 2021; Yu et al., 2024; Zamanian et al., 2012).

Upregulation of GFAP and hypertrophy are traditionally used as markers of astrocyte reactivity (Anderson et al., 2014; Eng et al., 1971). These two markers are often present across many CNS pathologies, however new research and sequencing strategies have revealed other more specific markers (Cahoy et al., 2008; Zamanian et al., 2012). Most of these newly uncovered markers appear to label distinct subsets of RAs (Liddelow et al., 2017; Zamanian et al., 2012). This heterogeny of RAs can further be explored by generation of new tools that can specifically target and manipulate subsets of RAs. Our previous work utilized the *lipocalin 2* (*Lcn2*) gene, which is upregulated between 200-300-fold in astrocytes in mouse models of neuroinflammation, to drive expression of a tamoxifen-dependent Cre recombinase (Agnew-Svoboda et al., 2022; Liddelow et al., 2017; Zamanian et al., 2012). The *Lcn2CreERT2* mouse line is capable of labeling large subsets of reactive cells under many different pathological conditions.

In our search to identify possible genetic drivers for targeting subsets of RAs we came upon Complement component 3 (C3) as an additional marker with increased expression in astrocytes across many pathologies (Zamanian et al., 2012). C3 is a central component of the complement cascade, which is part of

the innate immune system and plays a large role in defense against pathogens and regulation of the adaptive immune system (Dunkelberger & Song, 2010; Ricklin et al., 2016). In the CNS astrocytes are the primary source of C3 (Burda & Sofroniew, 2014; Sofroniew, 2009, 2015; Sofroniew & Vinters, 2010; Zhou et al., 2023). To continue developing the repertoire of genetic tools available, we have generated the *C3-FlpOER^{T2}* mouse line. The *C3-FlpOER^{T2}* line uses the endogenous C3 promoter to drive expression of a tamoxifen-dependent FlpO recombinase in subsets of reactive astrocytes. In this work we characterize the ability of the *C3-FlpOER^{T2}* line to label RAs in a discrete array of neuroinflammatory conditions.

Materials and Methods

Animals

Wild type C57BL/6N animals obtained from Taconic Biosciences (C57BL/6NTac) were used to examine *Complement 3* expression in healthy and inflamed brains. *C3-FlpOER^{T2}* animals were crossed into the Swiss Webster (Taconic) background for more than 10 generations before making the line homozygous for *C3-FlpOER^{T2}*. Homozygous *C3-FlpOER^{T2}* mice were crossed with the dual Flp and Cre recombinase reporter *RC::FLTG* (Jax, strain #026932). For combinatorial experiments the *Aldh1l1-CreER^{T2}* (Jax, strain #029655) line was crossed into *C3-FlpOER^{T2}* and offspring were then crossed with *RC::FLTG*. All experiments were done on animals between 6-20 weeks old. All animal

procedures performed were done according to the University of California Riverside's Institutional Animal Care and Use Committee (IACUC) guidelines.

Generation of C3-FlpOER^{T2} mice

C3-FlpOER^{T2} mice were generated by inserting P2A-*FlpOER^{T2}*-TGA at the end of the coding sequence for exon 41 of *Complement 3*, using CRISPR/Cas9 homology-directed repair in fertilized mouse eggs. Once the knock-in line was established, tail snips were taken, and genomic DNA was extracted using the Extracta DNA prep for PCR (Quanta, 95091-025). Genotyping of *C3-FlpOER^{T2}* mice was done via multiplexed PCR using the following primers: *C3-FlpOER^{T2}* forward 5'- TACTTCATCGCATTCCTTGC -3'; Wild type forward 5'-AGTTCATCAGCCACATCAAGTG -3'; Common reverse 5'-AGAGCACCTATAATCATGTGGC -3'. Expected product sizes are 609bp (wild type) and 382bp (*C3-FlpOER^{T2}*).

Tamoxifen gavage

Tamoxifen (Sigma, cat#T5648) was dissolved in corn oil (sigma, cat#C8267) at 20mg/ml and animals were dosed at 150ug tamoxifen per gram of mouse. In experiments where an oil (vehicle) control was used, dosage was calculated, and the same dose of corn oil was given. Animals were orally gavaged with an animal feeding needle (Fisher, cat#01-208-87).

Low- and high-dose LPS

LPS was dissolved in sterile saline and given intraperitoneally (IP). For the low-dose protocol tamoxifen in corn oil or corn oil alone (vehicle) was orally gavaged on days 0-5, low-dose LPS (1.5mg/kg) or equal volume saline was given IP on day 1, and tissue was collected on day 7. For the high-dose protocol tamoxifen was dosed on days 0-2, high-dose LPS (10mg/kg) or equal volume saline was given on day 1, and tissue was collected on day 3.

Intrastriatal LPS

Animals were orally gavaged with tamoxifen in corn oil or corn oil alone (vehicle) on days 0-2, 4, and 6. On day 1 intrastriatal injection of LPS or saline was done. Animals were anesthetized with isoflurane and a total of 1ul of 7.5mg/ml (250nl each site) LPS or saline was injected into the following 4 coordinates from bregma: A/P +1.18mm, M/L ±1.5mm, D/V -3.5mm and A/P -0.34, M/L ±2.5mm, D/V -3.2mm. Surgical incision was closed with Michel Suture Clips. Tissue was harvested on day 8. For the 7-14 day time points tamoxifen was given on day 7, 9, and 11, then collected on day 14. For the 14-28 day time point animals were given tamoxifen 3x per week and tissue was collected on day 28.

Toxoplasma gondii infection

The Me49 Toxoplasma strain was maintained *in vivo* by passaging consecutively in Swiss Webster mice. Toxoplasma cysts were collected by harvesting the brains of infected mice. Briefly, each infected brain was homogenized in 3mL of

sterile PBS and cysts counted on a light microscope. The average cyst burden per brain is about 3000.

C3-FlpOER^{T2}; RC::FLTG mice were infected by intraperitoneally injecting 200ml of sterile PBS containing 10 Me49 cysts. This initial infectious burden resembles a physiological infection that begins in the gut, travels through the bloodstream, enters the brain, and forms cysts in neurons. For the acute phase time point oral gavage of tamoxifen begins 5 days post infection and is given every other day until day 13 post infection and tissue is harvested on day 14. For the chronic time point oral gavage of tamoxifen began on day 14 post infection and was given 3x a week until day 42 post infection, then tissue was harvested on day 43. Only females were used for the acute condition because males did not survive.

Kainic Acid Injection

C3-FlpOER^{T2}; RC::FLTG mice were orally gavaged with tamoxifen in corn oil on days 0-2, 4, and 6. Kainic acid was injected on day one and mice were anesthetized with isoflurane during the surgery. 64nl of 20mM Kainic acid in sterile saline was injected into the following coordinated from bregma: A/P -1.80, M/L -1.60, D/V -1.80. After surgery animals were monitored for seizure activity. Only animals that reached at least a 3 on the modified Racine scale within one hour of surgery completion were used in this study. Tissues were collected on day 7. For the later 14-30d time point tamoxifen gavage began on day 14 post

injection and was given every other day until day 28 and tissue was harvested on day 30 post injection.

Traumatic brain injury

Traumatic brain injury was achieved via fluid percussion injury (FPI). Mice anesthetized with isoflurane underwent a stereotaxic craniectomy at the following coordinates: A/P -2.00mm, M/L -1.00mm. Following craniectomy a luer-lock syringe hub was bonded to the skull. The following day animals underwent a moderate (2.3 atm) FPI under isoflurane anesthesia received a 20ms impact on the dura using an FPI device (Virginia Commonwealth University, VA). Sham animals received the same treatment except for the pressure wave. At the first time point (0-7) animals were treated with FPI or sham injury on day 1 and given tamoxifen on days 0, 1, 2, 4, and 6. Tissue was harvested on day 7. For the 7-30 time point animals were treated with FPI or sham injury on day 1 and given tamoxifen 3x per week starting on day 7 and ending on day 28, then tissue was collected on day 30 post FPI. In the 30-60 day time point animals were treated with tamoxifen 3x per week starting on day 30 until day 58 and then collected on day 60 post FPI.

5-ethynyl-2'-deoxyuridine (EdU)

C3-FlpOER^{T2}; RC::FLTG mice were treated according to the intrastriatal injection days 0-7 protocol and given EdU IP (150mg/kg) on day 2, 4, and 6. Collected brains were fixed for 2 hours. For cryopreservation brains were placed in 30%

sucrose that was replaced every 24 hours until the brain sank. Brains were mounted in optimum cutting temperature medium (OCT) and frozen at -80°C until ready to cryosection. For EdU experiments, the Click-iT EdU Cell Proliferation Kit from Invitrogen was used according to manufacturer instructions.

Fluorescent in situ hybridization

Brains were fixed overnight, followed by cryopreservation as described above. RNAscope was performed following manufacturers suggested protocol on 15mm sections. If IHC was performed following RNAscope, brains were blocked with 3% bovine serum albumin (BSA) in PBS for one hour and then incubated with primary antibodies diluted in 1% BSA overnight at 4°C in a humidifying chamber. The following day tissue was washed 8x 10min in PBS at RT. Secondary antibodies and DAPI were diluted in 1% BSA and incubated on slides for 1-2 hours at RT. Following secondary incubation slides were washed 4x 10min in PBS at RT, then mounted using Fluoro-Gel.

Immunofluorescence

Animals were sacrificed via CO_2 inhalation followed by transcardial perfusion with 30mL of PBS, then 30mL with 4% paraformaldehyde (PFA). Brains were then harvested and post fixed in 4% PFA for 4 hours to overnight (2 hours for EdU treated animals). Floating vibratome sections were cut at 150mm and all cryosections except for those used in RNAscope were cut at 30mm. Vibratome sectioned tissue was blocked in permeabilization solution (PBS, 3%BSA, 0.3%

Triton-X) supplemented with 10% goat serum for 1 hour on an orbital shaker at low speed. Primary antibodies were diluted in permeabilization solution supplemented with 1% goat serum and incubated overnight at 4°C on an orbital shaker at low speed. The next day tissue was washed 8x 15min at RT with PBS on an orbital shaker. Secondary antibodies were diluted in permeabilization solution supplemented with 1% goat serum and incubated for 4 hours at RT or overnight at 4°C on an orbital shaker. The tissue was then washed 4x 15min in PBS at RT on an orbital shaker, then mounted with Fluro-Gel. Cryosectioned tissue was washed in PBS to remove OCT before being blocked with blocking solution (10% goat serum, 0.3% Triton-X100, PBS) for 1 hour at RT in a humidifying chamber. Primary antibodies were then diluted in antibody solution (1% goat serum, 0.1% Triton-X100, PBS) and incubated on tissue at 4°C overnight in a humidifying chamber. The next day tissue was washed 8x 10min in PBS at RT. Secondary antibodies were then diluted in antibody solution and incubated on the tissue at RT for 1-2 hours. Slides were then washed 4x 10min in PBS and mounted with Fluoro-Gel.

Antibody	Dilution	Supplier	Catalog #
Rabbit anti ALDH1L1	1:500	Cell Signaling	85828S
Rabbit anti DsRed	1:500	TAKARA	632496
Rat anti GFAP	1:500	Invitrogen	13-0300
Rabbit anti Iba1	1:500	FUJIFILM	019-19741
Chicken anti mCherry	1:500	AVES	MCHERRY-0020
Chicken anti NeuN	1:500	AVES	NUN-0020
Chicken anti GFP	1:500	AVES	GFP-1010
Tomato lectin	1:75	Vector Labs	B-1175-1
Mouse anti Tyrosine Hydroxylase	1:500	R&D Systems	MAB7566
Mouse anti Vimentin	1:500	HUABIO	EM0401TR
Goat anti Chicken 488	1:1000	Invitrogen	A11039
Goat anti Chicken 546	1:1000	Invitrogen	A11040
Goat anti Chicken 647	1:1000	Invitrogen	A21449
Goat anti Mouse 488	1:1000	Invitrogen	A32723
Goat anti Mouse 647	1:1000	Invitrogen	A21236
Goat anti Rabbit 546	1:1000	Invitrogen	A11035
Goat anti Rabbit 488	1:1000	Invitrogen	A11034
Goat anti Rabbit 647	1:1000	Invitrogen	A21244
Goat anti Rat 488	1:1000	Invitrogen	A11006
Goat anti Rat 647	1:1000	Invitrogen	A21247
Streptavidin 488	1:1000	Invitrogen	S11223
Streptavidin 647	1:1000	Invitrogen	S32357

Table 4.1: List of antibodies, dilutions, suppliers, and catalog numbers used in this work.

Quantification and statistical analysis

All image handling and processing was done in FIJI (Schindelin et al., 2012). RNAscope data was quantified by using the measure function in FIJI to measure *C3* and Aldh1l1 integrated densities. All other quantifications of cells was done manually in FIJI. Datasets in which statistical testing was done were all checked for normality using the Shapiro-wilk test. All statistical tests were carried out using GraphPad Prism Version 10.2.1.

Results

Complement 3 is highly upregulated during direct insults to the brain

Upregulation of *Complement 3* (*C3*) has been shown across many disease models as well as in human postmortem tissue (Sofroniew, 2015; Zamanian et al., 2012). To confirm this strong upregulation in mouse tissue we performed intrastriatal injection of LPS (IS LPS), traumatic brain injury, and single high dose of LPS (Fig. 4.1). IS LPS is used to model acute encephalitis that subsequently leads to a Parkinsonian disorder through the progressive cell death of dopaminergic neurons in the substantia nigra (SN) (R. L. Hunter et al., 2009). C57BL/6N animals were intrastriatally injected with a total of 1ul (250nl each site) of 7.5mg/ml LPS from *E. coli* or sterile saline and tissue was harvested 2 days later. RNAscope, a form of fluorescent *in situ*, was then performed on the tissue for *C3*. IS LPS treated sections displayed a significant increase in *C3* expression in astrocytes over saline injected animals (P=0.0052, unpaired t-test) (Fig. 4.1A,E). This confirmed that C3 is a marker for a subset of RAs in certain neuroinflammatory conditions.

We next analyzed a mouse model of traumatic brain injury by performing fluid percussion injury (FPI) on C57BL/6N animals. A cranial window was placed A/P -2.00mm, M/L -1.00mm from bregma. The following day animals were randomly selected to receive an FPI or sham injury and brains were collected 2 days post injury/sham. FPI injured animals had significantly increased *C3*

expression over their sham counterparts, though this increase was not as dramatic as the one seen in the IS LPS animals (P=0.0051, unpaired t-test) (Fig. 4.1A,B,C,F).

A single high-dose of LPS (10mg/kg) given intraperitoneally (IP) can be used as a model for acute systemic inflammation that results in neuroinflammation (Kim et al., 2022). Animals were given a single high-dose of LPS and brains collected 2 days later. LPS treated brains did not show a significant change in C3 expression compared to saline injected controls (P=0.5205, unpaired t-test) (Fig. 4.1D,G). Thus, while systemic inflammation did not result in a notable change in C3 expression, direct insult to the brain in the form of TBI or encephalitis did. With this knowledge, we proceeded to generate the *C3-FlpOER*^{T2} mouse.

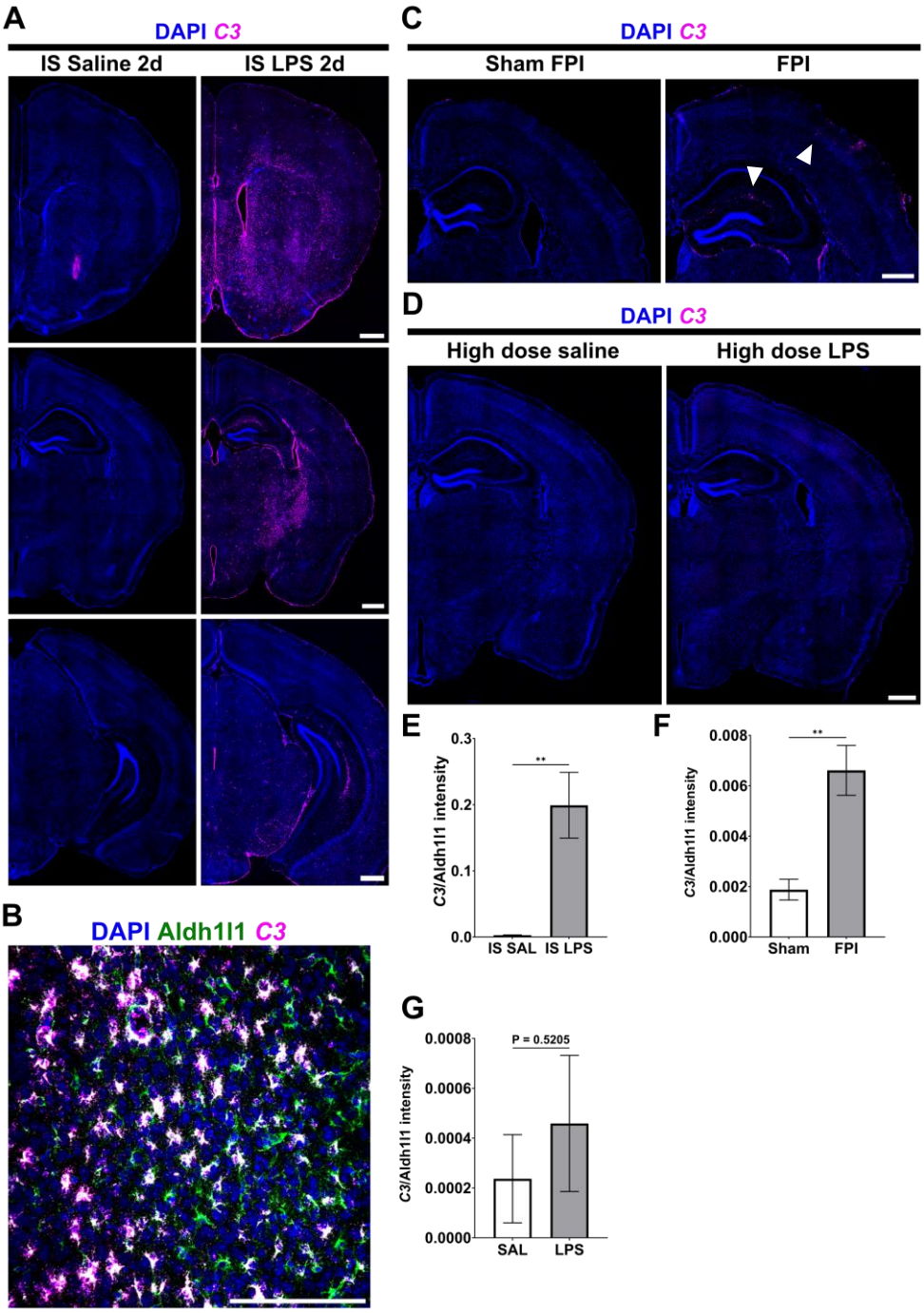


Figure 4.1: *Complement 3* is upregulated during direct insults to the brain. (A) RNAscope of wild type animals 2 days after intrastriatal injection with LPS or saline. **(B)** High magnification of the striatum of an IS LPS treated animal showing Aldh1l1 immunohistochemistry and *C3* RNAscope. **(C)** RNAscope of wild type animals 2 days after FPI or sham FPI. **(D)** RNAscope of animals 2 days after a single high-dose of LPS or saline given IP. **(E)** Quantification of puncta in (A). P = 0.0052 (unpaired t-test). **(F)** Quantification of puncta in (C). P = 0.0051 (unpaired t-test). **(G)** Quantification of puncta in (D). P =0.5205 (unpaired t-test). N=3 animals per condition. Scale A, C, D 500mm; B 50mm.

Design and generation of the *C3-FlpOER^{T2}* mouse

To design the *C3-FlpOER^{T2}* mouse line, we targeted the endogenous *C3* locus and introduced a cassette at the end of the coding sequence for exon 41 with a *Peptide 2A* site to separate FlpOER^{T2} from the C3 protein, the *FlpOER^{T2}* sequence, and a *TGA* stop sequence (Fig. 4.2). Thus, FlpOER^{T2} expression would be controlled by the endogenous *C3* promoter without disrupting endogenous *C3* expression. Additionally, the use of a tamoxifen-dependent FlpO allows for the control of the timing of FlpO recombinase activation.



Figure 4.2: Design of the C3-FlpOERT2 mouse. A cassette containing a *P2A* sequence, *FlpOER^{T2}* sequence, and a *TGA* stop was inserted at the end of the coding sequence in exon 41 of *C3*.

Validation of the C3-FlpOER^{T2} mouse during direct and systemic neuroinflammation

To characterize this new mouse line, the *C3-FlpOER^{T2}* line was crossed with the RC::FLTG reporter line. The RC::FLTG reporter expresses tdTomato upon FlpO-mediated recombination (Plummer et al., 2015). Using offspring from this cross (*C3-FlpOER^{T2}; RC:FLTG*) we proceeded to test *C3-FlpOER^{T2}* expression after IS LPS. *C3-FlpOER^{T2}; RC::FLTG* mice were injected into the striatum and orally gavaged with tamoxifen for three time points: 0-7 days, 7-14 days, and 14-28 days (see Material and Methods). In the saline injected animals, the only tdTomato+ cells were seen in striatal sections (a') and averaged

0.67±0.57 tdTomato+ cells per section. The IS LPS 0-7day time point had the most tdTomato positive cells of all the time points with an average of 496±18.5 tdTomato+ cells per 150mm section containing the striatum (a') and 414.3±60.2 tdTomato+ cells per section containing the cerebral peduncle (b'), and 0.43± 0.25 cells per section containing the substantia nigra (c') (Fig. 4.3). The 7-14day time point had averages of 0.43±0.29 tdTomato+ cells in striatal sections, 2.33±0.89 tdTomato+ in cerebral peduncle sections, and no tdTomato positive cells in substantia nigra sections (Fig. 4.3). Finally, the 14-28 day time points had an average of 0.11±0.11 tdTomato positive cells in striatal sections and no tdTomato positive cells in either the cerebral peduncle sections nor the substantia nigra sections. The robust activation seen in the 0-7 time point is thus consistent with the endogenous activation of *C3* by IS LPS.

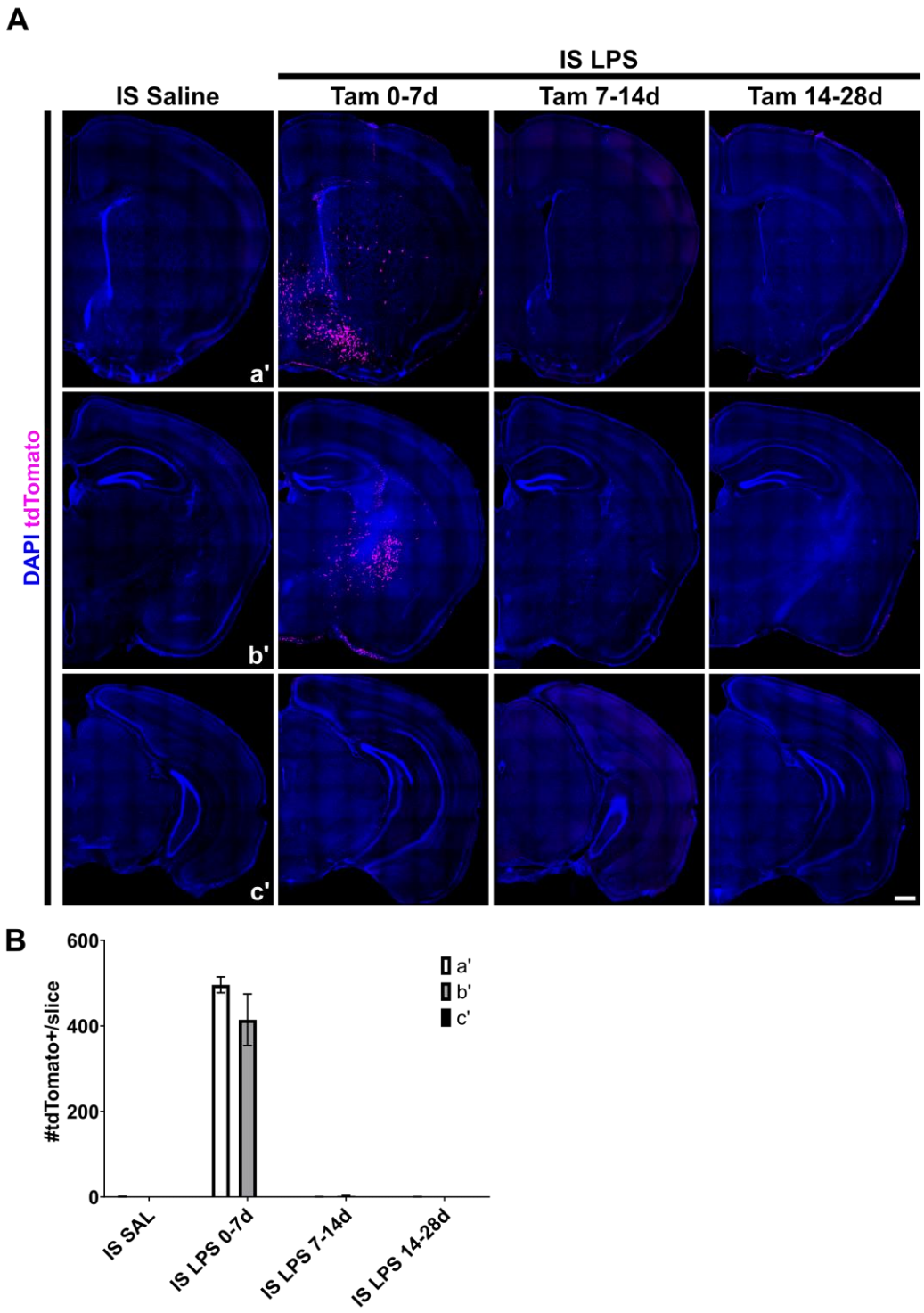


Figure 4.3: Intrastriatal LPS labeling in *C3-FlpOERT2; RC::FLTG* mice. (A) Labeling of intrastriatally injected animals treated with tamoxifen from days 0-7, 7-14, and 14-28. tdTomato+ cells are primarily seen in the 0-7 day time point in striatal sections (a'). **(B)** Quantifications of sections from near the striatum (a'), cerebral peduncle (b'), and the substantia nigra (c'). N=3. Scale 500μm.

To determine which cell types were labeled by the *C3-FlpOER^{T2}* line, we then performed a suite of cell-type immunohistochemical stains on 0-7day tissue. Aldh1l1, GFAP, and vimentin are all markers that label and identify astrocytes (Escartin et al., 2021). In the striatal and thalamic regions, 98.78±0.66% of tdTomato labeled cells were positive for Aldh1l1, 96.75±1.25% were positive for GFAP, and 97.46±0.27% were positive for vimentin. Tomato lectin labels endothelial and microglial cells. Of the tdTomato labeled cells, 2.24±0.90% were positive for tomato lectin. Finally, no tdTomato positive cells co-labeled with the neuronal marker NeuN nor the microglial marker Iba1. From this information we can conclude *C3-FlpOER^{T2}* primarily labels astrocytes in the IS LPS model of neuroinflammation.

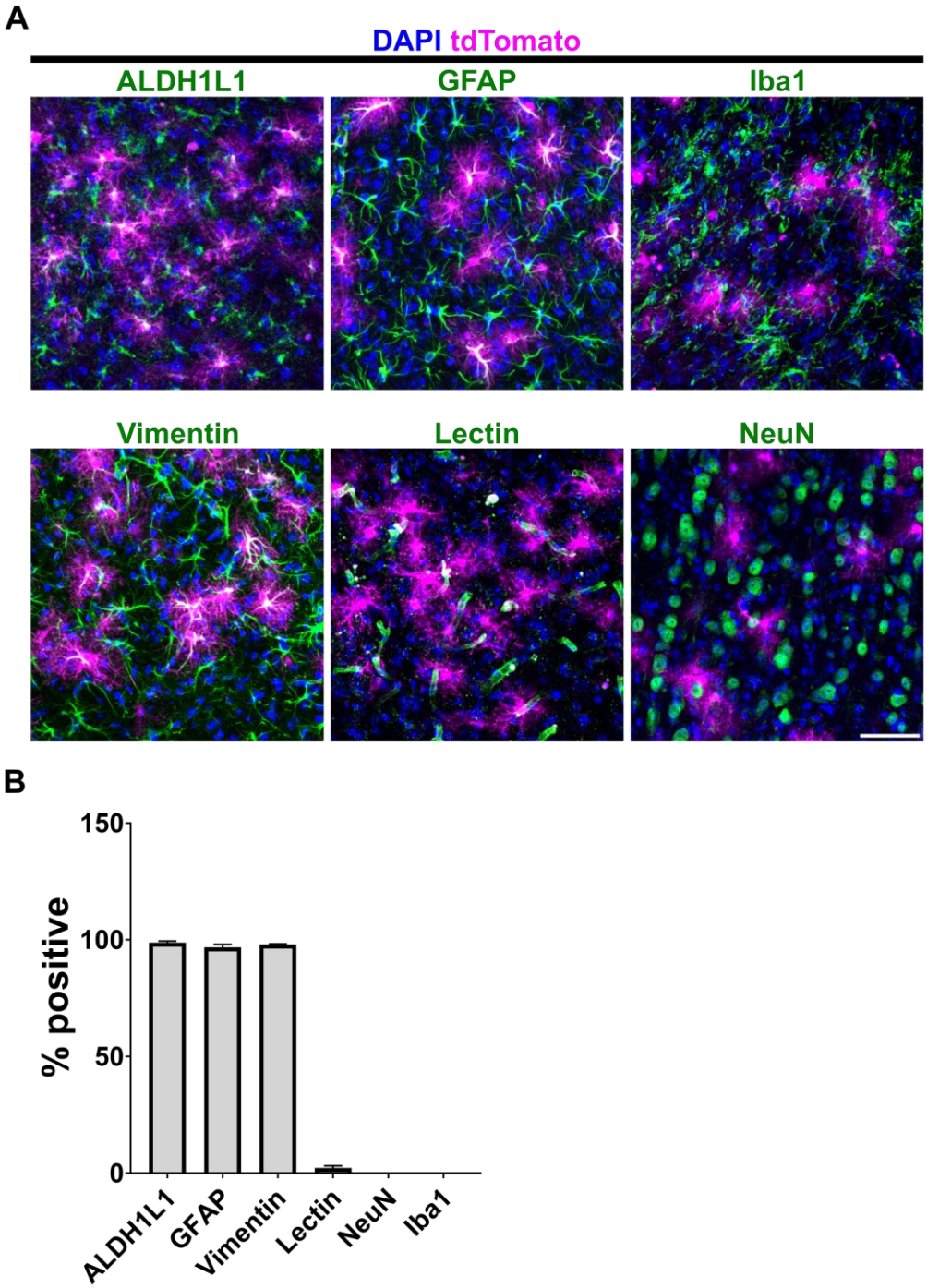


Figure 4.4: Cells labeled in the *C3-FlpOERT2* line are primarily astrocytes. (A) Tissue from intrastriatal LPS injected 0-7day treatment immunohistochemically stained for Aldh1l1, GFAP, vimentin, tomato lectin, NeuN, and Iba1. **(B)** Quantification of the labeled cell types in (A). Of the labeled cells quantified in the striatum and thalamic regions 98.78±0.66 are positive for Aldh1l1, 96.75±1.25 are positive for GFAP, 97.46±0.27 are positive for vimentin, 2.24±0.90 are positive for tomato lectin, and no cells stained positive for either NeuN nor Iba1. N=3 animals per stain. Scale 50μm.

We then tested *C3-FlpOER^{T2}* in other models that would cause systemic inflammation rather than direct brain inflammation as seen in the IS LPS model. We performed two different protocols for systemic IP LPS: low-dose (LD) and high-dose (HD) LPS. In the HD LPS protocol, *C3-FlpOER^{T2}; RC::FLTG* animals were injected IP with a single high dose of LPS (10mg/kg) on day 1 and given tamoxifen on day 0, 1, and 2. HD LPS brains were collected on day 3. In the LD protocol, animals are injected IP with a low dose of LPS (1.5mg/kg) on days 1-5 and given tamoxifen on days 0-5. LD LPS brains were collected on day 7. No tdTomato positive cells were seen in the LD treated animals and very few tdTomato positive cells were seen in the lateral ventricles (2.0±1.0 cells/slice) (Fig. 4.5). As expected from the RNAscope data for endogenous C3 expression (Fig. 4.2), activation of *C3-FlpOER^{T2}* is negligible after LPS-induced systemic induction.

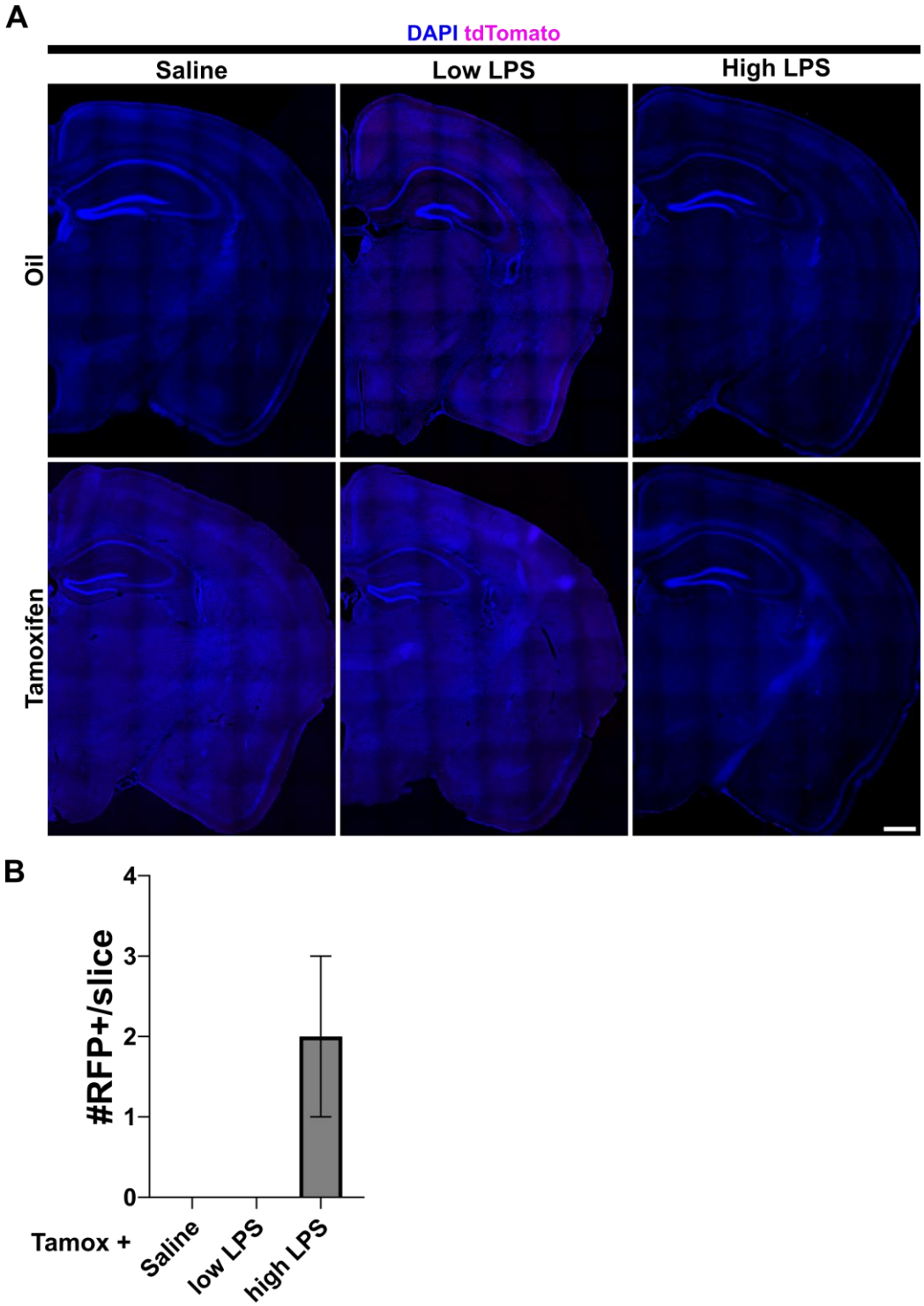


Figure 4.5: Low and high-dose LPS in C3-FlpOERT2; RC::FLTG animals. (A) Brains collected from animals treated with oil and LPS or tamoxifen and LPS. (B) Quantification of tdTomato cells in animals treated with tamoxifen and saline, low-dose LPS, or high-dose LPS. Quantification revealed there are 2.0±1.0 tdTomato positive cells per slice in the high-dose LPS and tamoxifen treated brains. N= 3 animals per condition. Scale 500μm.

We next explored *C3-FlpOER^{T2}; RC::FLTG* labeling after fluid percussion injury (FPI) at various time points. Prior to FPI or sham injury, a cranial window was placed at A/P -2.00mm, M/L -1.00mm from bregma. The next day animals were treated with either a moderate FPI (2.3atm) or sham injury. Tamoxifen was given 3 times per week at each time point with the exception of the 0-7 day time point which received additional doses the day before and day of injury. No tdTomato+ cells were seen in the 0-7 nor the 7-30 day time points in the sham or FPI treated animals. tdTomato positive cells are only seen in the 30-60 day time point (2.67±0.33 tdTomato+ cells/slice) (Fig. 4.6). tdTomato expression was not seen in the 0-7 day time point as expected form the *in situ* data (Fig. 4.1C, F). Overall, *C3-FlpOER^{T2}* labels few RAs after FPI. This could be due to a combination of the somewhat modest increase in endogenous C3 expression after FPI (as detected by RNAscope (Fig. 4.2)) and inefficient recombination by FlpO.

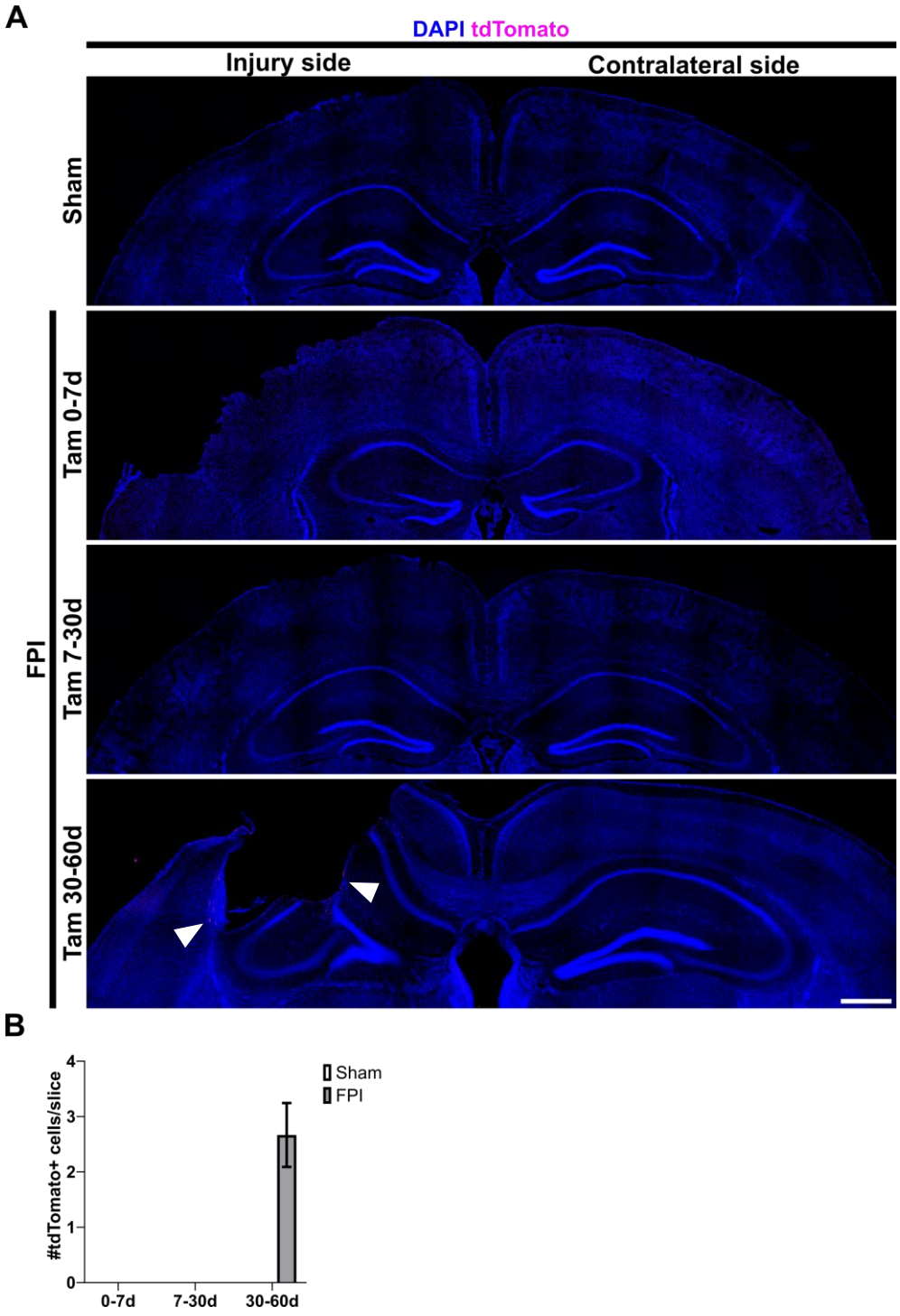


Figure 4.6: *C3-FlpOERT2; RC::FLTG* tdTomato expression 7, 30, and 60 days after FPI. Animals were treated with FPI or sham and then given tamoxifen during week 1, weeks 2-4, and weeks 4-8. tdTomato positive cells are seen only in the 30-60 day time point (arrowheads) (2.67±0.33 tdTomato+ cells/slice). N=3 animals for each condition. Scale bar 500μm. mean±SEM.

An additional neuroinflammatory model we tested in *C3-FlpOER^{T2}; RC::FLTG* animals was intrahippocampal kainic acid (IHKA). IHKA can be used as a model for medial temporal lobe epilepsy (MTLE). When treated with IHKA, mice develop spontaneous seizures, sclerosis of the hippocampus, and reactive gliosis (Ghouli et al., 2023). The acute phase of the IHKA model occurs up to day 7 post injection and the chronic phase lasts from approximately day 14 to 30 post injection. To encompass these phases, we chose to treat with tamoxifen from days 0-7 and 14-30. Animals received an injection of 20mM kainic acid into the CA1 region of the hippocampus and were monitored after surgery to ensure they developed seizures that met the criteria for at least a 3 on the modified Racine scale (Ihara et al., 2016; Lüttjohann et al., 2009). Tamoxifen was given 3 times per week with the exception of the 0-7 day time point which received 2 additional doses the day before and day of injection. Surprisingly, no tdTomato positive cells were seen at any time point (Fig. 4.7). Given that tdTomato+ RAs are not seen forming around the injection path in the IS LPS model it was not expected to see any around the injection site in this model, however sclerosis is expected at the chronic time point and possibly *C3-FlpOER^{T2}* RA labeling. Sclerosis was not overtly seen and it is possible that the current strain background is resistant to seizures and neuronal death induced by this model (McLin & Steward, 2006). In this background the *C3-FlpOER^{T2}* line does not label RAs in the IHKA model of MTLE.

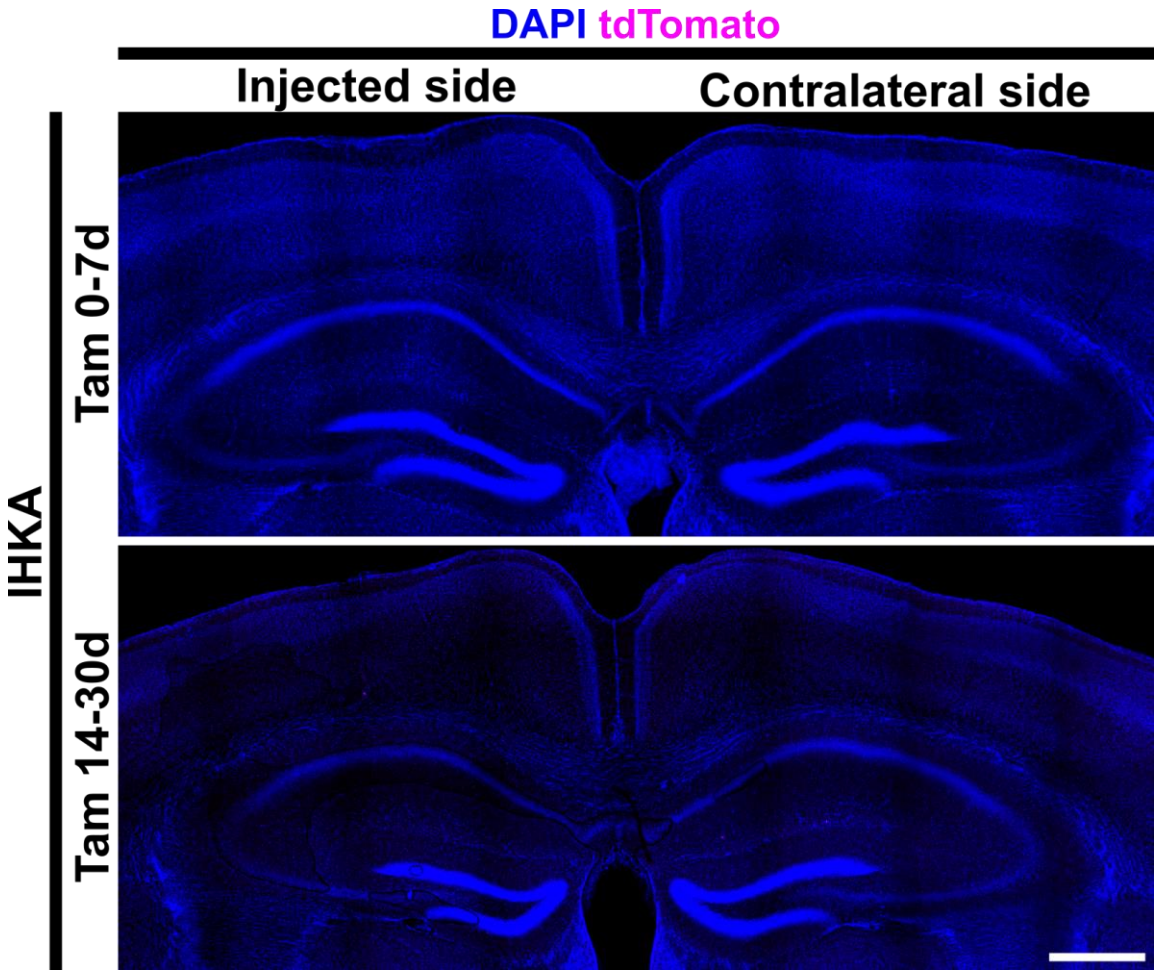


Figure 4.7: Intrahippocampal kainic acid does not induce labeling of cells in C3-FlpOERT2 mice. No tdTomato positive cells are seen in either the acute (0-7d) or chronic (14-30) phases after IHKA injection. N=4 animals each condition. Scale 500μm

C3-FlpOER^{T2} labels astrocytes during Toxoplasma gondii infection

Toxoplasma gondii is a parasite that causes neuroinflammation, cyst formation in neurons, and reactive astrocytosis (Wilson et al., 2009). Astrocytes become reactive during both the acute and chronic phases of *T. gondii* infection (C. A. Hunter et al., 1992; Wilson et al., 2009). To determine if the *C3-FlpOER^{T2}* line is capable of labeling RAs during *T. gondii* infection, we infected *C3-FlpOER^{T2}; RC::FLTG* mice with the Me49 strain of *T. gondii* and treated with tamoxifen during the acute or chronic phases. No tdTomato positive cells are seen in sham infected animals (Fig. 4.8A, top row). After *T. gondii* infection, tdTomato labeled cells are extremely sparse at the acute time point with about 3.67±0.69 labeled cells per 30mm section (Fig. 4.8A, middle row). tdTomato labeled cells are more abundant after chronic infection (67.13±1.70 tdTomato+ cells/slice) and appear to cluster around areas of inflammatory infiltration (Fig. 4.8A, C). During chronic infection of *T. gondii* areas of inflammatory infiltration are seen near areas of free tachyzoites and are likely the result of bursting cysts and reactivation of the immune response (Zhang et al., 2014; X. Y. Zhao & Ewald, 2020). In these areas neutrophils, lymphocytes, densely clustered nuclei, and cell debris can be seen surrounding areas of free tachyzoites (Zhang et al., 2014). In *C3-FlpOER^{T2}* mice, labeled RAs are seen surrounding areas of dense DAPI staining and observed cell debris (Fig. 4.8C). In conclusion, the *C3-FlpOER^{T2}* line is able to label RAs during the acute and chronic phases of *T. gondii* infection.

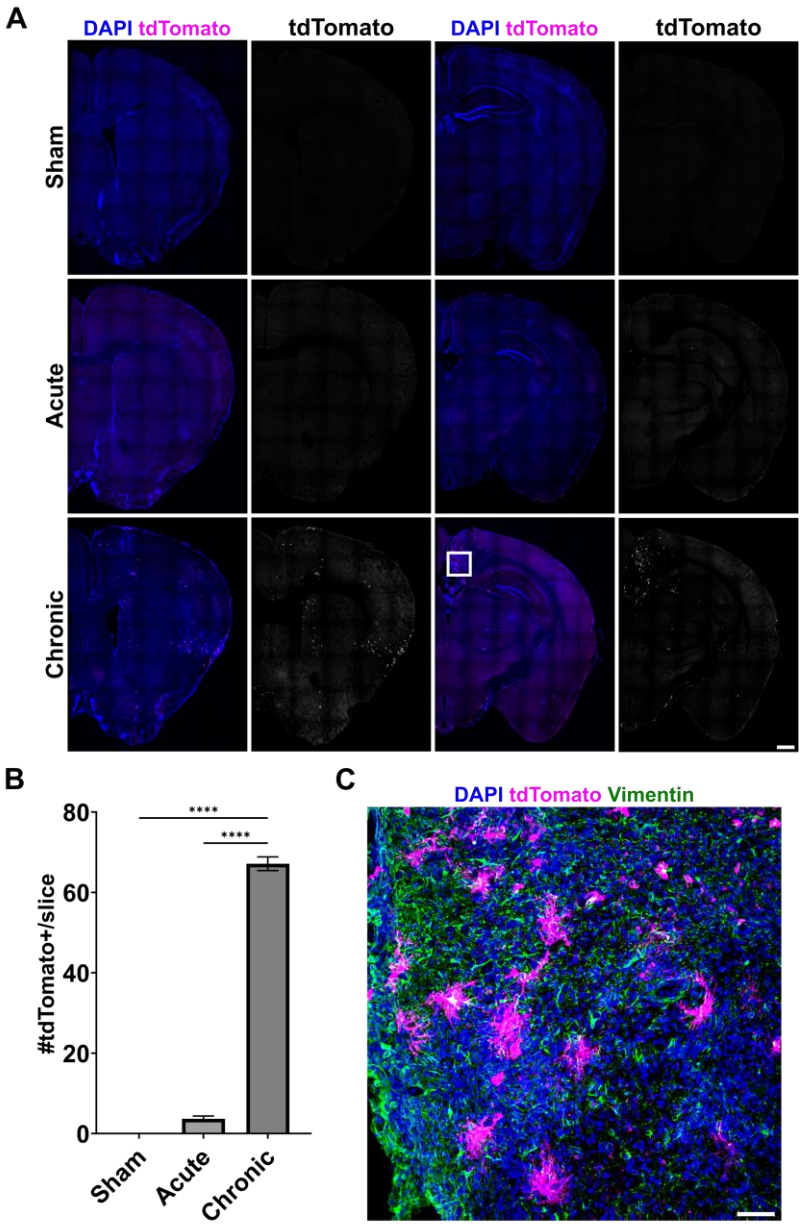


Figure 4.8: C3-FlpOERT2 labeling of astrocytes during acute and chronic *T. gondii* infection. (A) Representative images of *T. gondii* or sham infected brains. **(B)** quantification of cells seen in (A). No tdTomato labeled cells are seen in sham infected animals. There are significantly more tdTomato labeled cells in the chronic condition compared to both the acute and sham time points ($P<0.0001$, ANOVA with Tukey's multiple comparisons). At the acute time point an average of 3.67±0.69 cells per 30mm section are seen. At the chronic time point an average of 67.13±1.70 tdTomato+ cells per 30mm section. **(C)** Inset from white box in (A). In chronic infected brains, tdTomato+ cells appear to cluster around areas of dense DAPI staining that appear to be areas of immune infiltration. Scale (A) 500μm, (B) 50μm. N= 3 animals each condition. means±SEM.

C3-FlpOER^{T2} astrocytes are not proliferative

Given that *C3-FlpOER^{T2}; RC::FLTG* astrocytes are seemingly only present after direct insults to the brain and are primarily located in the white matter, it is possible that the labeled *C3-FlpOER^{T2}; RC::FLTG* astrocytes are a type of RA known as scar astrocytes. One prominent feature of scar astrocytes is they proliferate shortly after injury, peaking 3 days post injury (Yang et al., 2020). Thus, we next treated animals with EdU, a thymidine analog, on the day after injection, day 3, and day 5 post injection to label any proliferating cells (cells synthesizing DNA). Notably, after the 0-7 day IS LPS protocol no proliferative tdTomato+ astrocytes were seen, despite detection of EdU in other cells (Fig. 4.9). In conclusion, RAs labeled with *C3-FlpOER^{T2}* are not proliferative, and are thus unlikely to be scar astrocytes.

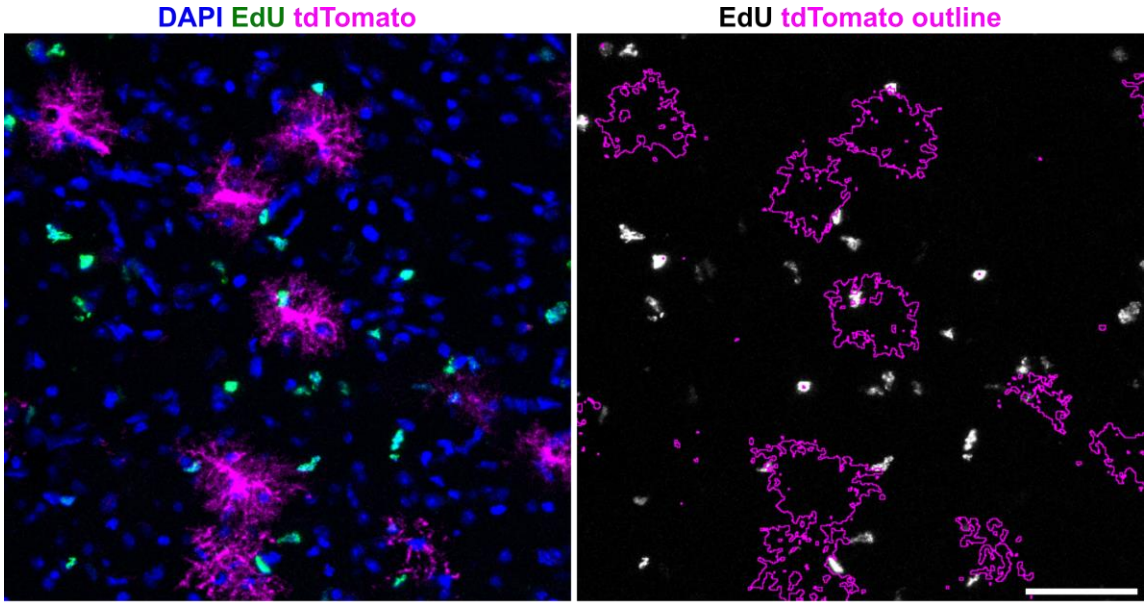


Figure 4.9: C3-FlpOERT2 labeled astrocytes are not proliferative. IS LPS 0-7 day treated *C3-FlpOER^{T2}; RC::FLTG* animals were also treated with EdU on days 2, 4, and 6. No tdTomato positive astrocytes are co-positive with EdU. N=3. Scale 50μm.

Combinatorial approaches to specifically label reactive astrocytes,

The main advantage of generating FlpO lines is that they can be used in combination with Cre lines to selectively label or manipulate specific subsets of cells. In the adult brain, *C3-FlpOER^{T2}* is only expressed after direct insult. While the majority of the cells expressing *C3-FlpOER^{T2}* after IS LPS are astrocytes, it is possible other reactive cells might activate it in other models of neuroinflammation. To filter out non-astrocytic reactive cells and show the utility of the *C3-FlpOER^{T2}* line for use in combinatorial approaches, we crossed the *C3-FlpOER^{T2}* with the astrocyte-specific *Aldh1l1-CreER^{T2}* and dual recombinase reporter *RC::FLTG* lines. The *RC::FLTG* line is a dual recombinase reporter for Cre and Flp. The RC::FLTG line has a frt-flanked stop sequence, a loxP-flanked tdTomato-stop, and an EGFP sequence. Flp recombinase activity will excise the frt-flanked stop, allowing for tdTomato expression. Cre recombinase activity will remove the tdTomato-stop sequence, allowing for EGFP expression only if Flp recombinase has also removed the frt-flanked stop. Therefore, only cells expressing both *Aldh1l1-CreER^{T2}* and *C3-FlpOER^{T2}* will experience full recombination and express EGFP in the presence of tamoxifen, while cells expressing only *C3-FlpOER^{T2}* will remain tdTomato+. *Aldh1l1-CreER^{T2}; C3-FlpOER^{T2}: RC::FLTG* mice were treated with the IS LPS 0-7 day protocol. EGFP positive and tdTomato positive astrocytes were observed (Fig. 4.10). The majority of reporter-labeled astrocytes were EGFP positive at 73.65% in striatal and 60.86% in cerebral peduncle-containing sections. A minority of reporter positive

cells expressed tdTomato only (26.36% and 39.14% in striatum and cerebral peduncle sections, respectively). Most of these are unequivocally astrocytes, based on morphology and co-expression of astrocytic markers (Fig and data not shown), suggesting incomplete recombination of this particular reporter by Cre - recombinase. Finally, there were some cells that expressed both tdTomato and GFP, 23.84% in striatal sections and 7.60% in cerebral peduncle sections. These co-positive cells represent a population where tdTomato expression perdured after reporter excision, possibly due to late recombination (Bapst et al., 2020). In summary, EGFP labeling of astrocytes in the IS LPS model demonstrates the ability of the *C3-FlpOER*^{T2} line to be utilized with other recombinase-dependent tools in combinatorial approaches.

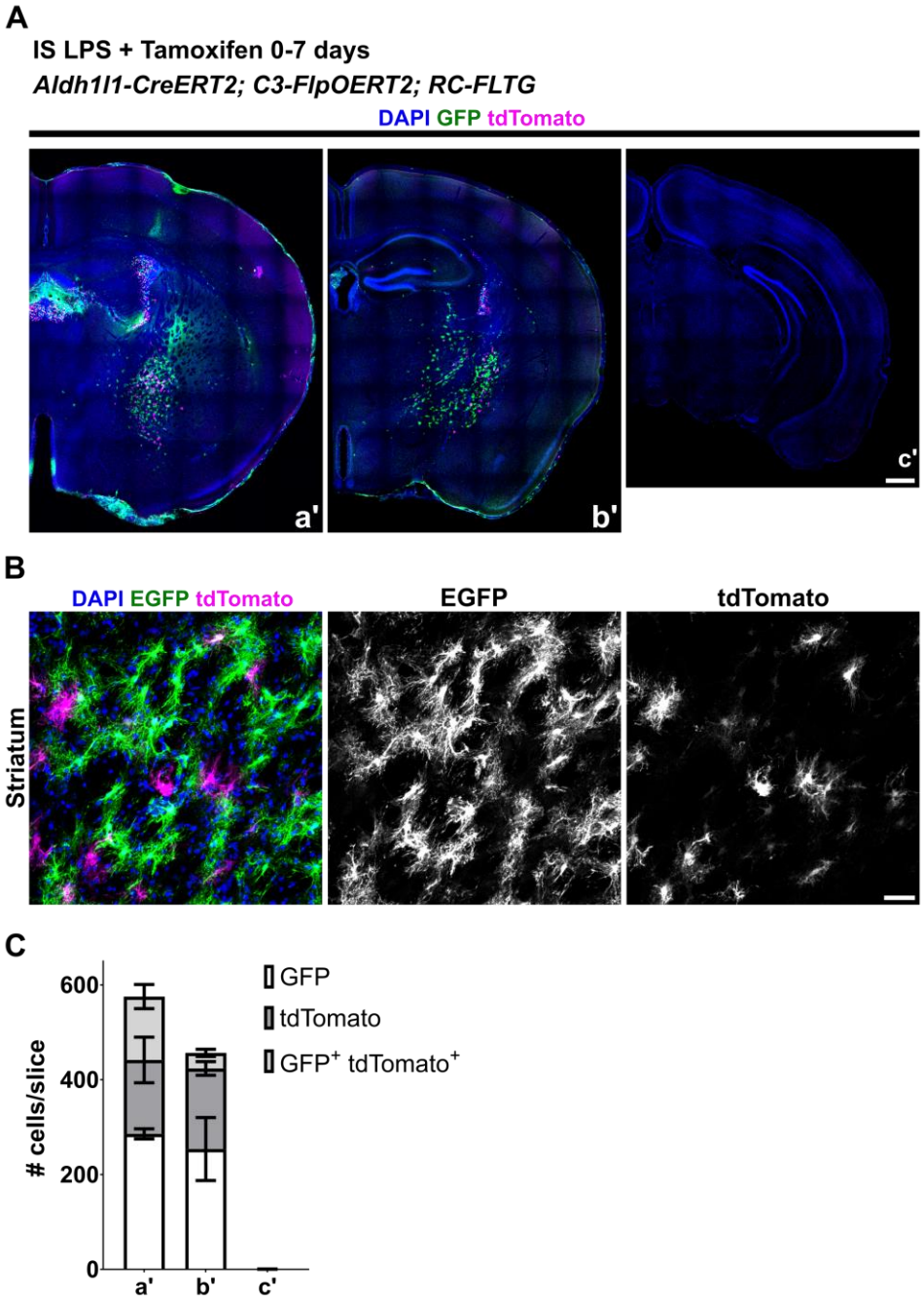


Figure 4.10: C3-FlpOERT2 can be used in combinatorial approaches. (A) *Aldh1l1-CreER^{T2}; C3-FlpOER^{T2}; RC::FLTG* mice treated with the IS LPS 0-7 day protocol. **(B)** high magnification of labeled astrocytes in the striatum. **(C)** Quantification of cells seen in (A). An average of 575.33±27.54 cells are seen in striatal sections (a'), 456±58.29 in cerebral peduncle sections (b'), and 0.33±0.27 cells in substantia nigra containing sections (c'). In striatal sections 26.36% are positive for tdTomato only, 49.81% positive for GFP only, and 23.84% are co-positive for tdTomato and GFP. In cerebral peduncle sections 39.14% of labeled cells are tdTomato positive only, 53.26% are tdTomato positive only, and 7.60% are positive for both tdTomato and GFP. mean±SEM. Scale (A) 500μm and (B) 50μm. N=3

Discussion

Though reactive astrocytes are seen across many neuroinflammatory conditions, we still understand very little about their heterogeneity and how these responses vary between diseases and injuries (Escartin et al., 2021). For example, reactive astrocytes isolated from ischemia induced by middle cerebral artery occlusion (MCAO) and systemic LPS were found to have overlapping, but distinct sets of differentially regulated genes (Zamanian et al., 2012). More recent single cell sequencing studies further reinforce this idea of extensive astrocyte diversity in health and disease (Burda et al., 2022; Endo et al., 2022; Hasel et al., 2021; Liddelow et al., 2017; Taha et al., 2022; Yu et al., 2024). This heterogeneity can be studied using new tools that can specifically target subsets of RAs. In this work we described a new mouse line, *C3-FlpOER^{T2}*, that is capable of labeling a subset of reactive astrocytes under some neuroinflammatory models.

This study presents the generation and characterization of the *C3-FlpOER^{T2}* mouse line. Our results demonstrate that the *C3-FlpOER^{T2}* is able to label a subset of RAs in a discrete set of neuroinflammatory models. Robust labeling is seen after both IS LPS injections and chronic Toxoplasma infection, but no labeling is observed in the IP LPS or IHKA models. Thus, *C3-FlpOER^{T2}* activation in RAs is so far only observed in models of direct brain insult. This is consistent with what we see by RNAscope analysis of endogenous expression (Fig. 4.1) and in previously reported studies (Benesova et al., 2009; Cameron et al., 2024; Hartmann et al., 2019a, 2019b; Liddelow et al., 2017; Voronkov et al.,

2023; Zamanian et al., 2012). The types of reactive astrocytes labeled with the *C3-FlpOER^{T2}* line are likely to be dependent on the starting type of astrocyte, the disease, the location, and the timing (Anderson et al., 2014; Bayraktar et al., 2015; Matyash & Kettenmann, 2010; Torres-Ceja & Olsen, 2022). This will be the subject of further study.

Utilizing the *C3-FlpOER^{T2}* line in combinatorial ways opens the possibility for greater manipulation of RAs and their subpopulations. In this work we show labeling with the reactive-cell-specific *C3-FlpOER^{T2}* line and the astrocyte-specific *Aldh1l1-CreERT2* line. Although we observed cells that were exclusively tdTomato+, most of these were unequivocally astrocytes, which suggests a potential lack of sensitivity of the reporter (Fig. 4.10). Regardless of the partial recombination observed for this particular reporter, this demonstrates the feasibility for this type of approach to manipulate C3+ reactive astrocytes. For example, some studies have concluded that C3+ astrocytes are “neurotoxic” and not beneficial to recovery. The *C3-FlpOER^{T2}* line could be used to ablate C3+ astrocytes and outcomes studied when these astrocytes are no longer present. It has been suggested that increased K_{ir}4.1 aids in the ability of astrocytes to regulate volume changes (Benesova et al., 2009). Using the *C3-FlpOER^{T2}* in combination with a Boolean exclusion tool such as ExBoX could regulate K_{ir}4.1 expression before and after injury to observe if this is indeed the case (Ubina et al., 2021).

Initially, after analyzing the pattern of labeled *C3-FlpOER^{T2}*; RC::FLTG being primarily in the white matter in the IS LPS model, we hypothesized that these astrocytes could be scar astrocytes. One feature of scar astrocytes is they proliferate shortly after injury (Yang et al., 2020). However, we did not see proliferation in any of the tdTomato+ astrocytes in the IS LPS model, suggesting that at least in this model C3+ astrocytes are not scar astrocytes. We now hypothesize that these astrocytes could be phagocytic based on the locations where they are primarily seen in the models we tested. In the IS LPS model, tdTomato+ astrocytes localize primarily in the white matter tracts of the nigrostriatal pathway as well as in areas of cell death and immune infiltration in chronic *T. gondii* infection. It has been shown that a subset of astrocytes function as phagocytes after ischemia, a direct insult to the brain though it is unclear if they are C3+ (Morizawa et al., 2017). Another group has shown the phagocytic-related gene *lgal3* is upregulated in C3+ astrocytes in optic nerve crush injury (Cameron et al., 2024). scRNA sequencing could help further elucidate the functions of these astrocytes.

One limitation of this model is that labeled cells seem to be less abundant in number than what is observed in RNAscope data for endogenous C3 expression (Figs. 4.1, 4.5, and 4.6). There are a few possibilities that may explain the disparity. In our hands expression of the *RC::FLTG* reporter is extremely dim in astrocytes and requires amplification to visualize as compared to the Ai9 line used previously (Agnew-Svoboda et al., 2022). It is possible that the expression

of this particular reporter is very low in this genetic background. This could be solved by utilizing a more sensitive reporter line. One other possibility is astrocytic death. Other groups have reported death of a subset of astrocytes shortly after neuroinflammatory induction in at least one of the models we tested and are reported to happen in others (Li et al., 1995; Newcomb et al., 1999; Samartino et al., 2010; Takuma et al., 2004; Van Kralingen et al., 2013; Wu et al., 2021). Another likely contributing factor is that FlpOER^{T2} has been reported to be notably less sensitive to tamoxifen than CreER^{T2} (Lao et al., 2012; C. Zhao et al., 2023). Though we have not explored expression of *C3-FlpOER^{T2}* beyond the CNS, this model could also prove useful in other areas of research as *C3* is known to be expressed in malignant epithelial cells during the epithelial to mesenchymal transition and is also expressed by other cell types of the body (Cho et al., 2016). Regardless, there are still a significant number of labeled astrocytes that could be studied and utilized in the study of this subset of RAs and in combinatorial approaches.

In summary, the *C3-FlpOER^{T2}* line is able to label a subset of RAs in models of direct neuroinflammatory insult. This further expands the toolkit available to neuroscientists to study reactive astrocyte heterogeneity and function. Future studies utilizing the *C3-FlpOER^{T2}* line could include single cell RNA sequencing (scRNA) studies to profile the transcriptomic changes and defining molecular signatures in this subset of labeled astrocytes. scRNA sequencing will provide deeper insights into the molecular pathways activated in

this subset of RAs and identify potential targets for therapeutic modulation. In addition to scRNA sequencing, other methods such as spatial -omics like 10x Visium or tDISCO could be utilized to further sus out changes in individual astrocyte transcriptomes and proteomes related to their proximity to injury (Scott et al., 2024; Ståhl et al., 2016).

CONCLUSION

This work shows the development and utilization of viral and genetically encoded tools for studying the heterogeneity, development, and function of subtypes of neural cells. The development of these genetic and AAV-based tools marks a step forward in the study of RAs and cellular heterogeneity in the brain. Each tool offers unique advantages for targeting specific cells populations and understanding their roles in health and disease.

The *Lcn2CreERT2* line is designed to permanently label a subset of reactive astrocytes. This inducible genetic tool is able to label a subset of RAs and reactive endothelial cells across a wide range of neuroinflammatory models including systemic LPS-induced inflammation, *T. gondii* parasitic infection, and intrastriatal LPS. After induction of neuroinflammation using systemic LPS RAs remain in the brain after the resolution of inflammation. Additionally, we showed that some of the morphological changes seen in these labeled RAs 24 hours after induction return to a pre-inflammatory state. We also show transcriptional changes in *Slc1a3* and *Lrrc8a* return to pre-inflammatory levels after 1 month. The results from this work suggest that the reactive state of this subset of RAs is mostly reversible, and observed changes in gene expression previously reported are likely to be from downregulation of RA markers and not from cell death.

The ExBoX (expression by Boolean exclusion) strategy offers a novel approach to define cell subpopulations by leveraging Boolean logic. This AAV-based system encodes a gene of interest (GOI) that is turned on by one

recombinase (Cre or Flp) and turned off by another. Allowing for precise control over gene expression in specific cell types. This approach enhances the specificity of genetic targeting, enabling detailed studies of cellular heterogeneity and temporal gene expression in neurons and potentially other cell types. The ExBoX system's ability to tightly regulate expression of fluorescent reporters both *in vitro* and *in vivo* reveals it to be a useful addition to the molecular tool kit available to target neural cells. It complements traditional transgenic mouse models and provides a versatile platform for investigating the complexities of diverse cell populations.

The *C3-FlpOER^{T2}* mouse line targets a subset of RAs by utilizing expression of C3 as a driver for FlpOER^{T2}. This line has tamoxifen inducible expression, allowing for control over the timing of labeling or manipulation of RAs. Here we show the *C3-FlpOER^{T2}* can label a subset of RAs after direct insults such as intrastriatal LPS, fluid percussion injury, and *T. gondii* parasitic infection when used with a fluorescent recombinase reporter. Additionally, we show that indirect or systemic insults do not induce reporter expression. Immunohistochemistry revealed this line primarily labels astrocytes, as cells co-label with the astrocytic markers Aldh1l1, GFAP, and Vimentin. Interestingly, labeling during the chronic phase of *T. gondii* infection seems to be concentrated around areas of immune infiltration. Lastly, to show utilization of the line in combinatorial approaches, *C3-FlpOER^{T2}* was crossed with Aldh1l1-CreERT2 and a dual recombinase reporter and showed robust fluorescent labeling of both

reporters. The *C3-FlpOER^{T2}* line opens new possibilities for combinatorial approaches with the many available Cre-dependent tools.

Future studies could focus on integrating these tools with other recombinase-dependent tools to investigate the interplay between different cell types in neurodevelopment or neuroinflammatory conditions. For example, crossing the *C3-FlpOER^{T2}* and *Lcn2CreERT2* lines with a dual recombinase reporter could reveal whether these populations overlap and if they do overlap, allow us the ability to manipulate them. Additionally, sequencing studies on the labeled cells in these lines under various inflammatory insults could provide further insights into the identity of these cells. Some functional roles of RAs are known to be beneficial to the survival of neurons during inflammatory insult and the resolution of inflammation. These lines could be used in combinatorial ways to “push” astrocytes towards these behaviors. The ExBoX, *Lcn2CreERT2*, and *C3-FlpOER^{T2}* tools each contribute uniquely to the field of neuroscience by allowing for precise control over gene expression in specific cell populations. Their development shows the importance of advancing genetic technologies to better understand the heterogeneity of cell types during development and their responses during injury or disease.

References

Adams, K. L., & Gallo, V. (2018). The diversity and disparity of the glial scar. *Nature Neuroscience, 21(1)*, 9–15. https://doi.org/10.1038/s41593-017-0033-9

Adesnik, H., & Naka, A. (2018). Cracking the Function of Layers in the Sensory Cortex. *Neuron*, *100*(5), 1028–1043. https://doi.org/10.1016/j.neuron.2018.10.032

Agnew-Svoboda, W., Ubina, T., Figueroa, Z., Wong, Y. C., Vizcarra, E. A., Roebini, B., Wilson, E. H., Fiacco, T. A., & Riccomagno, M. M. (2022). A genetic tool for the longitudinal study of a subset of post-inflammatory reactive astrocytes. *Cell Reports Methods*, *2*(8). https://doi.org/10.1016/j.crmeth.2022.100276

Anderson, M. A., Ao, Y., & Sofroniew, M. V. (2014). Heterogeneity of reactive astrocytes. *Neuroscience Letters, 565*, 23–29. https://doi.org/10.1016/j.neulet.2013.12.030

Anderson, M. A., Burda, J. E., Ren, Y., Ao, Y., O'Shea, T. M., Kawaguchi, R., Coppola, G., Khakh, B. S., Deming, T. J., & Sofroniew, M. V. (2016). Astrocyte scar formation AIDS central nervous system axon regeneration. *Nature*, *532*(7598), 195–200. https://doi.org/10.1038/nature17623

Anderson, S. A., Eisenstat, D. D., Shi, L., & Rubenstein, J. L. R. (1997). Interneuron migration from basal forebrain to neocortex: Dependence on Dlx genes. *Science*, *278*(5337), 474–476. https://doi.org/10.1126/science.278.5337.474

Andersson-Rolf, A., Mustata, R. C., Merenda, A., Kim, J., Perera, S., Grego, T., Andrews, K., Tremble, K., Silva, J. C. R., Fink, J. et al. (2017). One-step generation of conditional and reversible gene knockouts. *Nat. Methods* 14, 287-289. doi:10.1038/nmeth.4156

Atasoy, D., Aponte, Y., Su, H. H. and Sternson, S. M. (2008). A FLEX switch targets channelrhodopsin-2 to multiple cell types for imaging and long-range circuit mapping. *J. Neurosci*. 28, 7025-7030. doi:10.1523/JNEUROSCI.1954-08.2008

Awatramani, R., Soriano, P., Rodriguez, C., Mai, J. J. and Dymecki, S. M. (2003). Cryptic boundaries in roof plate and choroid plexus identified by intersectional gene activation. *Nat. Genet*. 35, 70-75. doi:10.1038/ng1228

Awatramanil, R., Soriano, P., Rodriguez, C., Mai, J. J., & Dymecki, S. M. (2003). Cryptic boundaries in roof plate and choroid plexus identified by intersectional gene activation. *Nature Genetics, 35(1)*, 70–75. https://doi.org/10.1038/ng1228

Bapst, A. M., Dahl, S. L., Knöpfel, T., & Wenger, R. H. (2020). Cre-mediated, loxP independent sequential recombination of a tripartite transcriptional stop cassette allows for partial read-through transcription. *Biochimica et Biophysica Acta - Gene Regulatory Mechanisms*, *1863*(8), 194568. https://doi.org/10.1016/j.bbagrm.2020.194568

Bayraktar, O. A., Bartels, T., Holmqvist, S., Kleshchevnikov, V., Martirosyan, A., Polioudakis, D., Ben Haim, L., Young, A. M. H., Batiuk, M. Y., Prakash, K., Brown, A., Roberts, K., Paredes, M. F., Kawaguchi, R., Stockley, J. H., Sabeur, K., Chang, S. M., Huang, E., Hutchinson, P., … Rowitch, D. H. (2020). Astrocyte layers in the mammalian cerebral cortex revealed by a single-cell in situ transcriptomic map. *Nature Neuroscience*, *23*(4), 500–509. https://doi.org/10.1038/s41593-020-0602-1

Bayraktar, O. A., Fuentealba, L. C., Alvarez-Buylla, A., & Rowitch, D. H. (2015). Astrocyte development and heterogeneity. *Cold Spring Harbor Perspectives in Biology*, *7*(1). https://doi.org/10.1101/cshperspect.a020362

Beckner, M. E. (2020). A roadmap for potassium buffering/dispersion via the glial network of the CNS. *Neurochemistry International*, *136*(November 2019), 104727. https://doi.org/10.1016/j.neuint.2020.104727

Ben Haim, L., & Rowitch, D. H. (2016). Functional diversity of astrocytes in neural circuit regulation. *Nature Reviews Neuroscience*, *18*(1), 31–41. https://doi.org/10.1038/nrn.2016.159

Benesova, J., Hock, M., Butenko, O., Prajerova, I., Anderova, M., & Chvatal, A. (2009). Quantification of astrocyte volume changes during ischemia in situ reveals two populations of astrocytes in the cortex of GFAP/EGFP mice. *Journal of Neuroscience Research*, *87*(1), 96–111. https://doi.org/10.1002/jnr.21828

Beyer, F., Lüdje, W., Karpf, J., Saher, G., & Beckervordersandforth, R. (2021). Distribution of Aldh1L1-CreERT2 Recombination in Astrocytes Versus Neural Stem Cells in the Neurogenic Niches of the Adult Mouse Brain. *Frontiers in Neuroscience*, *15*(September), 1–10. https://doi.org/10.3389/fnins.2021.713077

Binder, D. K., & Steinhäuser, C. (2009). Functional Changes in Astroglial Cells in Epilepsy. *Glia, 54(5)*, 358–368. https://doi.org/https://doi.org/10.1002/glia.20394

Birling, M. C., Dierich, A., Jacquot, S., Hérault, Y., & Pavlovic, G. (2012). Highly-efficient, fluorescent, locus directed cre and FlpO deleter mice on a pure C57BL/6N genetic background. *Genesis, 50(6)*, 482–489. https://doi.org/10.1002/dvg.20826

Bishop, K. M., Rubenstein, J. L. R., & O'Leary, D. D. M. (2002). Distinct actions of Emx1, Emx2, and Pax6 in regulating the specification of areas in the developing neocortex. *Journal of Neuroscience*, *22*(17), 7627–7638. https://doi.org/10.1523/jneurosci.22-17-07627.2002

Brambilla, R., Bracchi-Ricard, V., Hu, W. H., Frydel, B., Bramwell, A., Karmally, S., Green, E. J., & Bethea, J. R. (2005). Inhibition of astroglial nuclear factor κB reduces inflammation and improves functional recovery after spinal cord injury. *Journal of Experimental Medicine, 202(1)*, 145–156. https://doi.org/10.1084/jem.20041918

Branda, C. S. and Dymecki, S. M. (2004). Talking about a revolution: the impact of site-specific recombinases on genetic analyses in mice. *Dev. Cell* 6, 7-28. doi:10.1016/S1534-5807(03)00399

Burda, J. E., & Sofroniew, M. V. (2014). Reactive gliosis and the multicellular response to CNS damage and disease. *Neuron, 81(2)*, 229–248. https://doi.org/10.1016/j.neuron.2013.12.034

Burda, J. E., O'Shea, T. M., Ao, Y., Suresh, K. B., Wang, S., Bernstein, A. M., Chandra, A., Deverasetty, S., Kawaguchi, R., Kim, J. H., McCallum, S., Rogers, A., Wahane, S., & Sofroniew, M. V. (2022). Divergent transcriptional regulation of astrocyte reactivity across disorders. *Nature, 606(7914)*, 557–564. https://doi.org/10.1038/s41586-022-04739-5

Bush, T. G., Puvanachandra, N., Horner, C. H., Polito, A., Ostenfeld, T., Svendsen, C. N., Mucke, L., Johnson, M. H., & Sofroniew, M. V. (1999). Leukocyte Infiltration, Neuronal Degeneration, and Neurite Outgrowth after Ablation of Scar-Forming, Reactive Astrocytes in Adult Transgenic Mice provision of metabolic substrates for neurons, and inter-actions with endothelia to create and maintain the b. *Neuron*, *23*, 297–308.

Butt, A. M., & Jennings, J. (1994). Response of astrocytes to y-aminoburyric acid in the neonatal rat optic nerve. *Neuroscience Letters*, *168*, 53–56.

Butt, S. J. B., Fuccillo, M., Nery, S., Noctor, S., Kriegstein, A., Corbin, J. G., & Fishell, G. (2005). The temporal and spatial origins of cortical interneurons predict their physiological subtype. *Neuron*, *48*(4), 591–604. https://doi.org/10.1016/j.neuron.2005.09.034

Cahoy, J. D., Emery, B., Kaushal, A., Foo, L. C., Zamanian, J. L., Christopherson, K. S., Xing, Y., Lubischer, J. L., Krieg, P. A., Krupenko, S. A., Thompson, W. J., & Barres, B. A. (2008). A transcriptome database for astrocytes, neurons, and oligodendrocytes: A new resource for understanding brain development and function. *Journal of Neuroscience, 28(1)*, 264–278. https://doi.org/10.1523/JNEUROSCI.4178-07.2008

Cai, J., Chen, Y., Cai, W. H., Hurlock, E. C., Wu, H., Kernie, S. G., Parada, L. F., & Lu, Q. R. (2007). A crucial role for Olig2 in white matter astrocyte development. *Development*, *134*(10), 1887–1899. https://doi.org/10.1242/dev.02847

Cameron, E. G., Nahmou, M., Toth, A. B., Heo, L., Tanasa, B., Dalal, R., Yan, W., Nallagatla, P., Xia, X., Hay, S., Knasel, C., Stiles, T. L., Douglas, C., Atkins, M., Sun, C., Ashouri, M., Bian, M., Chang, K. C., Russano, K., … Goldberg, J. L. (2024). A molecular switch for neuroprotective astrocyte reactivity. *Nature*, *626*(7999), 574–582. https://doi.org/10.1038/s41586-023-06935-3

Capecchi, M. (1989). Altering the genome by homologous recombination. *Science* 244, 1288-1292. doi:10.1126/science.2660260

Catorce, N. M., & Gevorkian, G. (2016). LPS-induced Murine Neuroinflammation Model: Main Features and Suitability for Pre-clinical Assessment of Nutraceuticals. *Current Neuropharmacology, 14(2),* 155–164. https://doi.org/10.2174/1570159x14666151204122017

Cetin, A., Komai, S., Eliava, M., Seeburg, P. H. and Osten, P. (2007). Stereotaxic gene delivery in the rodent brain. *Nat. Protoc*. 1, 3166-3173. doi:10.1038/nprot. 2006.450

Chai, H., Diaz-Castro, B., Shigetomi, E., Monte, E., Octeau, J. C., Yu, X., Cohn, W., Rajendran, P. S., Vondriska, T. M., Whitelegge, J. P., Coppola, G., & Khakh, B. S. (2017). Neural Circuit-Specialized Astrocytes: Transcriptomic, Proteomic, Morphological, and Functional Evidence. *Neuron*, *95*(3), 531-549.e9. https://doi.org/10.1016/j.neuron.2017.06.029

Che, A., Babij, R., Iannone, A. F., Fetcho, R. N., Ferrer, M., Liston, C., Fishell, G. and De Marco García, N. V. (2018). Layer I interneurons sharpen sensory

maps during neonatal development. *Neuron* 99, 98-116.e7. doi:10.1016/j.neuron.2018.06.002

Cho, M. S., Rupaimoole, R., Choi, H.-J., Noh, K., Chen, J., Hu, Q., Sood, A. K., & Afshar-Kharghan, V. (2016). Complement Component 3 Is Regulated by TWIST1 and Mediates Epithelial–Mesenchymal Transition. *The Journal of Immunology*, *196*(3), 1412–1418. https://doi.org/10.4049/jimmunol.1501886

Clavreul, S., Abdeladim, L., Hernández-Garzón, E., Niculescu, D., Durand, J., Ieng, S. H., Barry, R., Bonvento, G., Beaurepaire, E., Livet, J., & Loulier, K. (2019). Cortical astrocytes develop in a plastic manner at both clonal and cellular levels. *Nature Communications*, *10*(1), 1–14. https://doi.org/10.1038/s41467-019-12791-5

Coulter, D. A., & Steinhäuser, C. (2015). Role of astrocytes in epilepsy. *Cold Spring Harbor Perspectives in Medicine, 5(3),* 1–12. https://doi.org/10.1101/cshperspect.a022434

Cuellar-Santoyo, A. O., Ruiz-Rodríguez, V. M., Mares-Barbosa, T. B., Patrón-Soberano, A., Howe, A. G., Portales-Pérez, D. P., Miquelajáuregui Graf, A., & Estrada-Sánchez, A. M. (2023). Revealing the contribution of astrocytes to glutamatergic neuronal transmission. *Frontiers in Cellular Neuroscience*, *16*(January), 1–15. https://doi.org/10.3389/fncel.2022.1037641

Dai, D. L., Li, M., & Lee, E. B. (2023). Human Alzheimer's disease reactive astrocytes exhibit a loss of homeostastic gene expression. *Acta Neuropathologica Communications, 11(1),* 1–19. https://doi.org/10.1186/s40478-023-01624-8

Daigle TL, Madisen L, Hage TA, Valley MT, Knoblich U, Larsen RS, Takeno MM, Huang L, Gu H, Larsen R, Mills M, Bosma-Moody A, Siverts LA, Walker M, Graybuck LT, Yao Z, Fong O, Nguyen TN, Garren E, Lenz GH, Chavarha M, Pendergraft J, Harrington J, Hirokawa KE, Harris JA, Nicovich PR, McGraw MJ, Ollerenshaw DR, Smith KA, Baker CA, Ting JT, Sunkin SM, Lecoq J, Lin MZ, Boyden ES, Murphy GJ, da Costa NM, Waters J, Li L, Tasic B, Zeng H. (2018). A Suite of Transgenic Driver and Reporter Mouse Lines with Enhanced Brain-Cell-Type Targeting and Functionality. *Cell.* 174(2):465-480. doi: 10.1016/j.cell.2018.06.035. PMID: 30007418; PMCID: PMC6086366

Daigle, T. L., Madisen, L., Hage, T. A., Valley, M. T., Knoblich, U., Larsen, R. S., Takeno, M. M., Huang, L., Gu, H., Larsen, R. et al. (2019). A suite of transgenic driver and reporter mouse lines with enhanced brain cell type targeting and functionality. *Cell* 174, 465-480. doi:10.1016/j.cell.2018.06.035

Darmanis, S., Sloan, S. A., Zhang, Y., Enge, M., Caneda, C., Shuer, L. M., Gephart, M. G. H., Barres, B. A., & Quake, S. R. (2015). A survey of human brain transcriptome diversity at the single cell level. *Proceedings of the National Academy of Sciences of the United States of America*, *112*(23), 7285–7290. https://doi.org/10.1073/pnas.1507125112

Deemyad, T., Lüthi, J., & Spruston, N. (2018). Astrocytes integrate and drive action potential firing in inhibitory subnetworks. *Nature Communications*, *9*(1). https://doi.org/10.1038/s41467-018-06338-3

Deneen, B., Ho, R., Lukaszewicz, A., Hochstim, C. J., Gronostajski, R. M., & Anderson, D. J. (2006). The Transcription Factor NFIA Controls the Onset of Gliogenesis in the Developing Spinal Cord. *Neuron*, *52*(6), 953–968. https://doi.org/10.1016/j.neuron.2006.11.019

Desai, A. R., & McConnell, S. K. (2000). Progressive restriction in fate potential by neural progenitors during cerebral cortical development. *Development*, *127*, 2863–2872. https://doi.org/10.1242/dev.127.13.2863

Diaz-Castro, B., Bernstein, A. M., Coppola, G., Sofroniew, M. V., & Khakh, B. S. (2021). Molecular and functional properties of cortical astrocytes during peripherally induced neuroinflammation. *Cell Reports, 36(6)*, 109508. https://doi.org/10.1016/j.celrep.2021.109508

Diaz-Castro, B., Gangwani, M. R., Yu, X., Coppola, G., & Khakh, B. S. (2019). Astrocyte molecular signatures in Huntington's disease. *Science Translational Medicine, 11(514),* 1–12. https://doi.org/10.1126/scitranslmed.aaw8546

Dong, J.-Y., Fan, P.-D. and Frizzell, R. A. (1996). Quantitative analysis of the packaging capacity of recombinant adeno-associated virus. *Hum. Gene. Ther.* 7, 2101-2112. doi:10.1089/hum.1996.7.17-2101

Du, Y., Kiyoshi, C. M., Wang, Q., Wang, W., Ma, B., Alford, C. C., Zhong, S., Wan, Q., Chen, H., Lloyd, E. E., Jr, R. M. B., Zhou, M., & Martina, M. (2016). Genetic Deletion of TREK-1 or TWIK-1 / TREK-1 Potassium Channels does not Alter the Basic Electrophysiological Properties of Mature Hippocampal Astrocytes In Situ. *Frontiers in Cellular Neuroscience*, *10*(February), 1–13. https://doi.org/10.3389/fncel.2016.00013

Duffy, S., & MacVicar, B. A. (1994). Potassium-dependent calcium influx in acutely isolated hippocampal astrocytes. *Neuroscience*, *61*(1), 51–61. https://doi.org/10.1016/0306-4522(94)90059-0

Dunkelberger, J. R., & Song, W. C. (2010). Complement and its role in innate and adaptive immune responses. *Cell Research*, *20*(1), 34–50. https://doi.org/10.1038/cr.2009.139

Dymecki, S. M., Ray, R. S. and Kim, J. C. (2010). Mapping cell fate and function using recombinase-based intersectional strategies. guide to techniques in mouse development, Part B: mouse molecular genetics*. Methods Enzymol..* 477,183-213. doi:10.1016/S0076-6879(10)77011-7

Economo, M. N., Viswanathan, S., Tasic, B., Bas, E., Winnubst, J., Menon, V., Graybuck, L. T., Nguyen, T. N., Smith, K. A., Yao, Z., Wang, L., Gerfen, C. R., Chandrashekar, J., Zeng, H., Looger, L. L., & Svoboda, K. (2018). Distinct descending motor cortex pathways and their roles in movement. *Nature*, *563*(7729), 79–84. https://doi.org/10.1038/s41586-018-0642-9

Emsley, J. G., & Macklis, J. D. (2006). Astroglial heterogeneity closely reflects the neuronal-defined anatomy of the adult murine CNS. *Neuron Glia Biology*, *2*(3), 175–186. https://doi.org/10.1017/S1740925X06000202

Endo, F., Kasai, A., Soto, J. S., Yu, X., Qu, Z., Hashimoto, H., Gradinaru, V., Kawaguchi, R., & Khakh, B. S. (2022). Molecular basis of astrocyte diversity and morphology across the CNS in health and disease. *Science*, *378*(6619). https://doi.org/10.1126/science.adc9020

Eng, L. F., Vanderhaeghen, J. J., Bignami, A., & Gerstl, B. (1971). An acidic protein isolated from fibrous astrocytes. *Brain Research*, *28*(2), 351–354. https://doi.org/10.1016/0006-8993(71)90668-8

Engelhardt, B., & Sorokin, L. (2009). The blood-brain and the blood-cerebrospinal fluid barriers: Function and dysfunction. *Seminars in Immunopathology, 31(4),* 497–511. https://doi.org/10.1007/s00281-009-0177-0

Escartin, C., Galea, E., Lakatos, A., O'Callaghan, J. P., Petzold, G. C., Serrano-Pozo, A., Steinhäuser, C., Volterra, A., Carmignoto, G., Agarwal, A., Allen, N. J., Araque, A., Barbeito, L., Barzilai, A., Bergles, D. E., Bonvento, G., Butt, A. M., Chen, W. T., Cohen-Salmon, M., … Verkhratsky, A. (2021). Reactive astrocyte nomenclature, definitions, and future directions. *Nature Neuroscience*, *24*(3), 312–325. https://doi.org/10.1038/s41593-020-00783-4

Fan, L. Z., Kheifets, S., Bö hm, U. L., Wu, H., Piatkevish, K. D., Xie, M. E., Parot, V., Ha, Y., Evans, K. E., Boyden, E. S. et al. (2020). All-optical electrophysiology reveals the role of lateral inhibition in sensory processing in cortical layer 1. *Cell* 180, 521-535.e18. doi:10.1016/j.cell.2020.01.001

Farago, A. F., Awatramani, R. B. and Dymecki, S. M. (2006). Assembly of the brainstem cochlear nuclear complex is revealed by intersectional and subtractive genetic fate maps. *Neuron* 50, 205-218. doi:10.1016/j.neuron.2006.03.014

Feil, R., Wagner, J., Metzger, D., & Chambon, P. (1997). Regulation of Cre Recombinase Activity by Mutated Estrogen Receptor Ligand-Binding Domains. *Biochemical and Biophysical Research Communications*, *237*, 752–757. https://doi.org/10.1006/bbrc.1997.7124

Fenno, L. E., Mattis, J., Ramakrishnan, C., Hyun, M., Lee, S. Y., He, M., Tucciarone, J., Selimbeyoglu, A., Berndt, A., Grosenick, L., Zalocusky, K. A., Bernstein, H., Swanson, H., Perry, C., Diester, I., Boyce, F. M., Bass, C. E., Neve, R., Huang, Z. J., & Deisseroth, K. (2014). Targeting cells with single vectors using multiple-feature Boolean logic. *Nature Methods, 11(7)*, 763–772. https://doi.org/10.1038/nmeth.2996

Fenno, L. E., Ramakrishnan, C., Kim, Y. S., Evans, K. E., Lo, M., Vesuna, S., Inoue, M., Cheung, K. Y. M., Yuen, E., Pichamoorthy, N., Hong, A. S. O., & Deisseroth, K. (2020). Comprehensive Dual- and Triple-Feature Intersectional Single-Vector Delivery of Diverse Functional Payloads to Cells of Behaving Mammals. *Neuron, 107(5),* 836-853.e11. https://doi.org/10.1016/j.neuron.2020.06.003

Ferrer-Acosta, Y., Gonzalez-Vega, M. N., Rivera-Aponte, D. E., Martinez-Jimenez, S. M., & Martins, A. H. (2017). Monitoring astrocyte reactivity and proliferation in vitro under ischemic-like conditions. *Journal of Visualized Experiments, 2017(128),* 1–9. https://doi.org/10.3791/55108

Fraser, D. D., Duffy, S., Angelides, K. J., Perez-Velazquez, J. L., Kettenmann, H., & MacVicar, B. A. (1995). GABAA/benzodiazepine receptors in acutely isolated hippocampal astrocytes. *Journal of Neuroscience*, *15*(4), 2720–2732. https://doi.org/10.1523/jneurosci.15-04-02720.1995

G. Kantzer, C., Boutin, C., Herzig, I. D., Wittwer, C., Reiß, S., Tiveron, M. C., Drewes, J., Rockel, T. D., Ohlig, S., Ninkovic, J., Cremer, H., Pennartz, S., Jungblut, M., & Bosio, A. (2017). Anti-ACSA-2 defines a novel monoclonal antibody for prospective isolation of living neonatal and adult astrocytes. *Glia, 65(6),* 990–1004. https://doi.org/10.1002/glia.23140

Gaiano, N., Nye, J. S., & Fishell, G. (2000). Radial glial identity is promoted by Notch1 signaling in the murine forebrain. *Neuron*, *26*(2), 395–404. https://doi.org/10.1016/S0896-6273(00)81172-1

Gallo, V., & Deneen, B. (2014). Glial development: The crossroads of regeneration and repair in the CNS. *Neuron*, *83*(2), 283–308. https://doi.org/10.1016/j.neuron.2014.06.010

Ge, W. P., & Jia, J. M. (2016). Local production of astrocytes in the cerebral cortex. *Neuroscience*, *323*, 3–9. https://doi.org/10.1016/j.neuroscience.2015.08.057

Gerfen, C. R., Paletzki, R. and Heintz, N. (2013). GENSAT BAC cre-recombinase driver lines to study the functional organization of cerebral cortical and basal ganglia circuits. *Neuron* 80, 1368-1383. doi:10.1016/j.neuron.2013.10.016

Ghouli, M. R., Jonak, C. R., Sah, R., Fiacco, T. A., & Binder, D. K. (2023). Regulation of the Volume-Regulated Anion Channel Pore-Forming Subunit LRRC8A in the Intrahippocampal Kainic Acid Model of Mesial Temporal Lobe Epilepsy. *ASN Neuro*, *15*. https://doi.org/10.1177/17590914231184072

Glover, C. P. J., Bienemann, A. S., Heywood, D. J., Cosgrave, A. S. and Uney, J. B. (2002). Adenoviral-mediated, high-level, cell-specific transgene expression: a SYN1-WPRE cassette mediates increased transgene expression with no loss of neuron specificity. *Mol. Ther*. 5, 509-516. doi:10.1006/mthe.2002. 0588

Gradinaru, V., Zhang, F., Ramakrishnan, C., Mattis, J., Prakash, R., Diester, I., Goshen, I., Thompson, K. R. and Deisseroth, K. (2010). Molecular and cellular approaches for diversifying and extending optogenetics. *Cell* 141, 154-165. doi:10.1016/j.cell.2010.02.037

Gu, H., Marth, J. D., Orban, P. C., Mosmann, H. and Rajewsky, K. (1994). Deletion of a DNA polymerase β gene segment in T cells using cell type-specific gene targeting. *Science* 265, 103-106. doi:10.1126/science.8016642

Gu, Y., Cheng, X., Huang, X., Yuan, Y., Qin, S., Tan, Z., Wang, D., Hu, X., He, C., & Su, Z. (2019). Conditional ablation of reactive astrocytes to dissect their roles in spinal cord injury and repair. *Brain, Behavior, and Immunity*, *80*(April), 394–405. https://doi.org/10.1016/j.bbi.2019.04.016

Haas, B., Schipke, C. G., Peters, O., Söhl, G., Willecke, K., & Kettenmann, H. (2006). Activity-dependent ATP-waves in the mouse neocortex are independent from astrocytic calcium waves. *Cerebral Cortex*, *16*(2), 237–246. https://doi.org/10.1093/cercor/bhi101

Haas, J. S., Nowotny, T., & Abarbanel, H. D. I. (2006). Spike-timing-dependent plasticity of inhibitory synapses in the entorhinal cortex. *Journal of Neurophysiology*, *96*(6), 3305–3313. https://doi.org/10.1152/jn.00551.2006

Habib, N., McCabe, C., Medina, S., Varshavsky, M., Kitsberg, D., Dvir-Szternfeld, R., Green, G., Dionne, D., Nguyen, L., Marshall, J. L., Chen, F., Zhang, F., Kaplan, T., Regev, A., & Schwartz, M. (2020). Disease-associated astrocytes in Alzheimer's disease and aging. *Nature Neuroscience, 23(6),* 701–706. https://doi.org/10.1038/s41593-020-0624-8

Hara, M., Kobayakawa, K., Ohkawa, Y., Kumamaru, H., Yokota, K., Saito, T., Kijima, K., Yoshizaki, S., Harimaya, K., Nakashima, Y., & Okada, S. (2017). Interaction of reactive astrocytes with type i collagen induces astrocytic scar formation through the integrin-N-cadherin pathway after spinal cord injury. *Nature Medicine*, *23*(7), 818–828. https://doi.org/10.1038/nm.4354

Hartmann, K., Sepulveda-Falla, D., Rose, I. V. L., Madore, C., Muth, C., Matschke, J., Butovsky, O., Liddelow, S., Glatzel, M., & Krasemann, S. (2019a). Complement 3+-astrocytes are highly abundant in prion diseases, but their abolishment led to an accelerated disease course and early dysregulation of microglia. *Acta Neuropathologica Communications*, *7*(1), 83. https://doi.org/10.1186/s40478-019-0735-1

Hasel, P., Rose, I. V. L., Sadick, J. S., Kim, R. D., & Liddelow, S. A. (2021). Neuroinflammatory astrocyte subtypes in the mouse brain. *Nature Neuroscience, 24(10),* 1475–1487. https://doi.org/10.1038/s41593-021-00905-6

Haydon, P. G., & Carmignoto, G. (2006). Astrocyte control of synaptic transmission and neurovascular coupling. *Physiological Reviews*, *86*(3), 1009–1031. https://doi.org/10.1152/physrev.00049.2005

He, M., Tucciarone, J., Lee, S., Nigro, M. J., Kim, Y., Levine, J. M., Kelly, S. M., Krugikov, I., Wu, P., Chen, Y. et al. (2016). Strategies and tools for combinatorial targeting of GABAergic neurons in mouse cerebral cortex. *Neuron* 91, 1228-1243. doi:10.1016/j.neuron.2016.08.021

Higashi, K., Fujita, A., Inanobe, A., Tanemoto, M., Doi, K., Kubo, T., & Kurachi, Y. (2001). An inwardly rectifying K+ channel, Kir4.1, expressed in astrocytes surrounds synapses and blood vessels in brain. *American Journal of Physiology - Cell Physiology*, *281*(3 50-3), 922–931. https://doi.org/10.1152/ajpcell.2001.281.3.c922

Houades, V., Koulakoff, A., Ezan, P., Seif, I., & Giaume, C. (2008). Gap junction-mediated astrocytic networks in the mouse barrel cortex. *Journal of Neuroscience*, *28*(20), 5207–5217. https://doi.org/10.1523/JNEUROSCI.5100-07.2008

Houades, V., Rouach, N., Ezan, P., Kirchhoff, F., Koulakoff, A., & Giaume, C. (2006). Shapes of astrocyte networks in the juvenile brain. *Neuron Glia Biology*, *2*(1), 3–14. https://doi.org/10.1017/S1740925X06000081

Hughes, A. C., Pittman, B. G., Xu, B., Gammons, J. W., Webb, C. M., Nolen, H. G., Chapman, P., Bikoff, J. B., & Schwarz, L. A. (2024). A single-vector intersectional AAV strategy for interrogating cellular diversity and brain function. *Nature Neuroscience*. https://doi.org/10.1038/s41593-024-01659-7

Hunter, C. A., Roberts, C. W., Murray, M., & Alexander, J. (1992). Detection of cytokine mRNA in the brains of mice with toxoplasmic encephalitis. *Parasite Immunology*, *14*(4), 405–413. https://doi.org/10.1111/j.1365-3024.1992.tb00015.x

Hunter, R. L., Cheng, B., Choi, D. Y., Liu, M., Liu, S., Cass, W. A., & Bing, G. (2009). Intrastriatal lipopolysaccharide injection induces Parkinsonism in C57/B6 mice. *Journal of Neuroscience Research, 87(8),* 1913–1921. https://doi.org/10.1002/jnr.22012

Ihara, Y., Tomonoh, Y., Deshimaru, M., Zhang, B., Uchida, T., Ishii, A., & Hirose, S. (2016). Retigabine, a Kv7.2/Kv7.3-channel opener, attenuates drug-induced seizures in knock-in mice harboring Kcnq2 mutations. *PLoS ONE*, *11*(2), 1–18. https://doi.org/10.1371/journal.pone.0150095

Jensen, P. and Dymecki, S. M. (2014). Essentials of recombinase-based genetic fate mapping in mice*. Methods Mol. Biol.* 1092, 437-454. doi:10.1007/978-1-60327-292-6_26

Jessen, N. A., Munk, A. S. F., Lundgaard, I., & Nedergaard, M. (2015). The Glymphatic System: A Beginner's Guide. *Neurochemical Research, 40(12),* 2583–2599. https://doi.org/10.1007/s11064-015-1581-6

Jin, S. M., Cho, H. J., Kim, Y. W., Hwang, J. Y., & Mook-Jung, I. (2012). Aβ-induced Ca2+ influx regulates astrocytic BACE1 expression via calcineurin/NFAT4 signals. *Biochemical and Biophysical Research Communications*, *425*(3), 649–655. https://doi.org/10.1016/j.bbrc.2012.07.123

Jiwaji, Z., Tiwari, S. S., Avilés-Reyes, R. X., Hooley, M., Hampton, D., Torvell, M., Johnson, D. A., McQueen, J., Baxter, P., Sabari-Sankar, K., Qiu, J., He, X., Fowler, J., Febery, J., Gregory, J., Rose, J., Tulloch, J., Loan, J., Story, D., … Hardingham, G. E. (2022). Reactive astrocytes acquire neuroprotective as well as deleterious signatures in response to Tau and Aß pathology. *Nature Communications*, *13*(1). https://doi.org/10.1038/s41467-021-27702-w

Jones, L. L., Margolis, R. U., & Tuszynski, M. H. (2003). The chondroitin sulfate proteoglycans neurocan, brevican, phosphacan, and versican are differentially regulated following spinal cord injury. *Experimental Neurology*, *182*(2), 399–411. https://doi.org/10.1016/S0014-4886(03)00087-6

Jurga, A. M., Paleczna, M., Kadluczka, J., & Kuter, K. Z. (2021a). Beyond the GFAP-astrocyte protein markers in the brain. *Biomolecules, 11(9).* https://doi.org/10.3390/biom11091361

Kakava-georgiadou, N., Zwartkruis, M. M., Bullich-Vilarrubias, C., Luijendijk, M. C. M., Garner, K. M., van der Plasse, G. and Adan, R. A. H. (2019). An intersectional approach to target neural circuits with cell- and projection-type specificity: validation in the mesolimbic dopamine system. *Front. Mol. Neurosci*. 12, 49. doi:10.3389/fnmol.2019.00049

Katsouri, L., Birch, A. M., Renziehausen, A. W. J., Zach, C., Aman, Y., Steeds, H., Bonsu, A., Palmer, E. O. C., Mirzaei, N., Ries, M., & Sastre, M. (2020). Ablation of reactive astrocytes exacerbates disease pathology in a model of Alzheimer's disease. *Glia, 68(5),* 1017–1030. https://doi.org/10.1002/glia.23759

Keizer, K., Kuypers, H. G. J. M., Huisman, A. M., & Dann, O. (1983). Diamidino yellow dihydrochloride (DY·2HCl); a new fluorescent retrograde neuronal tracer, which migrates only very slowly out of the cell. *Experimental Brain Research*, *51*(2), 179–191. https://doi.org/10.1007/BF00237193

Kim, H. J. and Magrané, J. (2011). Isolation and culture of neurons and astrocytes from the mouse brain cortex. In Neurodegeneration. *Methods in Molecular Biology (Methods and Protocols),* Vol. 793. (ed. G. Manfredi and H. Kawamata), pp. 63-75. Totowa, NJ: Humana Press.

Kim, J., Lee, H. ju, Park, J. H., Cha, B. Y., & Hoe, H. S. (2022). Nilotinib modulates LPS-induced cognitive impairment and neuroinflammatory responses by regulating P38/STAT3 signaling. *Journal of Neuroinflammation*, *19*(1), 1–28. https://doi.org/10.1186/s12974-022-02549-0

Kitanishi, T., Tashiro, M., Kitanishi, N., & Mizuseki, K. (2022). Intersectional, anterograde transsynaptic targeting of neurons receiving monosynaptic inputs from two upstream regions. *Communications Biology*, *5*(1), 1–8. https://doi.org/10.1038/s42003-022-03096-3

Kozorovitskiy, Y., Saunders, A., Johnson, C. A., Lowell, B. B. and Sabatini, B. L. (2012). Recurrent network activity drives striatal synaptogenesis. *Nature* 485, 646-650. doi:10.1038/nature11052

Laird, M. D., Vender, J. R., & Dhandapani, K. M. (2008). Opposing roles for reactive astrocytes following traumatic brain injury. *NeuroSignals, 16(2–3),* 154–164. https://doi.org/10.1159/000111560

Lao, Z., Raju, G. P., Bai, C. B., & Joyner, A. L. (2012). MASTR: A Technique for Mosaic Mutant Analysis with Spatial and Temporal Control of Recombination Using Conditional Floxed Alleles in Mice. *Cell Reports*, *2*(2), 386–396. https://doi.org/10.1016/j.celrep.2012.07.004

Lattke, M., Goldstone, R., Ellis, J. K., Boeing, S., Jurado-Arjona, J., Marichal, N., MacRae, J. I., Berninger, B., & Guillemot, F. (2021). Extensive transcriptional and chromatin changes underlie astrocyte maturation in vivo and in culture. *Nature Communications, 12(1).* https://doi.org/10.1038/s41467-021-24624-5

Laug, D., Glasgow, S. M., & Deneen, B. (2018). A glial blueprint for gliomagenesis. *Nature Reviews Neuroscience*, *19*(7), 393–403. https://doi.org/10.1038/s41583-018-0014-3

Lawal, O., Ulloa Severino, F. P., & Eroglu, C. (2022). The role of astrocyte structural plasticity in regulating neural circuit function and behavior. *Glia, 70(8),* 1467–1483. https://doi.org/10.1002/glia.24191

Lee, H. G., Wheeler, M. A., & Quintana, F. J. (2022). Function and therapeutic value of astrocytes in neurological diseases. *Nature Reviews Drug Discovery*, *21*(5), 339–358. https://doi.org/10.1038/s41573-022-00390-x

Lee, S., Park, J. Y., Lee, W. H., Kim, H., Park, H. C., Mori, K., & Suk, K. (2009). Lipocalin-2 is an autocrine mediator of reactive astrocytosis. *Journal of Neuroscience, 29(1),* 234–249. https://doi.org/10.1523/JNEUROSCI.5273-08.2009

Li, K., Li, J., Zheng, J., & Qin, S. (2019). Reactive astrocytes in neurodegenerative diseases. *Aging and Disease*, *10*(3), 664–675. https://doi.org/10.14336/AD.2018.0720

Li, Y., Chopp, M., Jiang, N., & Zaloga, C. (1995). In situ detection of DNA fragmentation after focal cerebral ischemia in mice. *Molecular Brain Research*, *28*(1), 164–168. https://doi.org/10.1016/0169-328X(94)00220-9

Liddelow, S. A., Guttenplan, K. A., Clarke, L. E., Bennett, F. C., Bohlen, C. J., Schirmer, L., Bennett, M. L., Münch, A. E., Chung, W. S., Peterson, T. C., Wilton, D. K., Frouin, A., Napier, B. A., Panicker, N., Kumar, M., Buckwalter, M. S., Rowitch, D. H., Dawson, V. L., Dawson, T. M.,…Barres, B. A. (2017). Neurotoxic reactive astrocytes are induced by activated microglia. *Nature, 541(7638),* 481–487. https://doi.org/10.1038/nature21029

Linnerbauer, M., & Rothhammer, V. (2020). Protective Functions of Reactive Astrocytes Following Central Nervous System Insult. *Frontiers in Immunology*, *11*(September), 1–18. https://doi.org/10.3389/fimmu.2020.573256

López-Bendito, G., Sturgess, K., Erdélyi, F., Szabó, G., Molnár, Z., & Paulsen, O. (2004). Preferential origin and layer destination of GAD65-GFP cortical interneurons. *Cerebral Cortex*, *14*(10), 1122–1133. https://doi.org/10.1093/cercor/bhh072

Lovick, T. A., Brown, L. A., & Key, B. J. (2005). Neuronal activity-related coupling in cortical arterioles: Involvement of astrocyte-derived factors. *Experimental Physiology*, *90*(1), 131–140. https://doi.org/10.1113/expphysiol.2004.028811

Luskin, M. B., Pearlman, A. L., & Sanes, J. R. (1988). Cell lineage in the cerebral cortex of the mouse studied in vivo and in vitro with a Recombinant Retrovirus. *Neuron*, *1*(8), 635–647. https://doi.org/10.1016/0896-6273(88)90163-8

Lüttjohann, A., Fabene, P. F., & van Luijtelaar, G. (2009). A revised Racine's scale for PTZ-induced seizures in rats. *Physiology and Behavior*, *98*(5), 579–586. https://doi.org/10.1016/j.physbeh.2009.09.005

Madisen L, Garner AR, Shimaoka D, Chuong AS, Klapoetke NC, Li L, van der Bourg A, Niino Y, Egolf L, Monetti C, Gu H, Mills M, Cheng A, Tasic B, Nguyen TN, Sunkin SM, Benucci A, Nagy A, Miyawaki A, Helmchen F, Empson RM, Knöpfel T, Boyden ES, Reid RC, Carandini M, Zeng H. Transgenic mice for intersectional targeting of neural sensors and effectors with high specificity and performance. Neuron. 2015 Mar 4;85(5):942-58. doi: 10.1016/j.neuron.2015.02.022. PMID: 25741722; PMCID: PMC4365051.

Madisen L, Mao T, Koch H, Zhuo JM, Berenyi A, Fujisawa S, Hsu YW, Garcia AJ 3rd, Gu X, Zanella S, Kidney J, Gu H, Mao Y, Hooks BM, Boyden ES,

Buzsáki G, Ramirez JM, Jones AR, Svoboda K, Han X, Turner EE, Zeng H. A toolbox of Cre-dependent optogenetic transgenic mice for light-induced activation and silencing. Nat Neurosci. 2012 Mar 25;15(5):793-802. doi: 10.1038/nn.3078. PMID: 22446880; PMCID: PMC3337962.

Madisen, L., Zwingman, T. A., Sunkin, S. M., Oh, S. W., Zariwala, H. A., Gu, H., Ng, L. L., Palmiter, R. D., Hawrylycz, M. J., Jones, A. R., Lein, E. S., & Zeng, H. (2010). A robust and high-throughput Cre reporting and characterization system for the whole mouse brain. *Nature Neuroscience, 13(1),* 133–140. https://doi.org/10.1038/nn.2467

Man, J. H. K., Groenink, L., & Caiazzo, M. (2018). Cell reprogramming approaches in gene- and cell-based therapies for Parkinson's disease. *Journal of Controlled Release*, *286*(June), 114–124. https://doi.org/10.1016/j.jconrel.2018.07.017

Mathiesen, S. N., Lock, J. L., Schoderboeck, L., Abraham, W. C. and Hughes, S. M. (2020). CNS transduction benefits of AAV-PHP.eB over AAV9 are dependent on administration route and mouse strain. *Mol. Ther. Methods Clin. Dev*. 19, 447-458. doi:10.1016/j.omtm.2020.10.011

Matho, K. S., Huilgol, D., Galbavy, W., He, M., Kim, G., An, X., Lu, J., Wu, P., Di Bella, D. J., Shetty, A. S., Palaniswamy, R., Hatfield, J., Raudales, R., Narasimhan, A., Gamache, E., Levine, J. M., Tucciarone, J., Szelenyi, E., Harris, J. A., … Huang, Z. J. (2021). Genetic dissection of the glutamatergic neuron system in cerebral cortex. *Nature*, *598*(7879), 182–187. https://doi.org/10.1038/s41586-021-03955-9

Matsuda, T. and Cepko, C. L. (2007). Controlled expression of transgenes introduced by in vivo electroporation. *Proc. Natl. Acad. Sci.* USA 104, 1027-1032. doi:10.1073/pnas.0610155104

Maturana, C.J., Verpeut, J.L., Kooshkbaghi, M. et al. Novel tool to quantify with single-cell resolution the number of incoming AAV genomes co-expressed in the mouse nervous system. *Gene Ther* 30, 463–468 (2023). https://doi.org/10.1038/s41434-021-00272-8

Matusova, Z., Hol, E. M., Pekny, M., Kubista, M., & Valihrach, L. (2023). Reactive astrogliosis in the era of single-cell transcriptomics. *Frontiers in Cellular Neuroscience*, *17*(April 2014). https://doi.org/10.3389/fncel.2023.1173200

Matyash, V., & Kettenmann, H. (2010). Heterogeneity in astrocyte morphology and physiology. *Brain Research Reviews*, *63*(1–2), 2–10. https://doi.org/10.1016/j.brainresrev.2009.12.001

McKeon, R. J., Hoke, A., & Silver, J. (1995). *Injury-induced proteoglycans inhibit the potential for laminin-mediated axon growth on astrocytic scars* (pp. 32–43). Experimental Neurology. https://doi.org/https://doi.org/10.1006/exnr.1995.1081

McKeon, R. J., Schreiber, R. C., Rudge, J. S., & Silver, J. (1991). Reduction of neurite outgrowth in a model of glial scarring following CNS injury is correlated with the expression of inhibitory molecules on reactive astrocytes. *Journal of Neuroscience*, *11*(11), 3398–3411. https://doi.org/10.1523/jneurosci.11-11-03398.1991

McLin, J. P., & Steward, O. (2006). Comparison of seizure phenotype and neurodegeneration induced by systemic kainic acid in inbred, outbred, and hybrid mouse strains. *European Journal of Neuroscience*, *24*(8), 2191–2202. https://doi.org/10.1111/j.1460-9568.2006.05111.x

Mishima, T., & Hirase, H. (2010). In vivo intracellular recording suggests that gray matter astrocytes in mature cerebral cortex and hippocampus are electrophysiologically homogeneous. *Journal of Neuroscience*, *30*(8), 3093–3100. https://doi.org/10.1523/JNEUROSCI.5065-09.2010

Miyoshi, G., Butt, S. J. B., Takebayashi, H., & Fishell, G. (2007). Physiologically distinct temporal cohorts of cortical interneurons arise from telencephalic Olig2-expressing precursors. *Journal of Neuroscience*, *27*(29), 7786–7798. https://doi.org/10.1523/JNEUROSCI.1807-07.2007

Miyoshi, G., Hjerling-Leffler, J., Karayannis, T., Sousa, V. H., Butt, S. J. B., Battiste, J., Johnson, J. E., Machold, R. P., & Fishell, G. (2010). Genetic fate mapping reveals that the caudal ganglionic eminence produces a large and diverse population of superficial cortical interneurons. *Journal of Neuroscience*, *30*(5), 1582–1594. https://doi.org/10.1523/JNEUROSCI.4515-09.2010

Molyneaux, B. J., Arlotta, P., Menezes, J. R. L., & Macklis, J. D. (2007). Neuronal subtype specification in the cerebral cortex. *Nature Reviews Neuroscience*, *8*(6), 427–437. https://doi.org/10.1038/nrn2151

Mongin, A. A. (2016). Volume-regulated anion channel—a frenemy within the brain. *Pflugers Archiv European Journal of Physiology, 468(3),* 421–441. https://doi.org/10.1007/s00424-015-1765-6

Moore, S. A., & Iulianella, A. (2021). Development of the mammalian cortical hem and its derivatives: The choroid plexus, Cajal-Retzius cells and hippocampus. *Open Biology*, *11*(5). https://doi.org/10.1098/rsob.210042

Morizawa, Y. M., Hirayama, Y., Ohno, N., Shibata, S., Shigetomi, E., Sui, Y., Nabekura, J., Sato, K., Okajima, F., Takebayashi, H., Okano, H., & Koizumi, S. (2017). Reactive astrocytes function as phagocytes after brain ischemia via ABCA1-mediated pathway. *Nature Communications*, *8*(28), 1–14. https://doi.org/10.1038/s41467-017-00037-1

Moulson, A. J., Squair, J. W., Franklin, R. J. M., Tetzlaff, W., & Assinck, P. (2021). Diversity of Reactive Astrogliosis in CNS Pathology: Heterogeneity or Plasticity? *Frontiers in Cellular Neuroscience*, *15*(July). https://doi.org/10.3389/fncel.2021.703810

Müller, T., Fritschy, J. M., Grosche, J., Pratt, G. D., Möhler, H., & Kettenmann, H. (1994). Developmental regulation of voltage-gated K+ channel and GABAA receptor expression in Bergmann glial cells. *Journal of Neuroscience*, *14*(5 I), 2503–2514. https://doi.org/10.1523/jneurosci.14-05-02503.1994

Nakajima, K. (2007). Control of tangential/non-radial migration of neurons in the developing cerebral cortex. *Neurochemistry International*, *51*(2-4 SPEC. ISS.), 121–131. https://doi.org/10.1016/j.neuint.2007.05.006

Nakazawa, K., Quirk, M. C., Chitwood, R. A., Watanabe, M., Yeckel, M. F., Sun, L. D., Kato, A., Carr, C. A. et al. (2002). Requirement for hippocampal CA3 NMDA receptors in associative memory recall. *Science* 297:211-218. doi:10.1126/science.1071795

Namihira, M., Kohyama, J., Semi, K., Sanosaka, T., Deneen, B., Taga, T., & Nakashima, K. (2009). Committed Neuronal Precursors Confer Astrocytic Potential on Residual Neural Precursor Cells. *Developmental Cell*, *16*(2), 245–255. https://doi.org/10.1016/j.devcel.2008.12.014

Newcomb, J. K., Zhao, X., Pike, B. R., & Hayes, R. L. (1999). Temporal profile of apoptotic-like changes in neurons and astrocytes following controlled cortical impact injury in the rat. *Experimental Neurology*, *158*(1), 76–88. https://doi.org/10.1006/exnr.1999.7071

Noor, S., Habashy, A. S., Nance, J. P., Clark, R. T., Nemati, K., Carson, M. J., & Wilson, E. H. (2010). CCR7-dependent immunity during acute toxoplasma gondii infection. *Infection and Immunity, 78(5)*, 2257–2263. https://doi.org/10.1128/IAI.01314-09

Oh, S. W., Harris, J. A., Ng, L., Winslow, B., Cain, N., Mihalas, S., Wang, Q., Lau, C., Kuan, L., Henry, A. M. et al. (2014). A mesoscale connectome of the mouse brain. *Nature*, 508, 207-214. doi:10.1038/nature13186

Okada, S., Nakamura, M., Katoh, H., Miyao, T., Shimazaki, T., Ishii, K., Yamane, J., Yoshimura, A., Iwamoto, Y., Toyama, Y., & Okano, H. (2006). Conditional ablation of Stat3 or Socs3 discloses a dual role for reactive astrocytes after spinal cord injury. *Nature Medicine, 12(7),* 829–834. https://doi.org/10.1038/nm1425

Okuda, H. (2018). A review of functional heterogeneity among astrocytes and the CS56-specific antibody-mediated detection of a subpopulation of astrocytes in adult brains. *Anatomical Science International*, *93*(2), 161–168. https://doi.org/10.1007/s12565-017-0420-z

Olsen, M. L., Campbell, S. L., & Sontheimer, H. (2007). Differential distribution of Kir4.1 in spinal cord astrocytes suggests regional differences in K+ homeostasis. *Journal of Neurophysiology*, *98*(2), 786–793. https://doi.org/10.1152/jn.00340.2007

Panatier, A., & Robitaille, R. (2016). Astrocytic mGluR5 and the tripartite synapse. *Neuroscience, 323,* 29–34. https://doi.org/10.1016/j.neuroscience.2015.03.063

Park, J. S., Kam, T. I., Lee, S., Park, H., Oh, Y., Kwon, S. H., Song, J. J., Kim, D., Kim, H., Jhaldiyal, A., Na, D. H., Lee, K. C., Park, E. J., Pomper, M. G., Pletnikova, O., Troncoso, J. C., Ko, H. S., Dawson, V. L., Dawson, T. M., & Lee, S. (2021). Blocking microglial activation of reactive astrocytes is neuroprotective in models of Alzheimer's disease. *Acta Neuropathologica Communications, 9(1),* 1–15. https://doi.org/10.1186/s40478-021-01180-z

Passini, M. A. and Wolfe, J. H. (2001). Widespread gene delivery and structure specific patterns of expression in the brain after intraventricular injections of neonatal mice with an adeno-associated virus vector. *J. Virol*. 75, 12382-12392. doi:10.1128/JVI.75.24.12382-12392.2001

Pastor, A., Chvátal, A., Syková, E., & Kettenmann, H. (1995). Glycine- and GABA-activated Currents in Identified Glial Cells of the Developing Rat Spinal Cord Slice. *European Journal of Neuroscience*, *7*(6), 1188–1198. https://doi.org/10.1111/j.1460-9568.1995.tb01109.x

Perego, C., Vanoni, C., Bossi, M., Massari, S., Basudev, H., Longhi, R., & Pietrini, G. (2000). The GLT-1 and GLAST glutamate transporters are expressed on morphologically distinct astrocytes and regulated by neuronal activity in primary hippocampal cocultures. *Journal of Neurochemistry*, *75*(3), 1076–1084. https://doi.org/10.1046/j.1471-4159.2000.0751076.x

Plummer, N. W., Evsyukova, I. Y., Robertson, S. D., de Marchena, J., Tucker, C. J. and Jensen, P. (2015). Expanding the power of recombinase-based labeling to uncover cellular diversity. *Development* 142, 4385-4393. doi:10.1242/dev.129981

Polleux, F. and Ghosh, A. (2002). The slice overlay assay: a versatile tool to study the influence of extracellular signals on neuronal development. *Science's STKE* 2002, pl9. doi:10.1126/stke.2002.136.pl9

Regan, M. R., Huang, Y. H., Yu, S. K., Dykes-Hoberg, M. I., Jin, L., Watkins, A. M., Bergles, D. E., & Rothstein, J. D. (2007). Variations in promoter activity reveal a differential expression and physiology of glutamate transporters by glia in the developing and mature CNS. *Journal of Neuroscience*, *27*(25), 6607–6619. https://doi.org/10.1523/JNEUROSCI.0790-07.2007

Reichenbach, A., & Wolburg, H. (2005). Astrocytes and ependymal glia. In *Neuroglia* (pp. 19–35).

Reid, J. K., & Kuipers, H. F. (2021). She Doesn't Even Go Here: The Role of Inflammatory Astrocytes in CNS Disorders. *Frontiers in Cellular Neuroscience*, *15*(September), 1–12. https://doi.org/10.3389/fncel.2021.704884

Retzius, G. (1894). Weitere beitrage zue kenntniss der Cajal'schen Zellen der grosshirnrinde des menschen. *Biol. Unters*, *6*, 29–34.

Ricklin, D., Reis, E. S., Mastellos, D. C., Gros, P., & Lambris, J. D. (2016). Complement component C3 – The "Swiss Army Knife" of innate immunity and host defense. *Immunological Reviews*, *274*(1), 33–58. https://doi.org/10.1111/imr.12500

Robel, S., Mori, T., Zoubaa, S., Schlegel, J., Sirko, S., Faissner, A., Goebbels, S., Dimou, L., & Götz, M. (2009). Conditional deletion of β1-integrin in astroglia causes partial reactive gliosis. *Glia, 57(15),* 1630–1647. https://doi.org/10.1002/glia.20876

Robles-Oteiza, C., Taylor, S., Yates, T., Cicchini, M., Lauderback, B., Cashman, C. R., Burds, A. A., Winslow, M. M., Jacks, T. and Feldser, D. M. (2015). Recombinase-based conditional and reversible gene regulation via XTR alleles. *Nat. Commun*. 6, 8783. doi:10.1038/ncomms9783

Rogers, S.,Wells, R. and Rechsteiner, M. (1986). Amino acid sequences common to rapidly degraded proteins: the PEST hypothesis*. Science* 234: 364-368. doi:10.1126/science.2876518

Roßner, S., Lange-Dohna, C., Zeitschel, U., & Perez-Polo, J. R. (2005). Alzheimer's disease β-secretase BACE1 is not a neuron-specific enzyme. *Journal of Neurochemistry*, *92*(2), 226–234. https://doi.org/10.1111/j.1471-4159.2004.02857.x

Ryoo, K., & Park, J. Y. (2016). Two-pore domain potassium channels in astrocytes. *Experimental Neurobiology*, *25*(5), 222–232. https://doi.org/10.5607/en.2016.25.5.222

Sabatini, P. V., Wang, J., Rupp, A. C., Affinati, A. H., Flak, J. N., Li, C., Olson, D. P. and Myers, M. G. (2021). tTARGIT AAVs mediate the sensitive and flexible manipulation of intersectional neuronal populations in mice. *eLife* 10, e66835. doi:10.7554/eLife.66835

Salic, A., & Mitchison, T. J. (2008). A chemical method for fast and sensitive detection of DNA synthesis in vivo. *Proceedings of the National Academy of Sciences of the United States of America, 105(7),* 2415–2420. https://doi.org/10.1073/pnas.0712168105

Samartino, C. G., Delpino, M. V., Godoy, C. P., Di Genaro, M. S., Pasquevich, K. A., Zwerdling, A., Barrionuevo, P., Mathieu, P., Cassataro, J., Pitossi, F., & Giambartolomei, G. H. (2010). Brucella abortus induces the secretion of proinflammatory mediators from glial cells leading to astrocyte apoptosis. *American Journal of Pathology*, *176*(3), 1323–1338. https://doi.org/10.2353/ajpath.2010.090503

Sanes, D. H., & Reh, T. A. (2019). *Development of the Nervous System*.

Sanosaka, T., Imamura, T., Hamazaki, N., Chai, M. C., Igarashi, K., Ideta-Otsuka, M., Miura, F., Ito, T., Fujii, N., Ikeo, K., & Nakashima, K. (2017). DNA Methylome Analysis Identifies Transcription Factor-Based Epigenomic Signatures of Multilineage Competence in Neural Stem/Progenitor Cells. *Cell Reports*, *20*(12), 2992–3003. https://doi.org/10.1016/j.celrep.2017.08.086

Sauer, B. (1987). Functional Expression of the cre-lox Site-Specific Recombination System in The yeast Saccharomyces cerevisiae. *Molecular and Cellular Biology*, *7*(6), 2087–2096.

Sauer, B. (2006). Cre– lox -Inducible Gene Targeting . *Encyclopedia of Life Sciences*, 1–3. https://doi.org/10.1038/npg.els.0005979

Sauer, B., & Henderson, N. (1988). Site-specific DNA recombination in mammalian cells by the Cre recombinase of bacteriophage P1. *Proceedings*

of the National Academy of Sciences of the United States of America, *85*(14), 5166–5170. https://doi.org/10.1073/pnas.85.14.5166

Saunders, A., Johnson, C. A. and Miyamichi, K. (2012). Novel recombinant adeno-associated viruses for Cre activated and inactivated transgene expression in neurons*. Front. Neural Circuits* 6, 47. doi:10.3389/fncir.2012.00047

Scemes, E., & Giaume, C. (2006). Astrocyte Calcium Waves: What They Are and What They Do. *Glia*, *54*, 716–725. https://doi.org/10.1002/glia

Schindelin, J., Arganda-Carreras, I., Frise, E., Kaynig, V., Longair, M., Pietzsch, T., Preibisch, S., Rueden, C., Saalfeld, S., Schmid, B. et al. (2012). Fiji: An open-source platform for biological-image analysis. *Nat. Methods* 9, 676-682. doi:10.1038/nmeth.2019

Schipke, C. G., Boucsein, C., Ohlemeyer, C., Kirchhoff, F., & Kettenmann, H. (2002). Astrocyte Ca2+ waves trigger responses in microglial cells in brain slices. *The FASEB Journal : Official Publication of the Federation of American Societies for Experimental Biology*, *16*(2), 255–257. https://doi.org/10.1096/fj.01-0514fje

Schnütgen, F., Doerflinger, N., Calléja, C., Wendling, O., Chambon, P. and Ghyselinck, N. B. (2003). A directional strategy for monitoring Cre-mediated recombination at the cellular level in the mouse. *Nat. Biotechnol*. 21, 562-565. doi:10.1038/nbt811

Scott, E. Y., Safarian, N., Casasbuenas, D. L., Dryden, M., Tockovska, T., Ali, S., Peng, J., Daniele, E., Nie Xin Lim, I., Bang, K. W. A., Tripathy, S., Yuzwa, S. A., Wheeler, A. R., & Faiz, M. (2024). Integrating single-cell and spatially resolved transcriptomic strategies to survey the astrocyte response to stroke in male mice. *Nature Communications*, *15*(1), 1–14. https://doi.org/10.1038/s41467-024-45821-y

Shinozaki, Y., Shibata, K., Yoshida, K., Shigetomi, E., Gachet, C., Ikenaka, K., Tanaka, K. F., & Koizumi, S. (2017). Transformation of Astrocytes to a Neuroprotective Phenotype by Microglia via P2Y1 Receptor Downregulation. *Cell Reports, 19(6),* 1151–1164. https://doi.org/10.1016/j.celrep.2017.04.047

Smith, A.M., Davey, K., Tsartsalis, S. et al. Diverse human astrocyte and microglial transcriptional responses to Alzheimer's pathology. *Acta Neuropathol 143*, 75–91 (2022). https://doi.org/10.1007/s00401-021-02372-6

Sofroniew, M. V. (2009). Molecular dissection of reactive astrogliosis and glial scar formation. *Trends in Neurosciences, 32(12),* 638–647. https://doi.org/10.1016/j.tins.2009.08.002

Sofroniew, M. V. (2015). Astrogliosis. *Cold Spring Harbor Perspectives in Biology, 16(3).*

Sofroniew, M. V., & Vinters, H. V. (2010). Astrocytes: Biology and pathology. *Acta Neuropathologica*, *119*(1), 7–35. https://doi.org/10.1007/s00401-009-0619-8

Sonninen, T. M., Hämäläinen, R. H., Koskuvi, M., Oksanen, M., Shakirzyanova, A., Wojciechowski, S., Puttonen, K., Naumenko, N., Goldsteins, G., Laham-Karam, N., Lehtonen, M., Tavi, P., Koistinaho, J., & Lehtonen, Š. (2020). Metabolic alterations in Parkinson's disease astrocytes. *Scientific Reports*, *10*(1). https://doi.org/10.1038/s41598-020-71329-8

Srinivasan, R., Lu, T. Y., Chai, H., Xu, J., Huang, B. S., Golshani, P., Coppola, G., & Khakh, B. S. (2016). New Transgenic Mouse Lines for Selectively Targeting Astrocytes and Studying Calcium Signals in Astrocyte Processes In Situ and In Vivo. *Neuron, 92(6),* 1181–1195. https://doi.org/10.1016/j.neuron.2016.11.030

Ståhl, P. L., Salmén, F., Vickovic, S., Lundmark, A., Navarro, J. F., Magnusson, J., Giacomello, S., Asp, M., Westholm, J. O., Huss, M., Mollbrink, A., Linnarsson, S., Codeluppi, S., Borg, Å., Pontén, F., Costea, P. I., Sahlén, P., Mulder, J., Bergmann, O., … Frisén, J. (2016). Visualization and analysis of gene expression in tissue sections by spatial transcriptomics. *Science*, *353*(6294), 78–82. https://doi.org/10.1126/science.aaf2403

Steinhaüser, C., Berger, T., Frotscher, M., & Kettenmann, H. (1992). Heterogeneity in the Membrane Current Pattern of Identified Glial Cells in the Hippocampal Slice. *European Journal of Neuroscience*, *4*(6), 472–484. https://doi.org/10.1111/j.1460-9568.1992.tb00897.x

Sternson, S. M., Atasoy, D., Betley, J. N., Henry, F. E. and Xu, S. (2016). An emerging technology framework for the neurobiology of appetite. *Cell Metab*. 23, 234-253. doi:10.1016/j.cmet.2015.12.002

Su Akdemir, E., Yu-Szu Huang, A., & Deneen, B. (2020). Astrocytogenesis: where, when, and how. *F1000Research*, *9*(233). https://doi.org/10.12688/f1000research.22405.1

Sulston, J. E., Schierenberg, E., White, J. G., & Thomson, J. N. (1983). The embryonic cell lineage of the nematode Caenorhabditis elegans.

Developmental Biology, *100*(1), 64–119. https://doi.org/10.1016/0012-1606(83)90201-4

Sung, B., Lim, G., & Mao, J. (2003). Altered expression and uptake activity of spinal glutamate transporters after nerve injury contribute to the pathogenesis of neuropathic pain in rats. *Journal of Neuroscience, 23(7)*, 2899–2910. https://doi.org/10.1523/jneurosci.23-07-02899.2003

Taha, D. M., Clarke, B. E., Hall, C. E., Tyzack, G. E., Ziff, O. J., Greensmith, L., Kalmar, B., Ahmed, M., Alam, A., Thelin, E. P., Garcia, N. M., Helmy, A., Sibley, C. R., & Patani, R. (2022). Astrocytes display cell autonomous and diverse early reactive states in familial amyotrophic lateral sclerosis. *Brain*, *145*(2), 481–489. https://doi.org/10.1093/brain/awab328

Takata, N., & Hirase, H. (2008). Cortical layer 1 and layer 2/3 astrocytes exhibit distinct calcium dynamics in vivo. *PLoS ONE*, *3*(6). https://doi.org/10.1371/journal.pone.0002525

Takuma, K., Baba, A., & Matsuda, T. (2004). Astrocyte apoptosis: Implications for neuroprotection. *Progress in Neurobiology*, *72*(2), 111–127. https://doi.org/10.1016/j.pneurobio.2004.02.001

Tamamaki, N., Fujimori, K. E., & Takauji, R. (1997). Origin and route of tangentially migrating neurons in the developing neocortical intermediate zone. *Journal of Neuroscience*, *17*(21), 8313–8323. https://doi.org/10.1523/jneurosci.17-21-08313.1997

Tang, F., Barbacioru, C., Wang, Y., Nordman, E., Lee, C., Xu, N., Wang, X., Bodeau, J., Tuch, B. B., Siddiqui, A., Lao, K., & Surani, M. A. (2009). mRNA-Seq whole-transcriptome analysis of a single cell. *Nature Methods*, *6*(5), 377–382. https://doi.org/10.1038/nmeth.1315

Tasic, B., Yao, Z., Graybuck, L. T., Smith, K. A., Nguyen, T. N., Bertagnolli, D., Goldy, J., Garren, E., Economo, M. N., Viswanathan, S., Penn, O., Bakken, T., Menon, V., Miller, J., Fong, O., Hirokawa, K. E., Lathia, K., Rimorin, C., Tieu, M., … Zeng, H. (2018). Shared and distinct transcriptomic cell types across neocortical areas. *Nature*, *563*(7729), 72–78. https://doi.org/10.1038/s41586-018-0654-5

Torres-Ceja, B., & Olsen, M. L. (2022). A closer look at astrocyte morphology: Development, heterogeneity, and plasticity at astrocyte leaflets. *Current Opinion in Neurobiology*, *74*, 102550. https://doi.org/10.1016/j.conb.2022.102550

Tremblay, R., Lee, S. and Rudy, B. (2016). GABAergic interneurons in the neocortex: from cellular properties to circuits. *Neuron* 91, 260-292. doi:10.1016/j. neuron.2016.06.033

Tropepe, V., Hitoshi, S., Sirard, C., Mak, T. W., Rossant, J., & Van Der Kooy, D. (2001). Direct neural fate specification from embryonic stem cells: A primitive mammalian neural stem cell stage acquired through a default mechanism. *Neuron*, *30*(1), 65–78. https://doi.org/10.1016/S0896-6273(01)00263-X

Tsien, J. Z., Chen, D. F., Gerber, D., Tom, C., Mercer, E. H., Anderson, D. J., Mayford, M., Kandel, E. R. and Tonegawa, S. (1996). Subregion- and cell type– restricted gene knockout in mouse brain. *Cell* 87, 1317-1326. doi:10.1016/S0092- 8674(00)81826-7

Ubina, T., Vahedi-Hunter, T., Agnew-Svoboda, W., Wong, W., Gupta, A., Santhakumar, V., & Riccomagno, M. M. (2021). ExBoX – A simple Boolean exclusion strategy to drive expression in neurons. *Journal of Cell Science*, *134*(20). https://doi.org/10.1242/jcs.257212

Valcanis, H., & Tan, S. S. (2003). Layer specification of transplanted interneurons in developing mouse neocortex. *Journal of Neuroscience*, *23*(12), 5113–5122. https://doi.org/10.1523/jneurosci.23-12-05113.2003

Van Duyne, G. D. (2015). Cre Recombinase. *Microbiology Spectrum, 3(1).* https://doi.org/10.1128/microbiolspec.mdna3-0014-2014

Van Kralingen, C., Kho, D. T., Costa, J., Angel, C. E., & Graham, E. S. (2013). Exposure to inflammatory cytokines IL-1β and TNFα induces compromise and death of astrocytes; implications for chronic neuroinflammation. *PLoS ONE*, *8*(12), 1–13. https://doi.org/10.1371/journal.pone.0084269

Volterra, A., & Meldolesi, J. (2005). Astrocytes, from brain glue to communication elements: The revolution continues. *Nature Reviews Neuroscience*, *6*(8), 626–640. https://doi.org/10.1038/nrn1722

Voronkov, D. N., Stavrovskaya, A. V., Potapov, I. A., Guschina, A. S., & Olshanskiy, A. S. (2023). Glial Reaction in a Neuroinflammatory Model of Parkinson's Disease. *Bulletin of Experimental Biology and Medicine*, *174*(5), 693–698. https://doi.org/10.1007/s10517-023-05772-8

Wang, Q., Wang, M., Choi, I., Sarrafha, L., Liang, M., Ho, L., Farrell, K., Beaumont, K. G., Sebra, R., De Sanctis, C., Crary, J. F., Ahfeldt, T., Blanchard, J., Neavin, D., Powell, J., Davis, D. A., Sun, X., Zhang, B., & Yue, Z. (2024). Molecular profiling of human substantia nigra identifies diverse

neuron types associated with vulnerability in Parkinson's disease. *Science Advances*, *10*(2), 1–18. https://doi.org/10.1126/sciadv.adi8287

Wanner, I. B., Anderson, M. A., Song, B., Levine, J., Fernandez, A., Gray-Thompson, Z., Ao, Y., & Sofroniew, M. V. (2013). Glial scar borders are formed by newly proliferated, elongated astrocytes that interact to corral inflammatory and fibrotic cells via STAT3-dependent mechanisms after spinal cord injury. *Journal of Neuroscience, 33(31),* 12870–12886. https://doi.org/10.1523/JNEUROSCI.2121-13.2013

Wheeler MA, Clark IC, Tjon EC, Li Z, Zandee SEJ, Couturier CP, Watson BR, Scalisi G, Alkwai S, Rothhammer V, Rotem A, Heyman JA, Thaploo S, Sanmarco LM, Ragoussis J, Weitz DA, Petrecca K, Moffitt JR, Becher B, Antel JP, Prat A, Quintana FJ. MAFG-driven astrocytes promote CNS inflammation. Nature. 2020 Feb;578(7796):593-599. doi: 10.1038/s41586-020-1999-0. Epub 2020 Feb 12. PMID: 32051591; PMCID: PMC8049843.

Wichterle, H., Turnbull, D. H., Nery, S., Fishell, G., & Alvarez-Buylla, A. (2001). In utero fate mapping reveals distinct migratory pathways and fates of neurons born in the mammalian basal forebrain. *Development*, *128*(19), 3759–3771. https://doi.org/10.1242/dev.128.19.3759

Wiesel, T. N. and Hubel, D. H. (1963). Single-cell responses in striate cortex of kittens deprived of vision in one eye. *J. Neurophysiol*. 26, 1003-1017. doi:10.1152/ jn.1963.26.6.1003

Wilson, E. H., Harris, T. H., Mrass, P., John, B., Tait, E. D., Wu, G. F., Pepper, M., Wherry, E. J., Dzierzinski, F., Roos, D., Haydon, P. G., Laufer, T. M., Weninger, W., & Hunter, C. A. (2009). Behavior of Parasite-Specific Effector CD8+ T Cells in the Brain and Visualization of a Kinesis-Associated System of Reticular Fibers. *Immunity*, *30*(2), 300–311. https://doi.org/10.1016/j.immuni.2008.12.013

Wu, Z., Deshpande, T., Henning, L., Bedner, P., Seifert, G., & Steinhäuser, C. (2021). Cell death of hippocampal CA1 astrocytes during early epileptogenesis. *Epilepsia*, *62*(7), 1569–1583. https://doi.org/10.1111/epi.16910

Xu, J., Jo, A., DeVries, R. P., Deniz, S., Cherian, S., Sunmola, I., Song, X., Marshall, J. J., Gruner, K. A., Daigle, T. L., Contractor, A., Lerner, T. N., Zeng, H., & Zhu, Y. (2022). Intersectional mapping of multi-transmitter neurons and other cell types in the brain. *Cell Reports*, *40*(1), 111036. https://doi.org/10.1016/j.celrep.2022.111036

Xu, Q., Cobos, I., De La Cruz, E. D., Rubenstein, J. L., & Anderson, S. A. (2004). Origins of Cortical Interneuron Subtypes. *Journal of Neuroscience*, *24*(11), 2612–2622. https://doi.org/10.1523/JNEUROSCI.5667-03.2004

Xue, M., Atallah, B. V. and Scanziani, M. (2014). Equalizing excitation-inhibition ratios across visual cortical neurons. *Nature* 511, 596-600. doi:10.1038/nature13321

Yang, J., Vitery, M. del C., Chen, J., Osei-Owusu, J., Chu, J., & Qiu, Z. (2019). Glutamate-Releasing SWELL1 Channel in Astrocytes Modulates Synaptic Transmission and Promotes Brain Damage in Stroke. *Neuron, 102(4),* 813-827.e6. https://doi.org/10.1016/j.neuron.2019.03.029

Yang, K., Liu, Y., & Zhang, M. (2024). The Diverse Roles of Reactive Astrocytes in the Pathogenesis of Amyotrophic Lateral Sclerosis. *Brain Sciences*, *14*(2). https://doi.org/10.3390/brainsci14020158

Yang, T., Dai, Y. J., Chen, G., & Cui, S. Sen. (2020). Dissecting the Dual Role of the Glial Scar and Scar-Forming Astrocytes in Spinal Cord Injury. *Frontiers in Cellular Neuroscience*, *14*(April). https://doi.org/10.3389/fncel.2020.00078

Yu, W., Li, Y., Zhong, F., Deng, Z., Wu, J., Yu, W., & Lü, Y. (2024). Disease-Associated Neurotoxic Astrocyte Markers in Alzheimer Disease Based on Integrative Single-Nucleus RNA Sequencing. *Cellular and Molecular Neurobiology*, *44*(1). https://doi.org/10.1007/s10571-024-01453-w

Yun, S. P., Kam, T. I., Panicker, N., Kim, S., Oh, Y., Park, J. S., Kwon, S. H., Park, Y. J., Karuppagounder, S. S., Park, H., Kim, S., Oh, N., Kim, N. A., Lee, S., Brahmachari, S., Mao, X., Lee, J. H., Kumar, M., An, D., … Ko, H. S. (2018). Block of A1 astrocyte conversion by microglia is neuroprotective in models of Parkinson's disease. *Nature Medicine, 24(7),* 931–938. https://doi.org/10.1038/s41591-018-0051-5

Zamanian, J. L., Xu, L., Foo, L. C., Nouri, N., Zhou, L., Giffard, R. G., & Barres, B. A. (2012). Genomic analysis of reactive astrogliosis. *Journal of Neuroscience*, *32*(18), 6391–6410. https://doi.org/10.1523/JNEUROSCI.6221-11.2012

Zhang, F., Aravanis, A. M., Adamantidis, A., de Lecea, L. and Deisseroth, K. (2007). Circuit-breakers: optical technologies for probing neural signals and systems. *Nat. Rev. Neurosci*. 8, 577-581. doi:10.1038/nrn2192

Zhang, Y. H., Chen, H., Chen, Y., Wang, L., Cai, Y. H., Li, M., Wen, H. Q., Du, J., An, R., Luo, Q. L., Wang, X. L., Lun, Z. R., Xu, Y. H., & Shen, J. L. (2014).

Activated microglia contribute to neuronal apoptosis in Toxoplasmic encephalitis. *Parasites and Vectors*, *7*(1), 1–11. https://doi.org/10.1186/1756-3305-7-372

Zhao J, Bi W, Xiao S, Lan X, Cheng X, Zhang J, Lu D, Wei W, Wang Y, Li H, Fu Y, Zhu L. Neuroinflammation induced by lipopolysaccharide causes cognitive impairment in mice. Sci Rep. 2019 Apr 8;9(1):5790. doi: 10.1038/s41598-019-42286-8. PMID: 30962497; PMCID: PMC6453933.

Zhao, C., Ries, C., Du, Y., Zhang, J., Sakimura, K., Itoi, K., & Deussing, J. M. (2023). Differential CRH expression level determines efficiency of Cre- and Flp-dependent recombination. *Frontiers in Neuroscience*, *17*(August), 1–14. https://doi.org/10.3389/fnins.2023.1163462

Zhao, X. Y., & Ewald, S. E. (2020). The molecular biology and immune control of chronic Toxoplasma gondii infection. *Journal of Clinical Investigation*, *130*(7), 3370–3380. https://doi.org/10.1172/JCI136226

Zhong, S., Du, Y., Kiyoshi, C. M., Ma, B., Alford, C. C., Wang, Q., Yang, Y., Liu, X., & Zhou, M. (2016). Electrophysiological behavior of neonatal astrocytes in hippocampal stratum radiatum. *Molecular Brain*, *9*(1), 1–16. https://doi.org/10.1186/s13041-016-0213-7